Institute of Physics, University of Latvia

THESIS

for obtaining of the degree
Doctor of Physics
in specialty of gas and liquid dynamics

by

Ilmārs Grants

Magnetically Driven Swirling Flow Guided by Steady Magnetic Field and Imposed Rotation

Salaspils – March, 1998

CONTENTS

Introduction

The present thesis concerns an azimuthal body force driven swirling flow and its stability. Controllable and stable rotating flows are needed in crystal growth technologies, where the motion of melt significantly influences the quality of grown crystals.

A rotating magnetic field induces a swirling flow of melt that usually has the conductivity of liquid metals. This artificial flow has a number of advantages in comparison to the natural buoyant one. However, there are too few possibilities to control and, thus, optimize the base flow. Besides, the swirling flow is unstable in most possible practical applications. My investigations were focused on two superimposed control tools: the steady axial magnetic field and imposed rotation of crucible. The investigations showed that both actions have a common promising feature to control the magnitude of induced flow and to stabilize it. A specific goal of the steady magnetic field application is a possibility to manipulate the pattern of secondary vortices of the meridional flow, which actually is of the most practical importance. The imposed rotation, in its turn, allows to change the direction of meridional recirculation, that otherwise is always fixed. The effect of the imposed rotation is similar to that of a steady field. So, essentially the same effect can be achieved by an energetically much lower cost.

The boundary layers of two types appear in magnetohydrodynamic and rotating flows. Horizontal rotating layers and magnetohydrodynamic Hartmann layers usually control the core flow. Much wider boundary layers appear near side wall. All these layers are subject of famous problems. The topic of the thesis introduces a close connection to these problems. At the same time, certain specific circumstances, as a rule, do not allow a straightforward use of the existing results. The main original theoretical results include the order of magnitude estimates illustrating the force balance in the rotating horizontal magnetohydrodynamic layer, an approximate analytical solution of a curved magnetohydrodynamic side layer, an approximate analytical solution of an almost rigidly rotating body force driven vertical layer, a simple and effective method to predict and optimize the shape of solidification interface, *etc.* I used different methods including scaling analysis, analytical solutions of indicative simplified cases, numerical axially symmetric simulation and experiment. Analogies to the related problems were extensively used.

The thesis consists of five chapters as independent contributions with their own abstracts, introducing and concluding sections. Since the models and governing equations are the same or similar for different flows considered, a certain overlapping occurs. The first chapter gives a review of a rotating field alone driven flow and related magnetohydrodynamic and rotating boundary layers. Chapter II deals with the stability of magnetic body force driven flow in a cylindrical vessel of variable length. A flow due to superimposed rotating and steady magnetic field is considered in the third chapter. The fourth chapter deals with a magnetic body force driven swirling flow in a rotating cylinder. Chapter V proceeds with the heat transfer as well as solidification interface controlled by the above artificial flows.

Magnetically driven swirling flow and related magnetohydrodynamic and rotating boundary layers

The current chapter presents a review of an azimuthal body force driven flow due to a rotating magnetic field in a cylinder. Besides, it deals with magnetohydrodynamic and rotating boundary layers related to those in such flow under superimposed steady axial magnetic field or rotation of the vessel. These boundary layers control the base flow and its stability. The present study shows that both superimposed actions may improve characteristics of the rotating magnetic field driven flow applied in crystal growth.

1. Introduction

The motion of melt plays an important role crucially affecting the quality of grown crystals. On the other hand, the flow conditions are not always certain and may turn out even contradictory. For example, a strong stirring reduces the large scale non-uniformity of dopant distribution. At the same time it is accompanied by an oscillating or even turbulent flow that increases microsegregation. So, more possibilities to control either the magnitude, pattern or stability of flow provide more possibilities to optimize each particular growth process. The current paper deals with a review of a body force driven axially symmetric swirling flow that is known to improve growth conditions in the melt. Besides, I made a review of boundary layer problems related to the previous one under the influence of superimposed control tools such as the steady axial magnetic field and imposed rotation of crucible.

A swirling flow of conducting liquid can be enforced by the azimuthal body force due to a magnetic field rotating in a plane perpendicular to the axis of symmetry. This artificial flow has several advantages if compared to the natural buoyant one (Priede 1993):

(i) elimination of asymmetry;
(ii) reduction of radial segregation;
(iii) control of heat transfer, hence, the solidification interface shape;
(iv) stabilization of motion.

To introduce the basics of problem and main previous results, I briefly reviewed a rotating magnetic field (RMF) driven flow in §2 (Other reviews by Gelfgat & Priede 1995, Davidson 1992).

Under the crystal growth conditions the RMF alone driven flow, however, has a fixed structure with too few possibilities for optimization. Different imposed actions such as the steady axial magnetic field (Grants, Priede & Gelfgat 1996) or the rotation of crucible (Priede 1993, 1994) may significantly widen these possibilities. Notice that the boundary layers that occur surrounding the inviscid core greatly determine both the base flow and its stability. Similar layers appear in other famous and well-studied problems. I reviewed these boundary layers with an eye to the original problem.

In case of an imposed strong steady magnetic field (SMF) the boundary layers of two types appear near the normal and tangential to the field walls. These boundary

layers are subject of classic magnetohydrodynamics (MHD). I examined them in §3. Several reviews of MHD flows under strong field are given by, e.g., Hunt & Shercliff (1971), Sterl (1990), Walker (1985).

Contrary to the SMF inducing additional body force, the imposed rotation alters the boundary conditions for angular velocity. The swirling flow in a layer between the crucible bottom and liquid bulk essentially controls the flow in the whole volume. This layer is described by the so-called one disk problem on the liquid bulk rotating above the differently rotating disk (Priede 1993, 1994). I reviewed this problem in §4. Other reviews by Zandbergen & Dijkstra (1987) and Lingwood (1997) were extensively used. Similarly to the flow in a strong SMF a much thicker boundary layer appears at the side wall under almost rigid rotation. It is a passive layer with no influence on the core. However, the thickness of this layer may become comparable to the crucible radius, so influencing all the flow.

The comparison of magnetohydrodynamic and rotating flow boundary layers is given in conclusions (§5) as well as the enumeration of main remaining questions, which make a body of the tasks for the current thesis paper.

2. Review on flow driven by a rotating magnetic field

An indicative example of rotating magnetic field (RMF) is the electric motor. It induces a magnetic field rotating in the plane perpendicular to the axis of symmetry. Similarly to the rotation of rotor, the swirling flow of conducting liquid is driven by RMF. The stirring due to RMF can be used, e.g., in the metallurgical applications (Davidson & Hunt 1987) and semiconductor crystal growth (see, review by Gelfgat and Priede 1995). Besides a certain practical aspect, the RMF driven flow turned out to be an attractive theoretical problem.

2.1 Body force

Consider magnetic field vector $\mathbf{B}_0$ rotating around the axis of cylindrical vessel with a constant angular velocity ω_0. The alternating magnetic field induces a purely axial alternating e.m.f. $\mathbf{B}_0\times\omega_0\times\boldsymbol{r}$ (Gelfgat, Priede & Sorkin 1991, Priede 1993). Since the fluid is electrically conducting, an oscillating current $\mathbf{j}_0$ appears. Interacting with RMF itself, it gives rise to an oscillating body force $\mathbf{j}_0\times\mathbf{B}_0$ with a frequency $2\omega_0$ and averaged value in the direction of RMF rotation.

2.2 Basic model and governing equations

The basic magnetic body force model considers the low frequency and induction of RMF. If $\omega_0 R_0^2\mu\sigma<3$ (μ is magnetic permeability and σ is conductivity of liquid; R_0 is vessel's radius), then the skin-effect can be ignored. In an infinitely long cylinder (or one truncated by perfectly conducting endwalls) the time-averaged azimuthal body force is $F_\theta^\infty(r)=0.5B_0^2\sigma\omega_0 r$ (Sneyd 1971, Davidson 1992). The average force $F_\theta(r,z)$ acting on a truncated cylinder is determined by the electric boundary conditions only (Priede 1993). Trombetta *et al.* (1997) obtained the expression:

$$F_\theta = B_0^2\sigma\omega_0\left(\frac{r}{2}-\sum_{k=1}^{\infty}\frac{R_0 I_1(\lambda_k r/R_0)}{(\lambda_k^2-1)I_1(\lambda_k)}\left\{\frac{\sinh\left(\lambda_k\dfrac{z+0.5L}{R_0}\right)-\sinh\left(\lambda_k\dfrac{z-0.5L}{R_0}\right)}{\sinh(\lambda_k L/R_0)}\right\}\right), \qquad (1)$$

for insulating end-walls. Axial coordinate z is measured from the mid-height of a cylinder of length L and radius R_0; $I_\nu(x)$ is the Bessel function of the first kind and λ_k are the roots of $I_\nu'(x)=0$.

Small induction of RMF implies negligible induced angular velocity of liquid if compared to that of the magnetic field rotation ($\Omega<<\omega_0$). On the one hand, it allows to ignore the oscillating part of body force since the amplitude of induced velocity oscillations scales as $\Omega'/\Omega\sim\Omega/\omega_0$ (Davidson & Hunt 1987). On the other hand, the induced swirl does not influence the RMF generated body force, if $\Omega<<\omega_0$. Priede (1993) showed that the condition is satisfied if $\mathrm{Re}_\omega>>\mathrm{Ha}_e^4$, where $\mathrm{Re}_\omega=(\omega_0 L^2/\nu)$ is the Reynolds number based on the field rotation frequency but $\mathrm{Ha}_e=(\sigma\rho/\nu)^{1/2}B_0 L$ is Hartmann number of RMF; ν is viscosity and ρ is density of liquid. The characteristic value of Re_ω under usual crystal growth conditions is more than 10^6, but Ha_e does not exceed $O(10)$.

Let us consider a laminar, incompressible axially symmetric flow. Researchers (e.g., Langlois 1987) traditionally use the vorticity-stream function formulation of Navier–Stokes equation. I believe that a modified form analogous to von Kármán similarity variables is more convenient. Let us introduce the functions Ω, H and W as $r\Omega=v_\theta$, $0.5r^2H=\psi$, $rW=w$, where w is vorticity $w=(\nabla\times\mathbf{v}, \mathbf{e}_\theta)$, and ψ is stream function $(v_r, v_z)=1/r(-\partial\psi/\partial z, \partial\psi/\partial r)$. Hence, $v_z=H+0.5r\partial H/\partial r$, $v_r=-0.5r\partial H/\partial z$. Then, the dimensionless[†] Navier-Stokes equation and the definition of both W and H yield the following set:

$$\frac{\partial\Omega}{\partial t}+H\frac{\partial\Omega}{\partial z}+\frac{r}{2}\left(\frac{\partial H}{\partial r}\frac{\partial\Omega}{\partial z}-\frac{\partial H}{\partial z}\frac{\partial\Omega}{\partial r}\right)-\frac{\partial H}{\partial z}\Omega=\frac{\partial^2\Omega}{\partial r^2}+\frac{3}{r}\frac{\partial\Omega}{\partial r}+\frac{\partial^2\Omega}{\partial z^2}+\mathrm{Te}f(r,z) \quad (2)$$

$$\frac{\partial W}{\partial t}+H\frac{\partial W}{\partial z}+\frac{r}{2}\left(\frac{\partial H}{\partial r}\frac{\partial W}{\partial z}-\frac{\partial H}{\partial z}\frac{\partial W}{\partial r}\right)-\frac{\partial\Omega^2}{\partial z}=\frac{\partial^2 W}{\partial r^2}+\frac{3}{r}\frac{\partial W}{\partial r}+\frac{\partial^2 W}{\partial z^2} \quad (3)$$

$$\frac{\partial^2 H}{\partial r^2}+\frac{3}{r}\frac{\partial H}{\partial r}+\frac{\partial^2 H}{\partial z^2}+2W=0 \quad (4)$$

Magnetic forcing is described by a source term $\mathrm{Te}f(r,z)$, where the magnetic Taylor number $\mathrm{Te}=(\Omega_f L^2/\nu)^2$ is based on angular velocity of forcing $\Omega_f=(0.5\sigma\omega_0/\rho)^{1/2}B_0$ (Davidson 1992), but the force distribution is described by $f(r,z)=F_\theta(r,z)/F_\theta^\infty(r)$. Notice, that the present definition of Ω_f differs from the referred one by a constant factor.

Ignoring the radial dependence of the functions above in neighborhood of the axis, we receive well-known similarity equations supplemented by a forcing term:

$$\frac{\partial\Omega}{\partial t}+H\Omega'-H'\Omega=\Omega''+T, \quad (5)$$

$$\frac{\partial H''}{\partial t}+HH'''+2(\Omega^2)'=H^{(4)}, \quad (6)$$

The dimensionless parameter T further referred as the Taylor number of forcing can be associated with a certain effective value of source $\mathrm{Te}f(r,z)$ according to the

[†] Vessel's height L and diffusion time $\tau=L^2/\nu$ has been used as characteristic values.

conditions below. Both Te and T coincide in case when liquid layer bounds with very thick or perfectly conducting end-walls.

2.3 Force balance in a truncated cylinder and core angular velocity

Consider an inertia dominated rotating flow due to RMF. Any axial non-uniformity of the angular velocity is accompanied by a centrifugal force drop that evokes a meridional flow smoothing angular velocity profile. Therefore, the flow tends to the solid body rotation (e.g., Davidson 1992, Priede 1993 experimentally confirmed by Short & Davidson 1994). The angular velocity falls to zero at the end-walls giving rise to radial inflow there. It passes through the liquid bulk producing the Coriolis force, which balances the magnetic forcing in the steady state. An inviscid core is surrounded by the boundary layers with a relative thickness proportional to the square root of Ekman number $E=\nu/(\Omega_0 L^2)$, where Ω_0 is core angular velocity (e.g., Greenspan 1968). Due to continuity returning meridional flow and, hence, Coriolis force in these layers is much larger than that in the core. Consequently, the magnetic forcing can be neglected in the boundary layer that results in a classic problem on fluid rotating above a rigid surface first solved by Bödewadt (1940).

Since the core rotates as a solid body, the core radial flow should adjust to the driving force distribution to provide proper balancing Coriolis force. On the other hand, the boundary layer flow near end-walls is determined only by the constant core angular velocity. Thus, the main flow characteristics are determined by the single parameter. Consequently, the source term $\mathrm{Te}f(r,z)$ can be often substituted by a constant "effective value" $\mathrm{T}=\mathrm{Te}M/M_0$, where M/M_0 is ratio of an actual driving torque to the one acting on a corresponding piece of infinite cylinder (cf., Davidson 1992, Ungarish 1997). Notice that T can be expressed by the total magnetic torque M as $\mathrm{T}=(2ML^4)/(mR_0^2\nu^2)$, where m is mass of liquid.

Applying a selfsimilar approach and Bödewadt's solution, Davidson (1992) obtained the core angular velocity $\Omega_0=\nu/L^2 0.52\mathrm{T}^{2/3}$. Grants (1997) numerically investigated the flow in an elongated vessel depending on the aspect ratio $1/8<R=R_0/L<1$ and he obtained the characteristic angular velocity $\Omega_0=\nu/L^2 0.52\mathrm{T}^{2/3}R^{1/2}$ in this range.

2.4 Unsteady flow, stability and turbulence

A strong coupling between the azimuthal swirl and secondary recirculation provides an environment for inertial waves. Inviscid oscillations in uniformly rotating flow has been investigated by Davidson (1989). It was found here that the characteristic oscillation period is $\tau\sim\Omega_0^{-1}$ or $\tau\sim R_0/v_0\ln(v_0/(\Omega_0 R_0))$ for small and large ($v_0\tau>>R_0$) amplitude oscillations, respectively (v_0 is characteristic velocity of poloidal flow). A transient flow during spin-up taking into account viscous boundary layers has been recently investigated by Ungarish (1997). He found out that 99% of steady-state swirl is achieved at time $t\approx 1.7(\Omega_0\nu)^{-1/2}$.

The analogy to the Taylor-Couette instability in a flow with an inner cylinder rotating was employed from very first papers in the field of RMF driven flow (Moffat 1965). Thus, main results on this topic worth mentioning. A dimensionless critical speed $\mathrm{Re}_T=\Omega R_1 c/\nu(2c/(R_1+R_2))^{1/2}\approx 42$ does not essentially depend on annulus length (Cole 1976). Here R_1 and R_2 are radii of inner and outer cylinders, but c is distance between them. Notice that the stability criterion of the Taylor-Couette flow is analogous to the Götler criterion $G_\theta=\mathrm{Re}_R(\delta_t/R_0)^{3/2}\approx 6$ (Tillman 1967) for a flow at spin down. The Reynolds number defined here as $\mathrm{Re}_R=\Omega R_0^2/\nu$, but δ_t is momentum

thickness of side layer. An experimental stability investigation of such flow in a vessel of aspect ratio L/R_0=18.7 was done by Mathis & Neitzel (1985). They reported their results being in a good agreement with those by Euteneuer (1972) who used a vessel of aspect ratio L/R_0=4. So, the effect of endwalls was found small or at least constant in the given range of aspect ratios. The numerical simulation of RMF driven flow, however, demonstrated that the decreasing of vessel's length delayed the onset of 2D instability (e.g., Gelfgat *et al.* 1991, Priede 1993, Barz *et al.* 1997) in comparison to an axially unbounded case investigated by Richardson (1974). It agrees qualitatively with the Götler criterion, since the decreasing of vessel's height increases the meridional flow that reduces the steady boundary layer thickness. The critical Reynolds number (based on maximum azimuthal velocity) Re=140 deduced from Richardson's results, agrees closely with the theoretical limit of global stability in flow at spin-down Re=141 (Neitzel 1982). According to Greenspan & Howard (1963), a related swirling flow during spin-up is determined by diffusion if $L/R_0>4\mathrm{Re}^{1/2}$. So, Richardson's results are expected to be applicable for aspect ratios $L/R_0>50$. Grants (1997) numerically investigated a 2D instability in RMF driven flow depending on the aspect ratio. He found that the critical Reynolds number based on maximum azimuthal velocity and vessels height $\mathrm{Re}=V_\theta L/\nu\approx2500$ was approximately constant in the range of aspect ratios $1<L/R_0<8$ that agrees with the results by Martin Witkowski (private communication).

Volz & Mazurk (1996) experimentally investigated stabilizing action of RMF on liquid heated below. They observed that at certain critical forcing flow came unstable even in the limits of zero temperature difference. Critical value $T_c\approx2.3\times10^6$ deduced from their contribution for aspect ratio $(L/R_0)\approx2$ agrees rather well with the corresponding numerical one found by Barz *et al.* (1997). Notice that sensors were placed on the side wall, so the obtained onset corresponds to the Taylor–Götler type instability of side layer.

More forcing applied rises turbulence, which violates the force balance reinforcing swirl at the axis of turbulent flow (Davidson 1992). He obtained "5/9"-law for maximum angular velocity $\Omega_0\approx2\mathrm{T}^{5/9}(L/R_0)^{-11/18}$ near the side wall. The theoretical explanations were shown in a good agreement with the experimental results by Robinson (1973) in a wide range of parameter T.

2.5 Control tools

The fixed pattern of the base flow as well as the oscillating velocity field is shortcoming in crystal growth technologies. Thus, additional means are needed to influence the base flow and to increase stability.

First, the flow can be influenced by the driving body force distribution. The arrangement of RMF allows to reinforce forcing near the side wall by a high frequency field as well as a field of higher order of symmetry (Abricka, Gelfgat and Krumins 1995, 1996, 1997). However, the role of force distribution decreases due to smoothing by meridional flow as flow velocities increase. Therefore, this means of control is restricted to small volumes.

Two cores counter-rotating and separated by a turbulent free shear layer can be obtained by opposite switching of two axially displaced RMF inductors. Such flows are suitable if intense stirring is needed (Abricka *et al.* 1995).

An additional driving magnetic body force can be applied to force meridional flow. AC current surrounding the cylinder with a conducting fluid induces currents within it. The induced current flows in the direction opposite to that in the winding. Parallel

opposite currents push each other back generating a radial inflow in front of the winding. The flow is somehow analogous to the buoyant one. However, it allows a much higher intensity and controllability of the stirring. AC field driven flows are marked by large amplitude oscillations (Gelfgat & Gorbunov 1994).

In this paper I focused on another two control tools, namely, the superimposed steady axial magnetic field (Grants *et al.* 1996) and the rotation of crucible (Priede 1993, 1994).

3. Review on MHD boundary layers

Steady magnetic field (SMF) is a standard means to suppress the oscillations of conducting liquid flow. Besides, SMF interferes the body force balance (Hunt & Shercliff 1971) providing a possibility to control the base flow due to RMF as well (Grants *et al.* 1996).

A moving conducting liquid in the steady magnetic field induces e.m.f. $\mathbf{v}\times\mathbf{B}$. Its rotational part induces electric currents with density $\mathbf{j}$. Their interaction with the steady magnetic field itself produces an e.m. body Lorentz force $\mathbf{j}\times\mathbf{B}$. In our case, two more parts of body force oscillating with the frequency of RMF appear; they are generated due to the interaction of SMF induced currents with RMF $\mathbf{j}\times\mathbf{B}_0$, and vice versa, $\mathbf{j}_0\times\mathbf{B}$.

3.1 Model and equations

Suppose the frequency of RMF is high enough to neglect the oscillating part of Lorentz force. The steady body force due to SMF is definitely flow determined. It has radial and azimuthal compounds since the imposed SMF is purely axial. The radial force is $f_r=j_\theta B$. From the Ohm's law it follows that $j_\theta=-\sigma v_r B$. The azimuthal force is $f_\theta=-j_r B$. The intensity of induced magnetic field $\mathcal{H}$ is more convenient than the current itself $\nabla\times\mathcal{H}=\mathbf{j}$. It yields the azimthal force $f_\theta=\partial\mathcal{H}_\theta/\partial z B$. A curl of Ohm's law introduces following link between $\mathcal{H}_\theta$ and the velocity:

$$\Delta\mathcal{H}_\theta=-\sigma B\partial v_\theta/\partial z \tag{7}$$

The boundary conditions for $\mathcal{H}_\theta$ are determined by the continuity of tangential electric field and normal current. Suppose walls are thin that the tangential current density is constant along their depth. Then the boundary condition for $\mathcal{H}_\theta$ is $\partial\mathcal{H}_\theta/\partial n=(\sigma/\sigma_n)\mathcal{H}_\theta/\Delta_n$ on the end walls and $\partial/\partial r(r\mathcal{H}_\theta)=(\sigma/\sigma_\tau)(r\mathcal{H}_\theta)/\Delta_\tau$ on the side wall (Shercliff 1956).

Consider a strong SMF, when inertia vanishes. Then the dimensionless[†] equations (2) and (7) take the following form:

$$\frac{\partial^2\Omega}{\partial r^2}+\frac{3}{r}\frac{\partial\Omega}{\partial r}+\frac{\partial^2\Omega}{\partial z^2}+\mathrm{Ha}^2\frac{\partial\Phi}{\partial z}+\mathrm{Te}f(r,z)=0 \tag{8}$$

$$\frac{\partial^2\Phi}{\partial r^2}+\frac{3}{r}\frac{\partial\Phi}{\partial r}+\frac{\partial^2\Phi}{\partial z^2}+\frac{\partial\Omega}{\partial z}=0, \tag{9}$$

[†] with characteristic density of induced current $\sigma(L/v)B$.

where $\Phi=\mathcal{H}_\theta/r$; $\mathrm{Ha}=(\sigma/(\rho\nu))^{1/2}LB$ is the Hartmann number. The boundary conditions for Φ are $\alpha_n\partial\Phi/\partial z\pm\Phi=0$, ($z=\pm1/2$) and $\alpha_\tau\partial/\partial r(\Phi r^2)+\Phi r^2=0$, ($r=R_0/L=R$) on the end and side walls, respectively; $\alpha_n=\sigma L/(\sigma_n\Delta_n)$ and $\alpha_\tau=\sigma L/(\sigma_\tau\Delta_\tau)$ denote the corresponding relative wall conductances.

The problem essentially differs from the one of a fully developed (2D) flow in duct only with curvature terms $\sim3/r$, non-uniform force distribution $f(r,z)$ and electric boundary conditions on the side wall, where the curvature term appears as well. In the presence of the considered strong field the flow split up into several regions (Hunt & Stewartson 1965):

(i) core;

(ii) $O(\mathrm{Ha}^{-1})$ normal to the field layer controlling the core velocity, called the Hartmann layer;

(iii) $O(\mathrm{Ha}^{-1/2})$ side layer with possibly its own velocity scale near a parallel to field wall;

(iv) corner $O(\mathrm{Ha}^{-1})\times O(\mathrm{Ha}^{-1/2})$, essentially the intersection of normal and side layers;

(v) inner corner $O(\mathrm{Ha}^{-1})\times O(\mathrm{Ha}^{-1})$, a part of the previous corner near side wall.

3.2 Core flow and Hartmann layer

A related classic MHD boundary layer problem in a rectangular duct is traditionally formulated for a constant driving pressure gradient. Suppose the force distribution is not essential in our case and the source of motion can be substituted by a certain "effective" value T. Consider a region far from parallel-to-field walls, where functions depend only on the height. Then $\partial\Phi/\partial z$ in (8) can be integrated from (9) yielding

$$\Omega''+\mathrm{T}-\mathrm{Ha}^2\left(\Omega-\frac{\overline{\Omega}}{2\alpha_n+1}\right)=0, \tag{10}$$

where the bar sign denotes the averaging over the height of layer (Grants *et al.* 1996) Asymptotic solution for core velocity is a constant

$$\Omega_0=\frac{\mathrm{T}}{\mathrm{Ha}^2}\frac{0.5+\alpha_n}{\alpha_n+\mathrm{Ha}^{-1}}. \tag{11}$$

determined by the solution in the boundary layer. Three asymptotic cases of wall conductivity can be introduced:

(i) insulating, $\alpha_n\ll\mathrm{Ha}^{-1}$; ($\Omega_0=0.5\mathrm{THa}^{-1}$);

(ii) perfectly conducting, $\alpha_n\gg1$; ($\Omega_0=\mathrm{THa}^{-2}$) and

(iii) poorly conducting, $\mathrm{Ha}^{-1}\ll\alpha_n\ll1$; ($\Omega_0=\mathrm{THa}^{-1}\alpha_n^{-1}$).

The boundary layers near the end-walls have exponential form $\Omega=\Omega_0(1-e^{-\zeta})$, $\zeta=\mathrm{Ha}(0.5\pm z)$; the plus sign corresponds to the lower and minus sign to the upper boundary layer. Equivalent forms of the solution are given by, e.g., Hartmann (1937) for insulating ends; Branover & Tsinober (1970) for arbitrary wall conductance. Now an axial non-uniformity of the core angular velocity due to ignored axial force distribution can be estimated. Integrating (9), it follows that an angular velocity drop is $\Delta\Omega=O(\partial\Phi/\partial z)$, which, in turn, can be estimated from (8) as $\partial\Phi/\partial z=O(\mathrm{T}/\mathrm{Ha}^2)$. Comparing to the core velocity itself (11), one can deduce that the force distribution is significant only for well conducting walls, when it actually becomes uniform.

3.3 Side layer

In their review Hunt & Shercliff (1971) examined all four cases with opposite walls either insulating or perfectly conducting. The case with a perfect normal and non-conducting side wall was the most surprising. Hunt (1965) found an analytical solution for perfect ends and an arbitrary conducting side wall in a form of expansion

$$h(\eta,z)=\sum_{n=0}^{\infty}h_n(\eta)\sin(\lambda_n z),\ \text{and}\quad g(\eta,z)=\sum_{n=0}^{\infty}g_n(\eta)\cos(\lambda_n z) \tag{12}$$

where $\lambda_n=(2n+1)\pi$, $n=0,1,2....$ and η is stretched side layer coordinate (factor $Ha^{1/2}$). He obtained the following asymptotic velocity expressions (written out here in our terms):

$$\Omega\sim T\sum_{n=0}^{\infty}\frac{4(-1)^n}{Ha\lambda_n{}^2}\cos(\lambda_n z)e^{-\kappa_n\eta}\sin(\kappa_n\eta)\ \text{and} \tag{13}$$

$$\Omega\sim T\sum_{n=0}^{\infty}\frac{4(-1)^n}{Ha^2\lambda_n}\cos(\lambda_n z)\left\{1-e^{-\kappa_n\eta}\left(\cos(\kappa_n\eta)-\sin(\kappa_n\eta)\right)\right\} \tag{14}$$

near an insulating and perfectly conducting side wall, respectively; $\kappa_n=(0.5\lambda_n)^{1/2}$. One can deduce that (13) has O(Ha) times higher velocity scale than the core (11) and the velocity profile has a spatially oscillating character with the reversals of velocity sign. Another limiting case (14) with all perfect walls, in its turn, has the velocity of the same order as that of the core. The velocity profile also has spatial oscillations but never changes the sign. Similar solutions are received by Uflyand (1961) and Chang & Lundgren (1961). Branover & Gelfgat (1968) and Alty (1971) performed corresponding experiments.

The case of non-conducting walls has been first solved by Shercliff (1953). The same solution was also received by, e.g., Williams (1963), Chang & Lundgren (1961) and Hunt (1965) using different methods. Shercliff (1953) obtained a selfsimilar solution exhibiting the boundary layers with a parabolically changing thickness and monotically rising profiles of no particular novelty. Corresponding confirmatory experiments have been carried out by Branover & Gelfgat (1968).

Hunt (1965) obtained a solution for case with insulating ends and an arbitrary conducting side-wall. It follows from his results that conductivity of side wall does not significantly change the profile of side layer. The case with insulating ends and a perfect side has a special practical interest in MHD devices. It was investigated by Grinberg (1961, 1962) as well. For corresponding experiments see Baylis (1964) and Alty (1971).

3.4 Stability

Branover & Tsinober (1970) reported (with a reference to Lock 1955) the onset of linear instability of Hartmann layer at a very high Reynolds number $Re_\delta^{cr}\approx 5\times10^4$ based on the layer's height. It coincides with the results of Priede (private communication). However, the experimental results summarized by Branover & Tsinober reveal instability and transition to turbulence at much lower (in 200 times) Reynolds numbers. Experimental investigations on the stability of flow within rectangular ducts yielded a laminar flow for Re<130Ha and a turbulent one at Re>215Ha (Branover and Tsinober 1970). Their conclusions were based on the

experimental data with Reynolds number below some 2×10^4. The numerical investigations by Grants (1997) showed that an imposed strong steady field allowed to obtain a stable rotating flow with $\mathrm{Re}=O(\mathrm{Ha}^{3/2})$, $(O(\mathrm{Re})\leq10^4)$.

4. Review on hydrodynamic boundary layers in rotating flows

We saw in §2 that the core of RMF alone driven flow tended to solid body rotation. Its angular and radial velocities couple via the force balance in the core. On the other hand, steady values of these characteristics are coupled via the steady solution of the boundary layer problem (e.g., Bödewadt's solution for a vessel in rest). Contrary to the imposed steady magnetic field, which interferes the force balance in the bulk, the imposed rotation modifies the boundary conditions of the boundary layer problem. The condition of force balance in the core requires a fixed product of core angular and radial velocities. Thus, one can be expressed from another, yielding famous, the so-called, one-disk problem (Priede 1993, 1994). It deals with a steady self-similar flow uniformly rotating in infinity above a differently rotating laterally unbounded disk. This problem was examined by different methods starting with rigorous provements of existence and uniqueness and ending with numerical solutions. Some indicative particular cases of this flow are:

(i) Von Kármán (1921) flow due to the rotating disk in the resting liquid solved by Cohran (1934);

(ii) Bödewadt (1940) flow due to rotating liquid over the disk in rest;

(iii) Ekman flow due to almost equally rotating disk and fluid (Rogers and Lance 1960). The only parameter determining the flow traditionally is velocity ratio $s=\Omega_f/\Omega_d$ or $\sigma=\Omega_d/\Omega_f$, where Ω_d and Ω_f are angular velocities of disk and liquid bulk, respectively. Thus, $s=0$, $\sigma=0$ and $s\to1$ correspond to von Kármán, Bödewat and Ekman boundary layers, respectively.

4.1 One disk problem

Consider an unbounded flow uniformly rotating with angular velocity Ω_f above the disk rotating with angular velocity Ω_d. According to von Kármán similarity principle, the velocity field compounds are given by

$$\mathrm{v}_r = r\Omega f'(x), \qquad \mathrm{v}_\theta = r\Omega g(x), \qquad \mathrm{v}_z = -2(\nu\Omega)^{1/2} f(x), \tag{15}$$

where $x=z(\Omega/\nu)^{1/2}$, but Ω is a characteristic angular velocity, e.g., Ω_d. Then the incompressible, laminar stationary Navier-Stokes equations take the following form (Zandbergen & Dijkstra 1987):

$$f''' + 2ff'' = f'^2 + s^2 - g^2, \tag{16}$$

$$g'' + 2fg' = 2f'g, \tag{17}$$

with boundary conditions

$$f=f'=0,\ g=1,\ x=0 \qquad \text{and} \qquad f'\to0,\ g\to s,\ x\to\infty \tag{18}$$

4.2 Existence and uniqueness

The existence of a solution for $s=0$ has been proved by McLeod (1969). The solution has monotone angular and axial velocity, in agreement with the Cohran's

(1934) numerical solution. A more general class of equations was considered by Lan (1971). His proof of the existence for $s=0$ was different from that of McLeod.

McLeod (1971) proved the theorem that guaranteed the existence of a solution for $s\geq 0$. Uniqueness of the solution considered, which has the fixed sign of angular velocity, has not been proved, although the numerical results hint to this. A direct consequence of the McLeods theorem is the uniqueness of trivial solution for $s=1$ and the absence of solution for $s=-1$. Besides, solution does not exist in a certain range of negative s (Evans 1969). An important rigorous result concerns the asymptotic behavior at infinity. McLeod (1969) showed that the solution must have a specific asymptotic behavior as the distance to the disk grows.

4.3 Expansions

Traditionally the solution is expressed in power series in the vicinity of the disk and "sewed" with an asymptotic solution at infinity (e.g., Schlihting 1979). Rogers and Lance (1960) linearized the solution about the state at infinity. The obtained expression of the asymptotic solution essentially depends on three real parameters, namely, axial velocity at infinity and a complex constant.

Another method of expansion is to linearize the flow over the full range of x about the state of almost solid rotation. It produces power series in powers of $s-1$. The first term of the expansion (Rogers & Lance 1960) describes the so-called Ekman layer of, probably, the most practical importance in our problem:

$$g_1=\cos x e^{-x},\quad f_1=0.5(1-(\sin x+\cos x)e^{-x})). \tag{19}$$

In an axially bounded volume the relative (to the axial lenghtscale L) thickness of this layer is $O(\mathrm{E}^{1/2})$, where $\mathrm{E}=\nu/(|\Omega_d|L^2)$ is the Ekman number. Since the trivial solution is $f_0=0$ for $s=1$, the sign of axial velocity depends on the sign of $(s-1)$ i.e., the sign of differential rotation of the disk. An estimate of the radius of convergence of expansion yields a singularity developing at $s=-0.16$ (Zandbergen & Dijkstra 1987 with a reference to van Hulzen 1980).

Priede (1993, 1994) has solved the problem expanding the solution in a form of double sum of complex exponentials. Substituting in the equations he received a recurrence formula expressing all coefficients from three real parameters, namely axial velocity at infinity and a complex constant that is the first non-diagonal coefficient of angular velocity expansion. These parameters were found as the root of a set of three non-linear equations expressing the boundary conditions on the disk (18).

4.4 Numerical solutions

Traditionally the numerical solution is obtained by shooting technique from or towards the disk (Rogers & Lance 1960, Evans 1969). Besides, finite difference technique and asymptotic behavior to reduce x-range has been employed as referred by Zandbergen and Dijkstra (1987). Numerical solution disappears at $s=-0.161$. Zandbergen and Dijkstra (1977) designed a special method to clarify the solution as s approaches a critical value from above and obtained two branches. The second branch merges to the first one at $s^{cr}=-0.16054$ and continues up to $s=0.0745$, where a third branch appears. In a subsequent paper Dijkstra & Zandbergen (1978) showed an infinity of the solution branches oscillating around $s=0$. These branches are marked by the occurrence of basic inviscid solutions or a chain of such solutions.

4.5 Unsteady solutions and stability

There may be several types of instabilities depending on the type of perturbation. The first is an instability of basic similarity solution against truly 3D perturbations. The second is an instability with respect to self-similar perturbations. It implies an assumption that an unsteady flow is constrained to (15). Another type of instability may appear due to an unstable force balance in the bulk of liquid. The flow due to a rotating magnetic field in a rotating vessel provides an example of such instability. The closure of meridional flow at infinity (i.e. core) provides the Coriolis force balancing the magnetic one. Let us consider a quasi-solid perturbation virtually increasing the core angular velocity. The instability takes place if the Coriolis force increases too, giving rise to further growth of perturbation. Such instability is first considered by Priede (1993, 1994). He examined the dependence between steady core radial and angular velocities instead of dynamic terms. Notice that different types of instability stand in certain "hierarchy". It worth nothing to investigate 3D instability if the solution is unstable with respect to the self-similar or even "quasi-solid" core perturbation.

An unsteady selfsimilar flow was investigated numerically by Bodonyi (1978). He recovered a limit-cycle character of unsteady solution at $\sigma=-0.1$, but beyond $\sigma=-0.15$ the calculation diverged. Bodonyi & Ng (1984) considered the stability problem for $\sigma<0$. They obtained a continuum spectrum of stable modes and a discrete spectrum rising the instability of Bödewadt type solution below the critical value $\sigma^{cr}=-0.03$. Besides, they concluded all higher branches near $s=0$ to be linearly unstable.

3D instabilities of rotating boundary layers were being studied both theoretically and experimentally during several decades. The review of these studies as well as recent investigations recovering the absolute instability are presented by Lingwood (1995, 1996, 1997). An inviscid crossflow instability of the Ekman flow occurs at $\mathrm{Re}_\delta=125$ observed experimentally by Faller (1963). It agrees closely with Lilly's (1966) and Lingwood's (1997) calculations that yields $\mathrm{Re}_\delta=115$ and 116, correspondingly. The flow has a second unstable mode that is stable in inviscid limit and has a lower critical Reynolds number $\mathrm{Re}_\delta=56$ (Lilly 1966, Melander 1983). The Reynolds number is defined here as $\mathrm{Re}_\delta=\Delta v_\theta l/\nu$; Δv_θ is local differential azimuthal velocity, l is characteristic boundary layer thickness $l=(\nu/\Omega_d)^{1/2}$. Lingwood (1997) concluded the absolute instability occurring at a higher Reynolds number $\mathrm{Re}_\delta=198$ to be far more dangerous and responsible for the transition to turbulence. Her theoretical results agree with an experimentally observed transition at $\mathrm{Re}_\delta\approx200$ (Faller and Keylor 1966, Owen, Pincombe & Rogers 1985).

The Bödewadt type layer occurs in the original flow with the vessel in rest. Lingwood (1997) calculated the onset of absolute instability of the Bödewadt flow at $\mathrm{Re}_\delta=21.6$, which agrees with the experimental results by Savas (1987). He determined the critical local Reynolds number to be about 25.

According to Lingwood's (1997) calculations, the imposed counter-rotation has a more stabilizing action on horizontal layers than co-rotation does.

4.6 Side layer at almost rigid rotation

Stewartson (1957) investigated the flow in a rotating cylinder driven by small differential rotation of the side wall. The problem is similar to our case. A constant over the height angular velocity distribution appears. Stewartson found out that the main flow fitted simple exponential boundary layer of $O(\mathrm{E}^{1/4})$ thickness near the side

wall, at which the meridional flow had discontinuity smoothed out by a more complicated inner $O(E^{1/3})$ layer. It led to correction of $O(E^{1/6})$ for the angular velocity.

A variety of vertical layers appear in a more complicated geometry. Stewartson (1966) investigated an almost rigid flow in a volume between two concentric rotating spheres and found two more types of vertical layers of $O(E^{2/5})$ and $O(E^{2/7})$ thickness.

4.7 Reviews on von Kármán swirling flows

Reviews on certain aspects of the problem under consideration are given by McLeod (1975), Parter (1982), van Wijngaarden (1985), Langlois (1985), Brady & Durlofsky (1986), Zandbergen and Dijkstra (1987), Lingwood (1997)

5. Conclusions and tasks for the current investigation

This chapter presents a review on the azimuthal body force driven swirling flow as well as on related rotating and magnetohydrodynamic boundary layers. This wide scope was truncated to fit practical aspects in the crystal growth technologies, where controllable axially symmetric and stable flows are needed. It is well-known that the azimuthal body force, e.g., due to a rotating magnetic field induces a swirling-recirculating flow. Its characteristics are greatly controlled by the boundary layers of different type occurring on both the flat endwalls and curved sidewall. As follows from various contributions, the rotating magnetic field driven flow has a number of advantages. However, sole rotating field does not provide enough options to guide the flow. Besides, a certain stabilizing action of RMF on a buoyancy driven flow is limited by different instabilities of the swirling flow itself. So, additional control tools are needed. In this chapter I refer to the investigations showing how similar flows are controlled by magnetohydrodynamic or rotating boundary layers.

It can be concluded that the action of a strong steady magnetic field is similar to the one due to rapid imposed rotation. Such rapid rotation of the vessel results in an almost rigid flow with $O(E^{1/2})$ Ekman layers and $O(E^{1/4})$ Stewartson layer on the endwalls and sidewall, respectively. Comparing to magnetohydrodynamic layers one can see the Hartmann number corresponding to an inverse Ekman number to the one half power.

Certain differences arise due to different ways how both imposed tools handle the core velocity. So, the steady magnetic field determines the core velocity via induced currents making the electric properties of rigid boundaries of primary importance. Notice that even a relatively small conductivity of semiconductor crystals may play an important role. SMF induced currents provide a magnetic transport mechanism smoothening the velocity profile. If endwalls are conducting, then a part of RMF produced angular momentum is delivered to them magnetically. In case of insulating ends, the whole produced momentum is carried away by the shear exactly in the way, which takes place in case of imposed rotation. Thus, we can expect similar characteristic angular velocity scalings both in a flow under a strong SMF with insulating walls and in an almost rigidly rotating flow.

Another essential difference takes place in the side layer, where MHD flow has the angular velocity drop in the axial direction, which leads to another source of meridional recirculation. The side layer of almost rigidly rotating flow, in its turn, has a constant along the height angular velocity profile and a more complicated inner layer. Contrary to the rotating flow, MHD sidelayer may have its own velocity scale.

Both imposed tools are expected to have stabilizing action. However, only the results for stability of rotating horizontal layers on the endwalls can be directly applied in our case. Summarizing the above, a possibility to control characteristics of the mean flow as well as to increase its stability by the considered control tools can be expected. However, a number of questions remain unclear. Let us enumerate main of them as a body of tasks for the present thesis paper. They fall into three groups depending on the type of flow they concern:

(i) Sole rotating magnetic field driven flow
   1) Effect of vessel's length on the thickness of steady side layer;
   2) Connection to related side layer stability problems;
   3) Limits to shear dominated and turbulent flows;
   4) Comparison to experiment in the range of moderate Reynolds numbers.

(ii) Rotating and steady axial magnetic field driven flow
   1) Role of driving force distribution at a strong SMF;
   2) Boundary layer solution near curved side wall;
   3) Meridional flow in the side layer;
   4) Stability of flow at a strong SMF;
   5) Comparison to experiment in order to:
      a) verify theoretical results;
      b) find the limit of laminar numerical model.

(iii) Rotating magnetic field driven flow in a rotating cylinder
   1) Numerical verifying of the results of similarity solution:
      a) meridional velocity direction change;
      b) control of characteristic velocities;
      c) multiple solutions;
   2) Numerical investigation of the flow in the range of absent similarity solution;
   3) Role of force distribution at almost rigid rotation;
   4) Side layer solution for almost rigid rotation;
   5) Stability of force balance in the core;

Besides the answers to these questions, I set a task to summarize the results on flows of the mentioned types from the point of view of practical application in crystal growth.

REFERENCES

Abricka, M., Gelfgat, Y. M. and Krumins, J. 1996 *Magnetohydrodynamics* 32

Abritcka, M., Gelfgat, Y. M. and Krumins, J. 1995 *Latvian J. Phys. and Tech. Sci.* 6, pp. 16–27 (in Russian)

Abritcka, M., Gelfgat, Y. M. and Krumins, J. 1997 *J. Cryst. Growth* 180, 388–400

Alty, C. J. N. 1971 *JFM* 48, 429

Barz, R. U., Gerbeth, G., Wunderwald, U., Buhrig, E., Gelfgat, Y. M. 1997 *J. Crystal Growth* 180, #3/4, 410

Baylis, J. A. 1964 *Nature* 204, 563

Bödewadt, U. T. 1940 *Die Drehströmung über festem Grunde. ZAMM* 20, 241–53

Bodonyi, R. J. & Ng, B. S. 1984 *JFM* 144, 311–28

Bodonyi, R. J. 1978 *Q. J. Mech. Appl. Math.* 31, 461–72

Brady, J. F. & Durlofsky, L. 1987 *JFM* 175, 363–394

Branover, G. G. and Gelfgat Y. M. 1968 *Izv. Akad. Nauk SSSR Mekh. Zhidk. Gaza* 1, 79

Branover, H. & Tsinober A. B. 1970 *Magnetohydrodynamics of incompressible media*, Nauka, Moscow (in Russian)
Chang, C. C. and Lundgren, T. S. 1961 *Z. angew. Math. Mech.* 12, 100–14.
Cochran, W. G. 1934 *Proc. Camb. Phil. Soc.* 30, 365–75
Cole, J. A. 1976 *JFM* 75, 1, pp. 1–15
Davidson, P. A. 1989 *JFM* 209, 35–55
Davidson, P. A. 1992 *JFM* 245, 669–699
Davidson, P. A. and Hunt, J. C. R. 1987 *JFM* 185, 67–106
Dijkstra, D., Zandbergen, P. J. 1978 *Arch. Mech. Stosow.* 30, 411
Dold, P. & Benz, K. W. 1995 *Cryst. Res. Technol.* 30, 1135–1145
Euteneuer, G. A. 1972 *Acta Mech.* 13, 215
Evans, D. J. 1969 *Q. J. Mech. Appl. Math.* 22, 467–85
Faller, A. J. 1963 *JFM* 15, 560–576
Faller, A. J. and Keylor, R. E. 1966 *J. Atmos. Sci.* 23, 466–480
Gelfgat Y. M. and Gorbunov, L. A. 1994 In: *Proc. on 2nd Int. Conf. on Energy transfer in MHD flows.* Vol. 1, pp. 1-14. Aussois, France.
Gelfgat, Yu. M. and Priede, J. 1995, *Magnetohydrodynamics* 32
Gelfgat, Yu. M. and Priede, J. 1996, *Magnetohydrodynamics* 33
Gelfgat, Yu. M., Priede, J., Sorkin, M. Z. 1991 *Proceed. on Int. Conf. on Energy Transf. in MHD Flows*, France, pp. 181–186.
Grants, I. 1997 In: *Proc. on 3rd Int. Conf. on Energy Transfer in MHD Flows.* Vol. 2, p. 409. Aussois, France.
Grants, I., Priede J., Gelfgat Y. M. *1996 Magnetohydrodynamics* 33
Greenspan, H. P. 1968 *The Theory of Rotating Fluids*. Cambridge University Press.
Greenspan, H. P. and Howard, L. N. 1963 *JFM* 17, 385
Grinberg, G. A. 1961 *Appl. Math. & Mech (PMM)* 25, 1536
Grinberg, G. A. 1962 *Appl. Math. & Mech (PMM)* 26, 106
Hartmann, J. 1937 Hg-Dynamics. I, Theory of the laminar flow of an ellectrically conductive liquid in a homogenous magnetic field, *Det. Kgl Danske Videnskab. Selskab. (Math.-fys. Medd.)* 15, 6
Hunt, J. C. R. 1965. *JFM* 21, 4, 577
Hunt, J. C. R. and Shercliff, J. A. 1971. *Ann. Rew. Fluid Mech.*, 3, 37
Hunt, J. C. R. and Stewartson, K. 1965. *JFM* 23, 3, 563
Lan, C. C. 1971 *Arch. Ration Mech. Anal.* 42, 24–39
Langlois, W. E. 1985 *Ann. Rev. Fluid Mech.* 17, 191–215.
Lilly, D. K. 1966 *J. Atmos. Sci.* 23, 481–494
Lingwood, R. J. 1995 *JFM* 299, 17–33
Lingwood, R. J. 1996 *JFM* 314, 373–405
Lingwood, R. J. 1997 *JFM* 331, 405–428
Lock, R. C. 1955 *Proc. Roy. Soc., London,* A233, 105.
Mathis, D. M. and Neitzel, G. P. 1985 *Phys. Fluids* 28, 2, 449–454
McLeod, J. B. 1969 *Arch. Ration. Mech. Anal.* 33, 91–102
McLeod, J. B. 1971 *Proc. R. Soc. London Ser. A* 324, 391–414
McLeod, J. B. 1975 *Lecture Notes in Mathematics*, 448, pp.242–55 Berlin: Springer-Verlag
Melander, M. V. 1983 *JFM* 132–293
Moffat, H. K. 1965 *JFM* 22, 521–528 (Corrigendum 1973 *JFM* 58, 823)
Neitzel, G. P. 1982 *Phys. Fluids* 25, 226
Owen, J. M., Pincombe, J. R., Rogers, R. H. 1985 JFM 155, 233–265.
Parter, S. V. 1982 *Lecture Notes in Mathematics*, 942, pp. 258-80 Berlin: Springer-Verlag
Priede, J. 1993 *Theoretical study of a flow in an axisymmetric cavity of finite length, driven by a rotating magnetic field.* Thesis, Salaspils
Priede, J. 1994 In: *Proc. on 2nd Int. Conf. on Energy Transfer in MHD Flows.* Vol. 1, pp. 87–97, Ausois, France

Richardson, A. T. 1974. *JFM* 63, 593
Robinson, T. 1973 *JFM* 60, 641–664
Rogers, M. H. & Lance, G. N. 1960 *JFM* 7, 617–31
Savas, Ö. 1987 *JFM* 183, 77–94
Shercliff, J. A. 1953. *Proc. Camb. Phil. Soc.* 49, 136
Shercliff, J. A. 1956 *JFM* 1, 644
Shlicting, H. 1979 *Boundary Layer Theory*, 7th edn. McGraw-Hill.
Short, D. J. and Davidson, P. A. 1994 In: *Proc. on 2nd Int. Conf. on Energy transfer in MHD flows.* Vol. 2, 729. Aussois, France.
Sneyd, A. J. 1971 *JFM* 49, 817
Sterl, A. 1990 *JFM* 216, 161
Stewartson, K. 1957 *JFM* 3, 17
Stewartson, K. 1966 *JFM* 26, 131–144
Tillmann, W. 1967 *Phys. Fluids Supl.* 10, 108
Trombetta, P., Marty, P., Martin Witkowski, L. and Tomasino, T. 1997 In: *Proc. on 3rd Int. Conf. on Energy Transfer in MHD Flows.* Vol. 2, p. 463. Aussois, France.
Uflyand, Y. S. 1961 *Sov. Phys.* 5, 1194
Ungarish, M. 1997 *JFM* 347, 105
Van Hulzen, J. A. 1980 *Sigsam Bull. ACM* 14, pp. 36–49.
Van Wijngaarden, L. 1985. *Fluid Dyn. Trans.* 12, 157–79
Volz, M. P. and Mazurk, K. 1996 *Exp. in Fluids* 20, 454
Von Kármán, T. 1921 *ZAMM* 1, 233–52
Walker, J. S. 1985 Laminar duct flows in a strong magnetic fields. In *Liquid metal Flows and Magnetohydrodynamics,* vol 2 (ed. H. Branover, P. S. Lykoudis & M. Moon), pp. 3–16. American Institute of Aeronautics and Astronautics, New York.
Williams, W. E. 1963 *JFM* 16, 2, 262
Zandbergen, P. J. and Dijkstra, D. 1977 *J. Eng. Math.* 11, 167
Zandbergen, P. J. and Dijkstra, D. 1987 *Ann. Rev. Fluid Mech.* 19, 465–91

Chapter II

Stability of a swirling flow driven by a rotating magnetic field

In this chapter, stability of swirling flow driven by a rotating magnetic field is investigated. The magnetic field is assumed to be weak and rotating at low frequency. First, it is shown by using various approaches that the self-similar solution is stable. Second, Taylor–Götler instability occurring at the side wall is investigated numerically. Onset of the instability is found to be determined by the Reynolds number based on the height of cylindrical vessel. This holds also for strongly elongated vessels. Stability criterion based on the thickness of the side boundary layer is close to that for the corresponding Taylor–Couette instability. Three dimensional instability in the Bödewadt boundary layers at the end walls is expected to set in first for vessels with radius to height ratio < 3.

1. Introduction

Rotating magnetic field (RMF) represents a powerful tool to control the flow of semiconductor melt in various crystal growth processes enabling production of crystals of improved quality (Priede 1993, Gelfgat & Priede 1995). The requirements to the melt flow are often contradicting. On the one hand, the flow is to be strong enough to sustain sufficient stirring necessary for homogeneity of the melt. On the other hand, strong mixing can cause undesirable flow instabilities and even turbulence. In order to ensure an optimal control, it is of primary importance to know under what conditions the flow may become unstable and what kind of instabilities can occur. It is the aim of the present chapter to investigate the stability of flow driven by a rotating magnetic field.

It is well known that behavior of the flow can crucially change with its characteristic velocity depending on the strength of the driving force. So initially steady flow can turn into oscillating one when forcing by rotating magnetic field exceeds certain critical threshold (Gelfgat, Priede & Sorkin 1991). At the same time, the RMF caused oscillations turned out to be less intense than those due to buoyancy (Dold & Benz 1995, Fischer *et al.* 1997).

Flow driven by RMF is similar to the well-studied spin-down flow occurring when rotating container with liquid is suddenly stopped. In this case, Taylor–Götler instability occurs at the side wall when momentum boundary layer there reaches a certain critical thickness defined according to so-called Götler criterion (Tillmann 1967) by $G_\theta=\mathrm{Re}_R(\delta_t/R_0)^{3/2}\approx 6$, where Re_R is the Reynolds number based on the radius of vessel R_0, but δ_t is the thickness of momentum boundary layer. This stability criterion has been confirmed by experiment of Mathis & Neitzel (1985) carried out in the vessel of aspect ratio $L/R_0=18.7$. The results of this experimental are in a good agreement with the findings of Euteneuer (1972) for vessel of aspect ratio $L/R_0=4$. The effect of end walls seems to be insignificant for the above mentioned range of aspect

ratios. However, the onset took place only at Re_R>351 while the theoretical limit of global stability in flow at spin-down was Re_R=141 (Neitzel 1982).

The stability of RMF driven flow in an infinite cylinder was first theoretically investigated by Richardson (1974). A critical Reynolds number Re_R=140 (based on maximum azimuthal velocity) following from his results is close to the global stability limit found by Neitzel. According to Greenspan & Howard (1963), a swirling spin-up flow is dominated by viscosity if $L/R_0>4Re^{1/2}$. So, Robinson's results are expected to be applicable for aspect ratios L/R_0>50. A numerical simulation of RMF-driven flow (Gelfgat *et al.* 1991, Priede 1993, Barz *et al.* 1997) demonstrated that reduction of height of the vessel increases the stability of axisymmetric disturbances. This is in a qualitative agreement with Götler's criterion: the shorter the vessel, the stronger meridional flow, and respectively, the thinner the boundary layer at the side wall. So far, most investigators have used critical forcing to define instability threshold. However, this choice is not very advantageous since the critical parameter directly related to the forcing involves the linear size to the forth power and thus it strongly depends on the aspect ratio. In the present study, it was found that a numerical 2D solution loses its stability at a fixed Reynolds number based on maximum azimuthal velocity V and vessel's length $Re=VL/\nu\approx2300$ in a wide range of aspect ratios $1<L/R_0<10$. To link this parameter to forcing, the characteristic velocity of a steady flow was determined as a function of aspect ratio (§4). The extrapolation of our numerical results intersect with Richardson's result for infinite cylinder at aspect ratio $L/R_0\approx16$.

Stabilizing action of RMF on the liquid heated from the below was experimentally investigated by Volz & Mazurk (1996). They observed that at certain critical forcing the flow became unstable even without any imposed heating. The critical value following from their results for the aspect ratio $(L/R_0)\approx2$ agrees well with the corresponding one numerically found by Barz *et al.* (1997).

Boundary layers at the end walls might be unstable with respect to 3D disturbances when the local Reynolds number $Re_\delta= v_\theta\delta^*/\nu$ based on the characteristic thickness of the boundary layer $\delta^*=(\nu/\Omega)^{1/2}$ exceeds same critical threshold. Such instabilities have been analyzed by Lingwood (1997) who predicted an absolute instability of a Bödewadt boundary layer at Re_δ=21.6. This is in a good agreement with experimental results of Savas (1987) who found the critical Reynolds number $Re_\delta\approx25$. Comparing this value to that of side layer instability, it follows that the 3D instability at end walls sets in first for aspect ratio $L/R_0 < 3$.

Strong enough forcing can lead to the development of turbulent flow considered by Davidson (1992) who obtained a "5/9"-law for angular velocity of such a flow. This prediction was shown to be in a good agreement with experimental results of Robinson (1973) for a wide range of applied forcing. Comparison of our numerical results with Davidson's prediction and recent experimental results reveals that a laminar model may be valid surprisingly far beyond the onset of instability.

This chapter is organized as follows. Section 2 introduces the governing equations. The stability of self-similar solution is discussed in §3. Section 4 presents the results of numerical 2D investigation of base flow and its stability. Section 5 proceeds with the discussion of the results.

2. Problem definition

Consider a uniform magnetic field $\mathbf{B}_0$ rotating at low frequency in a plane perpendicular to the axis of vessel filled with a conducting liquid. The electric currents induced by RMF interacting with this field produce a purely azimuthal body force. If the end walls of the vessel are well conducting, which is assumed to be the case here, the produced driving force is the same as that in infinite cylinder $F_\theta=0.5r\sigma\omega_0 B_0^2$. In addition, the induction of rotating field is assumed to be small so that its effect on the instability threshold may be neglected. After choosing height of the vessel L and viscous diffusion time $\tau = L^2/\nu$ as characteristic length and time scales, respectively, Navier–Stokes equation leads to the following set of dimensionless equations governing an axisymmetric flow driven by RMF:

$$\frac{\partial\Omega}{\partial t}+\mathrm{H}\frac{\partial\Omega}{\partial z}+\frac{r}{2}\left(\frac{\partial \mathrm{H}}{\partial r}\frac{\partial\Omega}{\partial z}-\frac{\partial \mathrm{H}}{\partial z}\frac{\partial\Omega}{\partial r}\right)-\frac{\partial \mathrm{H}}{\partial z}\Omega=\frac{\partial^2\Omega}{\partial r^2}+\frac{3}{r}\frac{\partial\Omega}{\partial r}+\frac{\partial^2\Omega}{\partial z^2}+\mathrm{T}, \tag{1}$$

$$\frac{\partial \mathrm{W}}{\partial t}+\mathrm{H}\frac{\partial \mathrm{W}}{\partial z}+\frac{r}{2}\left(\frac{\partial \mathrm{H}}{\partial r}\frac{\partial \mathrm{W}}{\partial z}-\frac{\partial \mathrm{H}}{\partial z}\frac{\partial \mathrm{W}}{\partial r}\right)-\frac{\partial\Omega^2}{\partial z}=\frac{\partial^2 \mathrm{W}}{\partial r^2}+\frac{3}{r}\frac{\partial \mathrm{W}}{\partial r}+\frac{\partial^2 \mathrm{W}}{\partial z^2}, \tag{2}$$

$$\frac{\partial^2 \mathrm{H}}{\partial r^2}+\frac{3}{r}\frac{\partial \mathrm{H}}{\partial r}+\frac{\partial^2 \mathrm{H}}{\partial z^2}+2\mathrm{W}=0, \tag{3}$$

where velocity components of the flow are expressed as follows:

$$v_\theta=r\Omega, \qquad v_z=\mathrm{H}+0.5r\partial \mathrm{H}/\partial r, \qquad v_r=-0.5\partial \mathrm{H}/\partial z; \tag{4}$$

$\psi=0.5r^2\mathrm{H}$ is the meridional stream function, $w=r\mathrm{W}$ is the corresponding vorticity. Taylor number $\mathrm{T}=(\Omega_f L^2/\nu)^2$ characterizes magnitude of the forcing, where $\Omega_f=(0.5\sigma\omega_0/\rho)^{1/2}B_0$ (cf., Davidson 1992). The introduced variables are closely related to the von Kármán similarity ones for a self-similar swirling flow in radially unbounded plane layer. In this case, functions Ω, H and W are invariant in the radial direction and the above equations take the following simple form

$$\frac{\partial\Omega}{\partial t}+\mathrm{H}\Omega'-\mathrm{H}'\Omega=\Omega''+\mathrm{T} \tag{5}$$

$$\frac{\partial \mathrm{H}''}{\partial t}+\mathrm{H}\mathrm{H}'''+2(\Omega^2)'=\mathrm{H}^{(4)} \tag{6}$$

3. Stability of self-similar flow

Before turning to the full stability problem, it is instructive to consider first its self-similar approximation. Results obtained on such very simplified model can give useful insight into much complicated solution of the whole problem.

The stability of self-similar flow with respect to self-similar disturbances was investigated by making use of Galerkin's spectral method. Gradual increase of the number of base functions up to 120 resulted in the sharply increasing critical Taylor number. So no actual instability of the self-similar flow was found. This agrees with the conclusion of Bodonyi & Ng (1984) about the stability of Bödewadt boundary layer with respect to self-similar perturbations.

Such a self-similar stability of the core region of the flow, where magnetic driving force is balanced by Coriolis force, can be proven by the following energetic arguments. Consider a small self-similar perturbation $g(z,t)$ and $h(z,t)$ of the core region rotating with a uniform angular velocity $\Omega_0(z)=\beta T^{2/3}$ in the presence of meridional recirculation with vertical velocity $H_0(z)=-\beta^{-1}T^{1/3}z$ ($\beta=0.516$), (Davidson 1992, Ungarish 1997). Substituting perturbed solution sought as $\Omega(z,t)=\beta T^{2/3}(1+g(z)\exp(\sigma t))$, $H(z,t)=\beta^{-1}T^{1/3}(-z+h(z)\exp(\sigma t))$ into Eqs. (5) and (6), we obtain the following eigenvalue problem defining the temporal growth rate σ:

$$\sigma g = g'' + \beta^{-1}T^{2/3}\left(zg' + h' - g\right) \tag{7}$$

$$\sigma h'' = h^{(4)} - 4\beta^3 T g' + \beta^{-1}T^{1/3} z h''' \tag{8}$$

Upon multiplying Eqs. (7) and (8) by $g(z)$ and $h(z)$, respectively, and then taking integral of booth equations over the depth of the layer and requiring the perturbations $g(z)$, $h(z)$ and $h'(z)$ to vanish at $z = \pm 1/2$ we obtain:

$$\int_{-0.5}^{0.5} gg''dz = -\int_{-0.5}^{0.5}(g')^2 dz < 0\,, \qquad \int_{-0.5}^{0.5} gg'zdz = -0.5\int_{-0.5}^{0.5} g^2 dz < 0$$

$$\int_{-0.5}^{0.5} hh^{(4)}dz = \int_{-0.5}^{0.5}(h'')^2 dz > 0\,, \qquad \int_{-0.5}^{0.5} hh'''zdz = -\int_{-0.5}^{0.5} hh''dz + 0.5\int_{-0.5}^{0.5}(h')^2 dz > 0$$

The sign of a remaining integral

$$\int_{-0.5}^{0.5} gh'dz = -\int_{-0.5}^{0.5} g'hdz = I$$

does not influence the sign of σ. Indeed, solving a set

$$\begin{aligned} \sigma &= -A + \beta^{-1}T^{1/3}I \\ \sigma &= -B - \beta^3 TI \end{aligned},$$

where A and B are definitely positive constants, we found $\sigma=-(A+B\beta^{-4}T^{-4/3})\times(1+\beta^{-4}T^{-4/3})^{-1}<0$ proving stability of the core flow against such self-similar perturbations. This conclusion is confirmed also by the numerical solution of Eqs. (5, 6) exhibiting only decaying oscillations at the spin-up of self-similar flow. Stability of the boundary layer flow over a disk at rest is also in agreement with numerical results of Bodonyi (1978).

4. Numerical results for axially symmetric flow

As originally noted by Moffat (1965), flow driven by RMF in cylindrical container close its side wall is similar to Cuette–Taylor flow between two coaxial differentially rotating cylinders when the outer one is kept at rest. Such a flow is prone to a Taylor–Görtler type instability. In order to investigate this instability, we performed numerical simulation of axisymmetric flow. We used the exponential finite difference scheme obtained by the control volume integral identity technique (Gelfgat *et al* 1991, Priede 1993). The integration over time was performed by the Peaceman-Rachford

alternating direction scheme. We refer to a corresponding code developed by J. Priede as *RTfield*. Besides, *FLUENT* package was used as an alternative method.

The Taylor number of forcing contains linear size to the fourth power. Therefore, the critical threshold significantly depends on the aspect ratio. In the current study we examined aspect ratios $R=R_0/L=0.125, 0.25, 0.5, 1$. Neither the height nor the radius used in T definition ensured invariance of the critical value T_c with respect to the aspect ratio. Instead of that noticed the numerical solution to lose its stability at a fixed Reynolds number based on the vessel height $\mathrm{Re}=VL/\nu=2300(\pm 10\%)$ (See, figure 1).

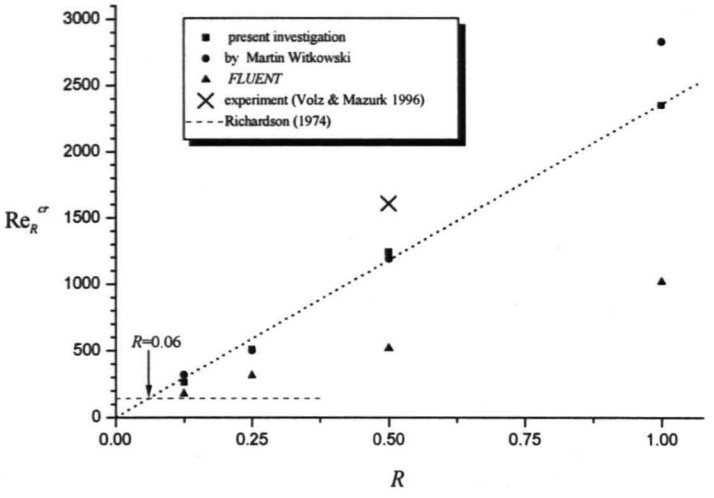

Figure 1 Critical Reynolds number (based on radius) depending on the aspect ratio R.

The instability appears as Taylor–Götler vortices slowly swept by the meridional flow from the mid-plane towards both end walls. The investigations by Martin Witkowski (private communication) confirmed these results. At the same time, a numerical solution by *FLUENT* becomes unstable at a much lower (though approximately constant) $\mathrm{Re}\approx 1000$. The comparison of critical Reynolds numbers from different studies is given in figure 1. The critical Reynolds number based on vessel's radius is used here to simplify comparison with Richardson's results for an infinite cylinder. The Reynolds number in experiment by Volz & Mazurk (1996) is deduced from the parameters of forcing.

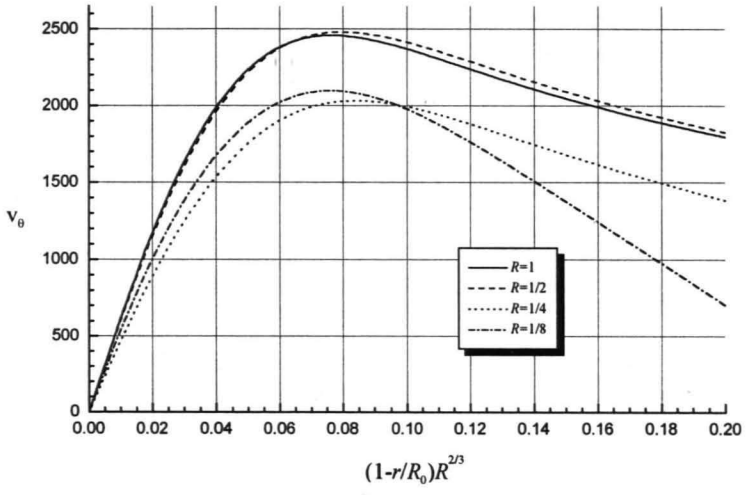

Figure 2. Radial profiles of azimuthal velocity near onset.

The obtained result (Re_R^{cr} = const R) agrees with that for Taylor–Cuette flow with the inner cylinder rotating, for which $\mathrm{Re}_R^{cr}(c/R_0)^{3/2} \approx 42$, (e.g., Cole 1976) if $R \sim (\delta^{cr}/R_0)^{-3/2}$ or $(\delta^{cr}/R_0) \sim R^{-2/3}$, where δ^{cr} is characteristic thickness of a critical side layer, but c is distance between cylinders. Figure 2 depicts radial profiles of the azimuthal velocity just below the stability threshold. One can see that maximum location does fit the expected scaling.

To link the critical Reynolds number with the corresponding forcing, we performed a numerical investigation of the characteristic velocity of the base flow depending on the aspect ratio. The characteristic angular velocity was found proportional to the square root of aspect ratio $R = R_0/L$. On the other hand, the dependence on the forcing matched a well-known "2/3"-law following from the similarity solution. At aspect ratio R=1 the numerical solution agreed with the self-similar one. Thus, the approximate expressions for the dimensionless core angular velocity

$$\Omega_0 = 0.52\mathrm{T}^{2/3}R^{1/2}, \tag{9}$$

and the Reynolds number

$$\mathrm{Re} = 0.52\mathrm{T}^{2/3}R^{3/2}, \tag{10}$$

were obtained. The numerical results are depicted in figure 3.

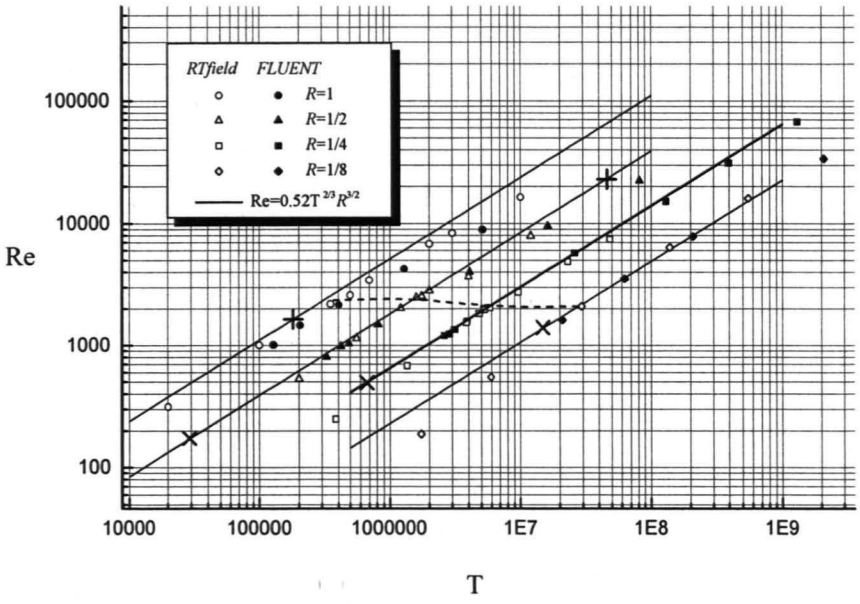

Figure 3. The Reynolds number of induced flow depending on forcing. Critical Reynolds numbers at different aspect ratios R depicted by dashed lines. Limits of viscosity controlled and turbulent flow are depicted by symbols × and +, respectively.

At R=1 expression (9) coincides with the self-similar solution for radially unbounded layer between parallel planes (Davidson 1992). Eq. (10) is not applicable for R >1 when a similarity solution $\mathrm{Re}=0.52\mathrm{T}^{2/3}R^{-1}$ seems to take place.

Figure 4 depicts the isolines of angular velocity and streamlines of meridional recirculation in vessels with aspect ratios R=1.0 and R=0.125. One can see that a spatially oscillating Bödewadt's type boundary layer is pushed by the side layer towards the axis together with eyes of meridional vortices.

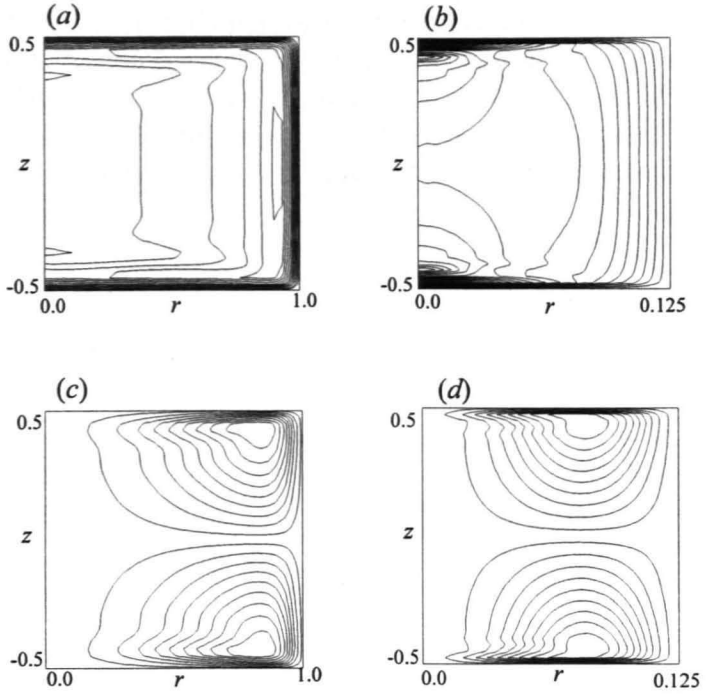

Figure 4. Isolines of angular velocity (a & b) and streamlines (c & d) of meridional flow near the onset of instability for aspect ratios R=1 (a & c) and R=1/8 (b & d).

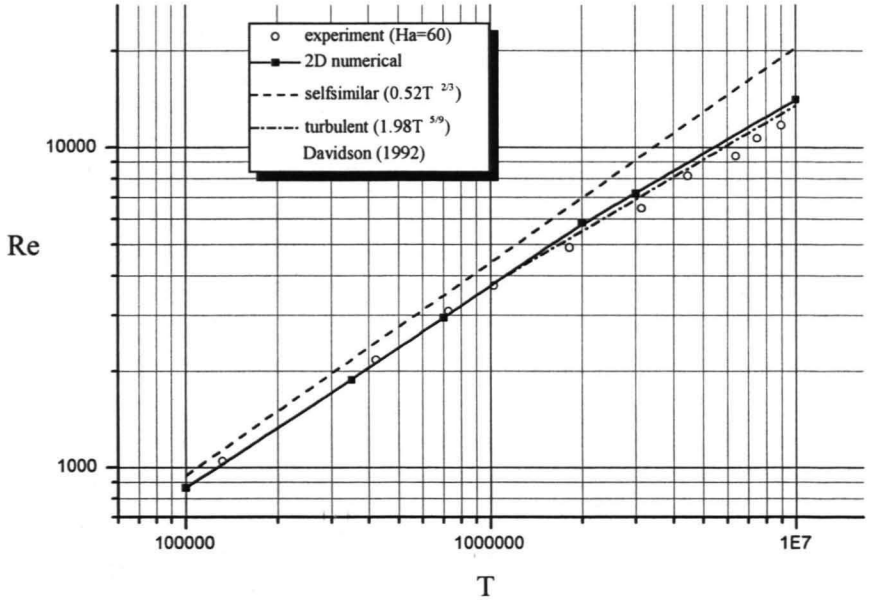

Figure 5. Reynolds number depending on forcing. Comparison of numerical and experimental results. R=1.

Let us estimate the range of applicability of Eq. (10). According to Richardson (1974), the Reynolds number of viscosity controlled flow is $\mathrm{Re}=0.048\mathrm{T}R^3$. A comparison to Eq. (10) yields a limiting value $\mathrm{T}=1300R^{-9/2}$, at which $\mathrm{Re}=62R^{-3/2}$. In order to assess the applicability limit due to turbulence, we compared Eq. (10) with an estimate found by Davidson (1992), according to which the Reynolds number of turbulent flow is $\mathrm{Re}=1.98\mathrm{T}^{5/9}R^{11/18}$. Both relations intersect at $\mathrm{T}=0.18\times10^6R^{-8}$ and $\mathrm{Re}=1645R^{-23/6}$. The limiting values are shown in figure 3.

We compared the Davidson's expression for tubulent flow with our numerical and recent experimental results (Grants 1998, ch. 3) in figure 5. Besides the characteristic velocity of turbulent flow, the laminar numerical model exhibited another feature of such flow as well. According to Davidson (1992), the swirl is reinforced near the axis of turbulent flow. The phenomenon manifested itself in our numerical simulation as shown in figure 6.

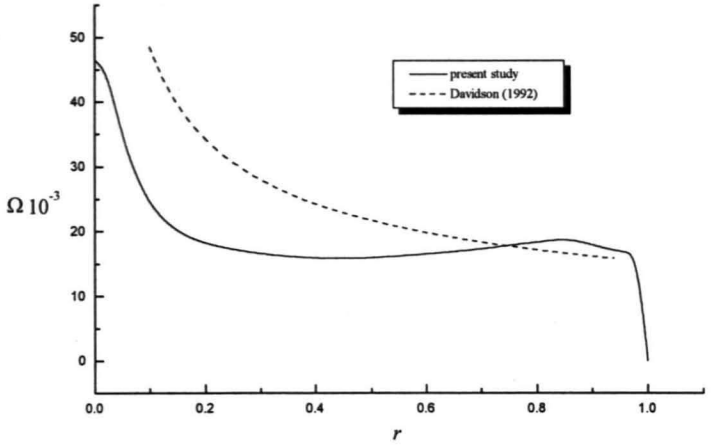

Figure 6. Radial profile of angular velocity at strong forcing $T=10^7$. Comparison of our numerical results to the profile for turbulent flow (Davidson 1992).

5. Summary and concluding remarks

This chapter concerns the stability of a liquid metal flow driven by a rotating magnetic field. The investigations by the Galerkin's spectral method as well as the numerical simulation and simple energetical estimates showed the stability of the core flow with respect to self-similar perturbations. A numerical 2D simulation revealed a Taylor-Götler type instability of the side layer at $\mathrm{Re}_T^{cr}=VR_0/\nu(\delta^{cr}/R_0)^{3/2}=46(\pm 10\%)$, which is close to the criterion for Taylor–Couette instability between rotating coaxial cylinders (for the inner cylinder rotating $\mathrm{Re}_T^{cr}\approx 42$. See, e.g. Cole 1976). The distance to the maximum in azimuthal velocity profile δ^{cr} corresponded to the distance between the cylinders. Our numerical simulation yielded $(\delta^{cr}/R_0)^{3/2}=0.02L/R_0$ for aspect ratios $1/8<R_0/L<1$. Hence, the onset occurs at a fixed Reynolds number based on the vessel's height $\mathrm{Re}^{cr}=VL/\nu=2300$ even in considerably elongated cylinders. The delay of the onset in comparison to a diffusion controlled flow $\mathrm{Re}_R^{cr}=140$ (Richardson 1974) is caused by meridional recirculation, that reduces the thickness of a steady side layer. Extrapolating our results beyond $R=1/8$ we deduced Richardson's analysis being valid for the aspect ratios R less than 1/16. It agrees with the conclusion of Martin Witkowski & Marty (1997) and Martin Witkowski (private communication). A numerical simulation with *FLUENT* yielded a significantly lower (though constant in a given range of aspect ratios) stability limit $\mathrm{Re}^{cr}=1000$. Critical Reynolds number $\mathrm{Re}^{cr}=3200$ deduced from the forcing parameters in experiment by Volz & Mazurk (1996) agrees better with the results obtained with our code. Grants (1998, ch. 3) investigated the stability of RMF driven flow in the presence of a steady axial field. An estimate $\mathrm{Re}^{cr}<1700$ was obtained for small steady field limit. However, the

observed instability could be due to 3D perturbation of a probe which was considerably larger than those used by Volz & Mazurk.

To link the critical Reynolds number with critical forcing, dependence of the base flow on the forcing was investigated close to the onset of instability. A characteristic velocity of the base flow was found to be $\mathrm{Re}\approx 0.52\mathrm{T}^{2/3}R^{3/2}$ leading to the critical Taylor number $\mathrm{T}^{cr}\approx 0.3\times 10^{6}R^{-9/4}$.

Experimental and theoretical investigations of 3D instability of a Bödewadt layer done by Savas (1987) and Lingwood (1997) led to the critical Reynolds number for local absolute instability $\mathrm{Re}_{\delta}^{cr}=v_{\theta}\delta^{*}/\nu=(\Omega/\nu)^{1/2}r^{cr}\approx 25$. Substituting the vessel's radius into this result, we find $\mathrm{Re}^{cr}=625R^{-1}$. The corresponding critical forcing is $\mathrm{T}^{cr}\approx 42\times 10^{3}R^{-15/4}$. The comparison of both critical values yields a simultaneous appearance of both instabilities at aspect ratio $R^{*}=0.27$. Below this value the instability appears first in the side layer. It should be noted that the critical forcing for 3D instability might be slightly overestimated for such an elongated cylinder, since the thickness of the side layer becomes considerable. The corner region, a part of the side layer adjacent to endwalls, has no spatially oscillating pattern and, therefore, is expected to be more stable.

It is interesting to note that the characteristic velocity supplied by the laminar model is surprisingly close the corresponding values resulting from the model of turbulent flow. So the numerical results for laminar flow agree well with experimental data (Grants 1998, ch. 3) even for Reynolds numbers $\mathrm{Re}=O(10^{4})$ which exceed the onset value at least four times. Besides, the reinforcing of swirl at the axis obtained by Davidson (1992) for turbulent flow reveals itself in our laminar numerical simulation as well.

In order to assess the range of applicability of the found relation for characteristic velocity of laminar flow, we compared it to the Davidson's formula. We obtained that for elongated cylinders ($R<0.25$) the latter holds only for very high Reynolds numbers. This suggests existence of an intermediate turbulent scaling.

The numerical simulation revealed that the relative thickness of the side layer considerably increases with a length of the vessel. As a result, the eyes of secondary recirculation move towards the axis. Location of these eyes may be important for crystal growth, since it determines the place where the influence of convection on heat transfer is inverted. It means that the heat flux through the solidification front is reduced or increased depending on whether the radius is smaller or larger than that of the eye. This heat flux determines the shape of the steady solidification interface (Grants & Gelfgat 1997). So, the aspect ratio of liquid zone can significantly influence the shape of solid-liquid interface.

REFERENCES

Barz, R. U., Gerbeth, G., Wunderwald, U., Buhrig, E., Gelfgat, Y. M. 1997 *J. Crystal Growth* 180, 410

Bodonyi, R. J. & Ng, B. S. 1984 *JFM* 144, 311-28

Bodonyi, R. J. 1978 *Q. J. Mech. Appl. Math.* 31, 461-72

Cole, J. A. 1976 *JFM* 75, 1

Davidson, P. A. 1992 *JFM* 245, 669-699

Dold, P. & Benz, K. W. 1995 *Cryst. Res. Technol.* 30, 1135

Euteneuer, G. A. 1972 *Acta Mech.* 13, 215

Fischer, B., Friedrich, J., Kupfer, C., Müller, G. and Vizman, D. 1997 In: *Proc. on 3rd Int. Conf. on Energy Transfer in MHD Flows.* Vol. 2, pp. 337-342. Aussois, France.
Gelfgat, Yu. M., Priede, J., Sorkin, M. Z. 1991 *Proceed. on Int. Conf. on Energy Transf. in MHD Flows*, France, pp. 181.
Gelfgat, Yu. M. and Priede, J. 1995, *Magnetohydrodynamics* 32
Grants, I. and Gelfgat, Y. M. 1997 In: *Proc. on 3rd Int. Conf. on Energy Transfer in MHD Flows.* Vol. 2, p. 351. Aussois, France.
Grants, I. 1998 *Magnetically driven swirling flow guided by steady magnetic field and imposed rotation.* Thesis, Salaspils, Latvia
Greenspan, H. P. and Howard, L. N. 1963 *JFM* 17, 385
Lingwood, R. J. 1997 *JFM* 331, 405
Martin Witkowski, L. and Marty, P. 1997 In: *Proc. on 3rd Int. Conf. on Energy Transfer in MHD Flows.* Vol. 2, pp. 357-362. Aussois, France.
Mathis, D. M. and Neitzel, G. P. 1985 *Phys. Fluids* 28, 2, 449
Moffat, H. K. 1965 *JFM* 22, 521–528 (Corrigendum 1973 *JFM* 58, 823)
Neitzel, G. P. 1982 *Phys. Fluids* 25, 226
Priede, J. 1993 *Theoretical study of a flow in an axisymmetric cavity of finite length, driven by a rotating magnetic field.* Thesis, Salaspils
Richardson, A. T. 1974. *JFM* 63, 593
Robinson, T. 1973 *JFM* 60, 641-664
Savas, Ö. 1987 *JFM* 183, 77
Ungarish, M. 1997 *JFM* 347, 105
Volz, M. P. and Mazurk, K. 1996 *Exp. in Fluids* 20, 454
Tillmann, W. 1967 *Phys. Fluids Supl.* 10, 108

Chapter III

On liquid metal flow generated by superimposed rotating and steady magnetic fields

Rotating magnetic field drives a swirling recirculating flow of conducting liquid. The fixed structure of this flow is shortcoming from the point of view of its application in crystal growth technologies. The current chapter deals with the influence of imposed steady axial magnetic field as a tool to control the induced flow. We used different methods: order of magnitude analysis, analytical solutions of simplified equations, 2D numerical simulation as well as experimental investigation. Conditions of overlapping of results, simple physical interpretations as well as analogy to a fully developed flow in duct have been introduced and illustrated. Estimates of the necessary field induction to influence the mean flow are given. The threshold value essentially depends on the wall conductivity and may differ for the core region and boundary layer. The presence of a strong steady field makes the flow in its middle part analogous to classic Hartmann flow. The parallel boundary layer appears near the side wall. The behavior of this layer has some peculiarities if compared to the corresponding classic one. The angular velocity drop along the side layer generates meridional flow, which vanishes slower than the "normal one." The Taylor–Götler type instability occurs at strong forcing. Flow oscillations disappear when the imposed SMF suppresses inertia in the side layer.

1. Introduction.

An obvious example of the source of rotating magnetic field (RMF) is the stator of electric motor. It induces a magnetic field rotating in the plane perpendicular to the axis of symmetry. Similarly to the rotation of the rotor, RMF drives the swirling flow of conducting liquid. The stirring due to RMF can be used, e.g., in metallurgy (Davidson & Hunt 1987) and semiconductor crystal growth (see, Gelfgat and Priede 1995). Besides a certain practical aspect, the RMF driven flow turns out to be an attractive theoretical problem. The exhaustive investigation by Davidson (1992) summarizes the key features of mean flow. It has a solid body resembling core surrounded by thin boundary layers of Bödewadt's type on end-walls. Any axial non-uniformity of angular velocity induces meridional flow, which tends to eliminate it. The balance of driving magnetic force and Coriolis force determines the core angular velocity. Thus, the core rotates as a solid body, but the core meridional flow is adjusted to the driving force distribution. The axial uniformity of the core rotation persists even when the forcing is highly localized. The theoretical explanations were shown in a good agreement with the experimental results by Robinson (1973).

A strong coupling between the azimuthal swirl and secondary recirculation provides an environment for inertial waves. An unsteady RMF driven flow was investigated by Davidson (1989), recently by Ungarish (1997). The numerical simulation (e.g., Gelfgat, Priede & Sorkin 1991, Barz *et al.* 1997) demonstrated that the recirculation stabilized the flow in comparison to an axially unbounded case investigated by Richardson (1974). However, the flow is unstable under usual crystal

growth conditions. A review on the RMF driven flow was presented by Gelfgat & Priede (1995).

The fixed pattern of the base flow as well as the oscillating velocity field is shortcoming in crystal growth technologies. The stabilizing action of steady axial magnetic field (SMF) is well known (e.g., Branover & Tsinober 1970). On the other hand, SMF influences the base flow as well (see, the review by Hunt and Shercliff 1971, Sterl 1990).

The flow due to superimposed rotating and steady magnetic fields has been investigated by Grants, Priede & Gelfgat (1996). They found the necessary induction to influence the flow for two limiting cases of insulating and perfectly conducting end-walls. However, the new solidified semiconductor crystal has a characteristic relative conductance of few percents. Such weak conductance plays an important role in spite of seeming negligibility (Hjelming & Walker 1986). In the current chapter we examined all three cases of wall conductance. The existence of two limiting values of SMF induction for both the core and boundary layer was found in the presence of perfectly or poorly conducting ends (§3).

The numerical simulation of selfsimilar problem (§4) confirmed the results of order of magnitude analysis and illustrated a consequent boundary layer widening due to SMF. A simple analytical selfsimilar solution coincides with the related Hartmann solution between the planes in the presence of a strong SMF. The numerical 2D simulation (§5) showed the role of the force distribution as well as revealed an analogy to a fully developed flow in the rectangular duct. However, an essentially different side layer behavior was detected in case of all perfectly conducting walls. We have found an analytical boundary layer type solution (§6) explaining this distinction.

The duct flow studies (Hunt and Shercliff 1971) as well as our 2D numerical solution predicted the angular velocity drop in the axial direction along the side layer. Thus, an additional meridional flow is induced there. The order of magnitude estimates and corresponding 2D numerical simulation (§7) showed that this flow was less suppressed by SMF than the one generated by normal layers. As a result, the inertia persists in the side layer for a higher induction value.

A strong SMF suppresses the mean flow. At the same time, the oscillating with the frequency of RMF azimuthal forces due to alternating radial currents and steady axial magnetic field grow together with the SMF induction. Section 8 discusses the estimated amplitude of induced oscillating flow velocity.

The appearance of thin boundary layers at the end walls is a characteristic feature of the rotating recirculating flows. Similar thin boundary layers for SMF induced currents usually appear, too. In such cases a couple of electrodes can be simply used to measure the angular velocity of flow. Using this favorable circumstance, we have verified some results experimentally, as well (§9).

2. Equations

Figure 1 depicts the sketch of investigated model. A liquid with a conductivity σ fills a cylindrical vessel of dimensions L and R_0. The vessel walls are thin $\Delta << L$ and their conductivity is σ_w. The induction of superimposed rotating and steady magnetic fields is $\mathbf{B}_0$ and $\mathbf{B}$, correspondingly. $\mathbf{B}_0$ rotates with an angular velocity ω_0.

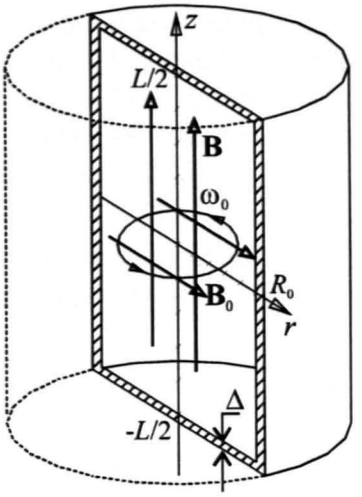

Figure 1. Sketch of the model

The alternating magnetic field in conducting media as well as a moving conducting liquid in the steady magnetic field induces currents. Their interaction with both imposed magnetic fields produces an e.m. body Lorentz force. It can be divided into several parts:

(i) A steady time-averaged part of the interaction between RMF induced axial current and RMF itself.

(ii) An oscillating with frequency $2\omega_0$ part of the above interaction. This one gives rise to flow oscillations with a relative velocity amplitude $u'/u \sim \Omega/\omega_0$, where Ω is angular velocity of base flow (Davidson & Hunt 1987).

(iii) A steady part due to the interaction of SMF induced current with SMF itself.

(iv) Two oscillating with the frequency ω_0 parts generated by the interaction of SMF induced currents with RMF, and vice versa.

We traditionally consider the induction of RMF too small to drive the flow with an angular velocity comparable to that of field rotation. On the one hand, it allows to ignore the effect of oscillating e.m. force (ii). On the other hand, if $\Omega << \omega_0$, the induced swirl does not influence the RMF generated body force. Besides, we dropped the part of Lorentz force oscillating with field frequency ω_0 (iv). This requires certain conditions, which are examined below in §8. The low frequency condition is usual for RMF applications. If $\omega_0 R_0^2 \mu\sigma < 3$ (μ is magnetic permeability), then the induced body force can be assumed purely azimuthal (Davidson 1992). We restricted the investigation to low-frequency fields, too. The azimuthal body force in an infinitely long cylinder then is $F_\theta^\infty(r) = 0.5 B_0^2 \sigma \omega_0 r$. The force acting on a truncated cylinder $F_\theta(r,z)$ is determined by the electric boundary conditions. Further we shall use the force distribution $f(r,z) := F_\theta(r,z)/F_\theta^\infty(r)$ and consider it to be defined (Gelfgat *et al.* 1991, Priede 1993, Gelfgat and Priede 1996, Trombeta *et al.* 1997). If the aspect ratio $R = R_0/L$ is of the order of unity or less and the Reynolds number is of the order of some thousand that is characteristic for crystal growth, the core rotates as a solid body. In this case the force distribution $f(r,z)$ can be substituted by an "effective" value a constant M/M_0 ratio of an actual driving torque to the one acting on a corresponding piece of infinite cylinder. We used the actual force distribution $f(r,z)$ in a 2D numerical simulation and the constant one in a selfsimilar formulation of the problem. The influence of force distribution, which appears under action of a strong steady field, is analyzed below in §5.

We consider the flow to be laminar and axially symmetric. Hence, it is described by 2D Navier-Stokes equations supplemented by the body forces due to RMF and SMF. The first one, as mentioned, is flow independent. The second one due to SMF, in its turn, is flow determined. There are radial and azimuthal parts since the imposed SMF is purely axial. The radial force is $f_r=j_\theta B$. From the Ohm's law it follows that $j_\theta=-\sigma v_r B$. The azimuthal force is $f_\theta=-j_r B$. Let us use $\mathcal{H}$ — induced magnetic field instead of **j**: $\nabla\times\mathcal{H}=\mathbf{j}$. It yields the azimthal force $f_\theta=\partial\mathcal{H}_\theta/\partial z B$. The Ohm's law introduces a link between $\mathcal{H}_\theta$ and the velocity:

$$\Delta\mathcal{H}_\theta=-\sigma B\partial v_\theta/\partial z \tag{1}$$

The continuity of tangential electric field and normal current determine the boundary conditions for $\mathcal{H}_\theta$. Suppose the walls are thin enough to consider the tangential current density through them as a constant along the depth. Then the boundary condition for $\mathcal{H}_\theta$ is $\partial\mathcal{H}_\theta/\partial n=(\sigma/\sigma_n)\mathcal{H}_\theta/\Delta_n$ on the end walls, and $\partial/\partial r(r\mathcal{H}_\theta)=(\sigma/\sigma_\tau)(r\mathcal{H}_\theta)/\Delta_\tau$ on the side wall.

With an eye to the further application of von Kármán similarity variables (e.g., Shlichting 1979), let us introduce the functions Ω, H, W, and Φ as: $r\Omega=v_\theta$; $0.5r^2H=\psi$; $rW=w$; $r\Phi=\mathcal{H}_\theta$, where w is vorticity: $w=(\nabla\times\mathbf{v},\mathbf{e}_\theta)$, and ψ is stream function: $1/r(-\partial\psi/\partial z,\partial\psi/\partial r)=\mathbf{v}=(v_r,v_z)=(-0.5r\partial H/\partial z, H+0.5r\partial H/\partial r)$. Then, the dimensionless Navier-Stokes equation, Ohm's law and definition of both W and H yield the following set:

$$\frac{\partial\Omega}{\partial t}+H\frac{\partial\Omega}{\partial z}+\frac{r}{2}\left(\frac{\partial H}{\partial r}\frac{\partial\Omega}{\partial z}-\frac{\partial H}{\partial z}\frac{\partial\Omega}{\partial r}\right)-\frac{\partial H}{\partial z}\Omega=\frac{\partial^2\Omega}{\partial r^2}+\frac{3}{r}\frac{\partial\Omega}{\partial r}+\frac{\partial^2\Omega}{\partial z^2}+Ha^2\frac{\partial\Phi}{\partial z}+Tef(r,z) \tag{2}$$

$$\frac{\partial W}{\partial t}+H\frac{\partial W}{\partial z}+\frac{r}{2}\left(\frac{\partial H}{\partial r}\frac{\partial W}{\partial z}-\frac{\partial H}{\partial z}\frac{\partial W}{\partial r}\right)-\frac{\partial\Omega^2}{\partial z}=\frac{\partial^2 W}{\partial r^2}+\frac{3}{r}\frac{\partial W}{\partial r}+\frac{\partial^2 W}{\partial z^2}+Ha^2\frac{\partial^2 H}{\partial z^2} \tag{3}$$

$$\frac{\partial^2 H}{\partial r^2}+\frac{3}{r}\frac{\partial H}{\partial r}+\frac{\partial^2 H}{\partial z^2}+2W=0 \tag{4}$$

$$\frac{\partial^2\Phi}{\partial r^2}+\frac{3}{r}\frac{\partial\Phi}{\partial r}+\frac{\partial^2\Phi}{\partial z^2}+\frac{\partial\Omega}{\partial z}=0 \tag{5}$$

The symmetry condition on the axis is $\partial/\partial r(\Omega,W,H,\Phi)=0$. The no-slip condition on rigid boundaries requires $\Omega=0$, $H=0$. The boundary conditions for Φ are $\alpha_n\partial\Phi/\partial z\pm\Phi=0$, $(z=\pm1/2)$ and $\alpha_\tau\partial/\partial r(\Phi r^2)+\Phi r^2=0$, $(r=R)$ on the end walls and the side wall, respectively.

The following dimensional scales were used: vessel's height L for the distance; characteristic time τ of swirl diffusion $\tau=L^2/\nu$; characteristic density of induced current $\sigma(L/\tau)B$.[†] The problem depends on the five dimensionless parameters (table 1), namely, magnetic Taylor number Te, Hartmann number of steady magnetic field Ha; aspect ratio R; relative conductance of end and side walls α_n and α_τ, respectively. As mentioned, the constant effective value $T=M/M_0Te$ often can substitute the actual source $Tef(r,z)$, the total torque remaining the same. Further we shall refer to it as a Taylor number of forcing. It can be defined directly by the total applied torque M, as well. This definition is convenient for the selfsimilar formulation. On the other hand,

[†] No special notation is introduced for the dimensional variables used further in scaling analysis.

it may turn out useful in experiment. Besides, it has a slightly more general physical content, i.e., it uses the total torque — the only essential parameter of forcing, instead of the parameters of RMF.

$\mathrm{Te} = \dfrac{\sigma\omega_0 B_0^2 L^4}{2\rho\nu^2}$	Magnetic Taylor number; expresses the ratio of e.m. torque induced in a piece of the infinite cylinder to the characteristic viscous torque.
$\mathrm{T} = \dfrac{M}{M_0}\mathrm{Te} = \dfrac{2ML^4}{mR_0^2\nu^2} = \dfrac{M}{0.5mR_0^2/t^2}$	Taylor number of forcing; expresses an actual dimensionless e.m. torque (m is mass of liquid metal).
$\mathrm{Ha} = \left(\dfrac{\sigma}{\nu\rho}\right)^{1/2} LB$	Hartmann number; the ratio of Lorentz force to frictional force.
$R=R_0/L$	Aspect ratio.
$\alpha_n = \dfrac{\sigma_n\Delta_n}{\sigma L}$	Relative conductance of end walls.
$\alpha_\tau = \dfrac{\sigma_\tau\Delta_\tau}{\sigma L}$	Relative conductance of side wall.

Table 1. Dimensionless criteria.

Under the aforementioned so-called selfsimilar approximation, the functions Ω, W, H and Φ are considered constant in the radial direction. Then the problem can be formally treated as a problem of the flow in a layer between two parallel infinite disks. The term $\partial\Phi/\partial z$ can be integrated from (5), but from (4) it follows that $\mathrm{W} = -2\partial^2\mathrm{H}/\partial z^2$. Therefore, the number of independent equations reduces to two:

$$\frac{\partial\Omega}{\partial t} + \mathrm{H}\Omega' - \Omega\mathrm{H}' = \Omega'' + \mathrm{T} - \mathrm{Ha}^2\left(\Omega - \frac{\overline{\Omega}}{2\alpha_n + 1}\right) \tag{6}$$

$$\frac{\partial\mathrm{H}''}{\partial t} + \mathrm{H}\mathrm{H}''' + 2(\Omega^2)' = \mathrm{H}^{(4)} - \mathrm{Ha}^2\mathrm{H}'' \tag{7}$$

Here the bar sign denotes the averaging over the height of layer.

3. Orders of Magnitude

First consider inertia dominated laminar flow due to sole RMF. The liquid rotates with a nearly constant angular velocity $\Omega_0 = 0.52\nu/L^2\mathrm{T}^{2/3}$ determined by the balance of driving Lorentz and braking Coriolis forces. Narrow boundary layers of thickness $\delta_n \sim L\mathrm{T}^{-1/3}$ occur at rigid walls. The radial velocity in the core is $v_0 \sim \nu/L\mathrm{T}^{1/3}$. The flow returns through narrow boundary layers, so, due to the continuity condition, the radial velocity is $L/\delta_n \sim \mathrm{T}^{1/3}$ times larger there. Therefore, the inertia in the boundary layer exceeds the driving force in $L/\delta_n \sim \mathrm{T}^{1/3}$ times, as well (Davidson 1992).

The imposed SMF in a non-uniformly rotating conducting fluid induces current with characteristic values j_0 and j_n in the core and boundary layer, respectively. Suppose temporarily, they are too small to influence the mean flow. To estimate their magnitude, let us integrate the Ohm's law over a closed contour A shown in figure 2

(Priede, private communication). In such a way we can get rid of the contribution of unknown potential.

$$(j_n + j_0)L \sim \sigma\Omega_0 L^2 B. \tag{8}$$

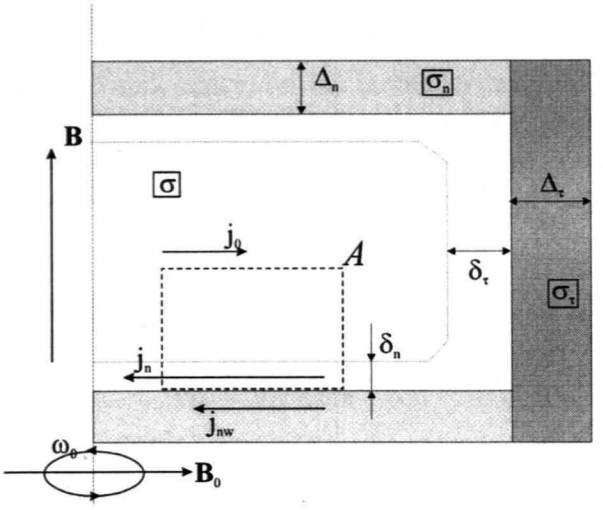

Figure 2. Induced currents

In case of a perfectly conducting wall, the current closes through it and enter the wall normally. Relation (8) simplifies:

$$j_0 \sim \sigma\Omega_0 LB, \; j_n \to 0. \tag{9}$$

If the end walls are insulating, the current completely closes through the boundary layer. Due to the continuity condition, j_n will be L/δ_n time larger than j_0. Consequently, the resistance of thin boundary layer determines the current as follows:

$$j_0 \sim \sigma\Omega_0\delta_n B, \; j_n \sim \sigma\Omega_0 LB. \tag{10}$$

In case of finite wall conductivity, the currents close partially through the boundary layer and partially through the end-wall, where its characteristic value is j_{nw}. The condition of continuity allows us to link these currents with the core current density: $j_0 L \sim j_n\delta_n + j_{nw}\Delta_n$. Together with the continuity condition of tangential to wall electric field: $j_n/\sigma \sim j_{nw}/\sigma_n$, it introduces the relationship between the current density in the core and that in the boundary layer (Priede, private communication):

$$j_0 L \sim j_n(\delta_n + \Delta_n\sigma_n/\sigma)$$

If the conductance of end wall is much lower than that of liquid layer and, at the same time, much higher than that of adjacent thin boundary layer ($1 >> \alpha_n >> \delta_n/L$), then the induced current is determined by a relative wall conductance as follows:

$$j_0 \sim \sigma\Omega_0 LB\alpha_n, \; j_n \sim \sigma\Omega_0 LB. \tag{11}$$

So, in spite of poor wall's conductivity, the latter plays an important role (Hjelming & Walker 1986). In this case, the radial current density in the boundary layer has the same order of magnitude as for insulating walls. In its turn, the current density in the core is α_n times smaller than in case of perfectly conducting walls.

When the induced currents are found, let us estimate the necessary SMF induction to considerably influence the mean flow. Notice that the force balance in the core and

boundary layer should be examined separately, since the characteristic inertia in the normal boundary layer is $O(L/\delta_n)$ times larger than the driving force. However, in case of insulating walls, the current density in the boundary layer exceeds that in the core exactly in the same number of times (10). Comparing the Lorentz force $O(j_0B)$ to the driving force $O(\rho\nu^2/L^3T)$, the threshold value of strong field

$$Ha \sim T^{1/3} \tag{12}$$

yields from (10) for the core and, hence, for the boundary layer, as well.

In case of perfectly conducting walls, the core current density (9) is $O(L/\delta_n)$ times larger than in the previous case. Consequently, the SMF induced Lorentz force become considerable at a lower SMF induction. The threshold value

$$Ha \sim T^{1/6} \tag{13}$$

follows from the force balance in the core. At further increase of the SMF induction the core angular velocity

$$\Omega_0 \sim \nu/L^2 THa^{-2} \tag{14}$$

is determined by the balance of driving and braking Lorentz forces due to RMF and SMF, respectively, $\rho\nu^2/L^3T \sim \sigma\Omega_0 LB^2$.

At the same time, the Lorentz force due to SMF vanishes at perfectly conducting end walls, since the electric current lines enter them normally. So in the boundary layer the balance of inertia and shear ($\rho v_n\Omega_0 \sim \rho\nu\Omega_0 L/\delta_n^2$) remains (Priede, private communication). The radial velocity of meridional flow v_n is determined by the balance of driving pressure gradient $O(\partial p/\partial r)=O(\rho\Omega_0^2 L)$ and shear $O(\rho\nu v_n/\delta_n^2)$. Thus, the characteristic thickness of rotating boundary layer (Greenspan 1968) persists:

$$\delta_n \sim (\nu/\Omega_0)^{1/2} \text{ and consequently } \delta_n \sim LHaT^{-1/2}. \tag{15}$$

The boundary layer thickness should increase with the field induction. Of course, the boundary layer growth must be limited. The phenomenon will take place while both the inertia and shear in the boundary layer dominate over the driving force, i.e., until

$$\rho\nu^2/L^3T \sim \rho\nu\Omega_0 L/\delta_n^2. \tag{16}$$

From (16) and (15) the second threshold for SMF induction follows. The inertia looses its determining role in the whole layer at:

$$Ha \sim T^{1/4}. \tag{17}$$

The region of Ha, where the phenomenon manifests itself, is rather narrow. The boundary layer thickness can increase in $O(T^{1/12})$ times.

Similarly the phenomenon can be shown to take place in case of poorly conducting end-walls as well. Indeed, in the boundary layer the current density (11) coincides with that at insulating walls but a corresponding ratio of the core current density is $O(L/\delta_n\alpha_n)>>1$, (cf., (10) and (11)). Expressing the Lorentz force due to SMF from (11) and comparing with the one provided by RMF, the first threshold value can be estimated as follows

$$Ha \sim T^{1/6}\alpha_n^{-1/2}. \tag{18}$$

Similarly to (14), the core angular velocity estimate $\Omega_0 \sim \nu/L^2 THa^{-2}\alpha_n^{-1}$ follows from (11). Contrary to the case of perfectly conducting walls, the characteristic radial

current density in the boundary layer is considerably larger (α_n^{-1} times) than in the core. As a result, the effect is restricted by the increase of SMF induced force rather than by the decay of inertia down to the magnitude of driving force. The comparison of the Lorentz force due to SMF $O(j_n B)$ with the shear $O(\rho\nu\Omega_0 L/\delta_n^2)$ together with (11) and (15) yield an estimate of the second threshold value

$$Ha \sim T^{1/4}\alpha_n^{-1/4}, \tag{20}$$

when the inertia vanishes in the whole layer.

Figure 3 shows the boundaries of regions with different flow behavior in the (α_n, Ha) plane. To the left from ABCD, the SMF influence on the mean flow is insignificant. To the right from FECD, the flow linearizes due to a strong SMF. Inside ABCEF the core is SMF dominated but the inertia dominates in the boundary layer. Note that in figure 3 the scale in both Ha and α_n directions is determined by the rate of forcing T.

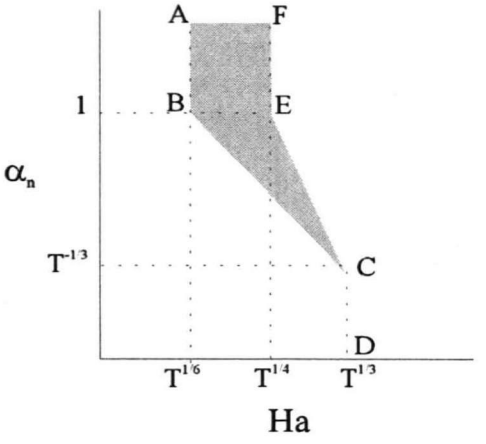

Figure 3. Intermediate range of steady magnetic field induction

4. Self-similar solution

A simple analytical solution for self-similar flow can be obtained in case of a strong SMF. As expected, it exactly coincides with the corresponding well-known Hartmann solution between the planes. The flow has the core angular velocity:

$$\Omega_0 = \frac{T}{Ha^2}\frac{0.5+\alpha_n}{\alpha_n + Ha^{-1}} \tag{21}$$

and exponentially boundary layers: $\Omega=\Omega_0(1-e^{-\zeta})$, $\zeta=Ha(0.5\pm z)$. Since SMF eliminates the inertia, the corresponding term may be dropped in (7), and a simple linear problem follows:

$$H''''-HaH''-2(\Omega^2)'=0,\ H(\pm 0.5)=H'(\pm 0.5)=0.$$

The solution yields the magnitude of axial velocity in the vicinity of rigid end-walls:

$$H_0=5/6\Omega_0^2 Ha^{-3}, \tag{22}$$

and the direction towards the liquid bulk. The radial velocity in the core is:

$$v_0=rH_0=5/6r\Omega_0^2 Ha^{-3} \tag{23}$$

Let us estimate the influence of axial non-uniformity of driving force. The order of velocity drop in the core $(\Omega - \overline{\Omega}) = O(\mathrm{THa}^{-2})$ follows from (6) for insulating or poorly conducting walls. It is much lower than the core velocity itself (21) in these cases. The angular velocity drop in the core becomes essential for perfectly conducting walls. However, the driving force distribution is constant then. Thus, a significant axial non-uniformity of the core rotation appears only when the relative conductivity α_n is about unity.

Notice that only the intermediate region has a certain novelty. If SMF is small, the mean flow stays nearly the same as the one driven by RMF alone. If SMF is large, the core flow coincides with the classic Hartmann flow. The performed numerical solution of self-similar problem has completely confirmed the above conclusions on scaling (§3). Figure 4 depicts characteristic value of angular and axial velocity in the core depending on the Hartmann number for both insulating and perfectly conducting walls. The Taylor number of forcing there is $T=10^8$. The estimated limiting values of SMF induction $Ha_{1/6}=21.5$, (13); $Ha_{1/4}=100$, (17); $Ha_{1/3}=464$, (12) are depicted by doted vertical lines. The numerical simulation has revealed that the constants in these estimates are about unity.

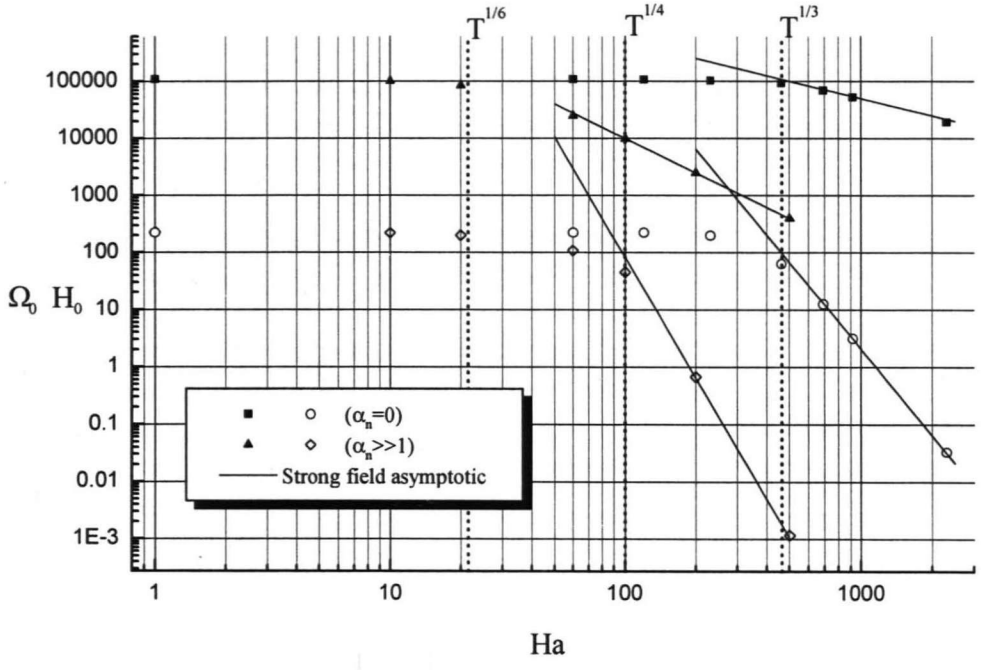

Figure 4. Core angular (solid dots) and maximum axial (hollow dots) velocities versus the Hartmann number. Numerical selfsimilar solution and strong field asymptotic ((21),(22)). $T=10^8$, the end walls insulating ($\alpha_n=0$) and perfectly conducting ($\alpha_n>>1$).

Figure 5 illustrates the effect of boundary layer widening in the numerical solution of self-similar problem. According to the estimates, the boundary layer thickness should increase $(10^8)^{1/12} \approx 4.6$ times.

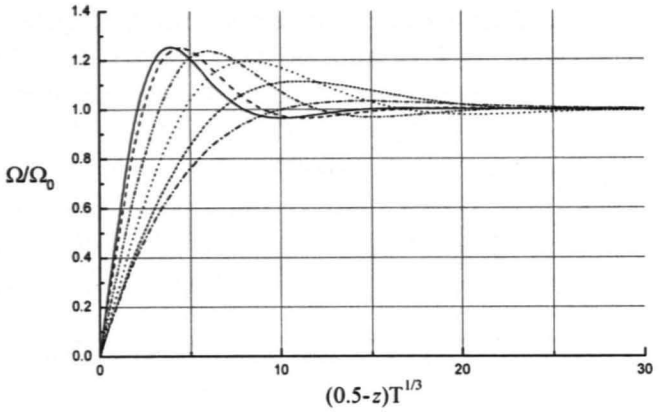

Figure 5. Characteristic boundary layer profiles in the intermediate range of SMF. Numerical selfsimilar solution. $T=10^8$, Ha=0, 20, 40, 60, 80, 100.

The distance to the velocity maximum increases as predicted by the scaling. At the same time, the distance of spatial oscillation vanishing does not change significantly.

5. Numerical 2D solution

In the previous section we examined a selfsimilar solution. A question on its usefulness for the central part of an actual radially bounded flow arises. To answer this question, we performed a numerical simulation of a corresponding 2D flow. The exponential type finite difference approximation, obtained by the integral identity technique, and the Peaceman–Rachford alternating direction time-stepping scheme were used. The code developed by J. Priede (Priede 1993, Gelfgat *et al.* 1991) was adapted.

When the end walls are perfectly conducting, the driving force distribution is $f(r,z)\equiv 1$. It assured a good agreement between selfsimilar and 2D solutions for a strong SMF (see, figure 6). In the intermediate range of Ha numbers this agreement was not so evident. However, the predicted boundary layer thickness increase occurs.

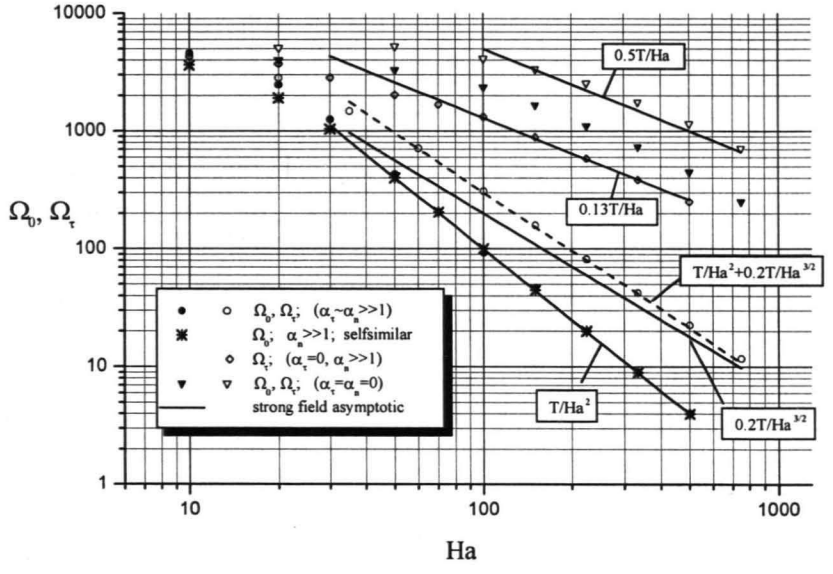

Figure 6. Characteristic angular velocity in the core and boundary layer versus Hartmann number. $T=10^6$, R=1.0

In case of insulating or poorly conducting end-walls, the driving force distribution differs significantly. Alternating currents due to RMF have to bend along the end walls. These currents have no boundary layers there, since the alternating e.m.f. $\omega_0 \times \boldsymbol{r} \times \mathbf{B}_0$ is purely axial (Priede 1993). Therefore, the e.m. driving force distribution is nearly the same in both above cases. The total driving torque obviously must come down because the currents pass nearly parallel to RMF at the end walls. For example, if the aspect ratio is R=1, the averaged torque is only about one fifth of that for perfectly conducting walls (table 2).

R	M/M_0	Ω_0/Ω_τ
0.25	0.72	0.95
0.5	0.48	0.81
1.0	0.20	0.40
2.0	0.061	0.05

Table 2. Average torque and rate of radial non-uniformity of the angular velocity distribution in case of strong SMF and insulating walls.

Let us examine the case of all insulating walls depicted in figure 6. We see in §4 that a strong SMF induced current smoothes the axial distribution of angular velocity as the meridional flow does. So, one can suppose the core rotation to be determined by the total magnetic torque again. The numerical 2D simulation has confirmed this assumption for the maximum angular velocity Ω_τ near the side wall. However, the current does not smooth the radial distribution of angular velocity. Consequently, the radial non-uniformity of core rotation appears. The ratio of minimum and maximum core angular velocities was found numerically $\Omega_0/\Omega_\tau \approx (1+1.5R^3)^{-1}$ (figure 7).

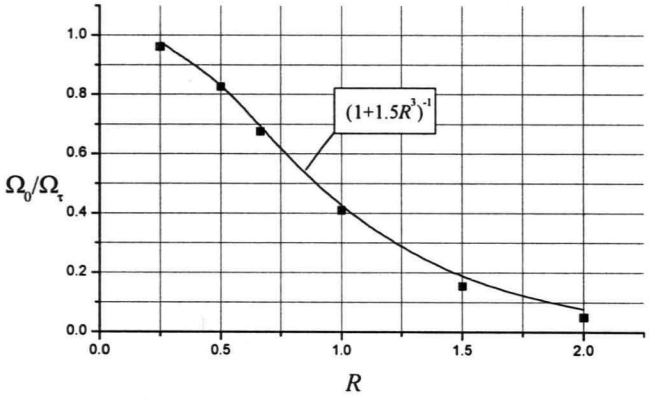

Figure 7. Radial non-uniformity of angular velocity distribution in the presence of strong SMF and all insulating walls as a function of aspect ratio.

The influence of tangential MHD boundary layer at the side wall may violate the agreement between the 2D and selfsimilar solutions, which usually takes place. This phenomenon is a subject of the following section. Since the tangential boundary layer is much thicker than the normal one, it may occupy all the volume. In such cases the core actually disappears, and the selfsimilar solution is evidently a nonsense.

6. Tangential boundary layer

We see in §4 that under a strong SMF the solution of selfsimilar problem coincides with the classic Hartmann problem on the flow between parallel walls. A certain analogy to the fully developed MHD duct flow with the so-called side layers of $O(\mathrm{Ha}^{-1/2})$ thickness is expected to appear as well. These boundary layers are well studied (See, Hunt & Shercliff 1971). The conductivity of both walls plays an important role. The most surprising is the case of a well conducting normal and insulating side wall, when the velocity in the tangential boundary layer is of a higher order than the core velocity. Besides, the velocity profile has spatial oscillations and can even change the sign. The boundary layer velocity is of the core velocity order ($O(\mathrm{Ha}^{-2})$), and the velocity sign does not change in case of all perfectly conducting walls (Chang & Lundgren 1961, Hunt 1965). Our numerical solution has revealed the difference for a rotating flow. The angular velocity scale $O(\mathrm{Ha}^{-3/2})$ in the tangential boundary layer turned out much larger than in the core. In order to explain this distinction, we found an analytical boundary layer type solution for an arbitrary conducting side wall and perfectly conducting ends similar to the one obtained by Hunt (1965).

Let us rewrite equations (2) and (5) for a strong SMF, when the inertia vanishes:

$$\frac{\partial^2\Omega}{\partial r^2}+\frac{3}{r}\frac{\partial\Omega}{\partial r}+\frac{\partial^2\Omega}{\partial z^2}+\mathrm{Ha}^2\frac{\partial\Phi}{\partial z}+\mathrm{Te}f(r,z)=0 \tag{24}$$

$$\frac{\partial^2\Phi}{\partial r^2}+\frac{3}{r}\frac{\partial\Phi}{\partial r}+\frac{\partial^2\Phi}{\partial z^2}+\frac{\partial\Omega}{\partial z}=0 \tag{25}$$

The boundary conditions for Φ are:

$$\partial\Phi/\partial z=0,\quad (z=\pm1/2),\qquad \text{and}\qquad \alpha_\tau\partial/\partial r(r^2\Phi)+r^2\Phi=0,\ (r=R). \tag{26}$$

If volume end walls are perfectly conducting, the e.m. driving force is $\mathrm{Te}f(r,z)\equiv\mathrm{T}$. Suppose, the induction of SMF is so high that the boundary layer appears at the side wall. It has to match the core solution (21). Let us introduce the boundary layer variables: $\Omega(r,z)=\mathrm{T}\mathrm{Ha}^{-1}g(\eta,z)$, $\Phi(r,z)=\mathrm{T}\mathrm{Ha}^{-2}(-z+h(\eta,z))$, $\eta=(R-r)\mathrm{Ha}^{-1/2}$. Then the problem (24–26) in the boundary layer at the side wall transforms into:

$$\frac{\partial^2 g}{\partial\eta^2}+\frac{\partial h}{\partial z}=O(\mathrm{Ha}^{-1/2}) \tag{27}$$

$$\frac{\partial^2 h}{\partial\eta^2}+\frac{\partial g}{\partial z}=O(\mathrm{Ha}^{-1/2}) \tag{28}$$

$$\partial h/\partial z=1,\qquad g=0,\qquad (z=\pm1/2), \tag{29}$$

$$\alpha_\tau\left(-Ha^{1/2}\frac{\partial h}{\partial\eta}+O(h)\right)+h=z\left(1+\frac{2\alpha_\tau}{R}\right),\qquad g=0,\quad (\eta=0). \tag{30}$$

"Sewing" with the core requires $h(\eta\to\infty)=0$, since $\Phi(r,z)=-\mathrm{T}\mathrm{Ha}^{-2}z$ in the core. Condition $g(\eta\to\infty)=\mathrm{Ha}^{-1}$ follows from the core angular velocity expression (21). The

form of Φ was chosen to ensure equal characteristic values of h and g, which do not exceed the unity order: $O(h)=O(g)\leq O(1)$.

Notice that the order of equations (27) and (28) is lower than the corresponding number of boundary conditions in the axial direction. Hence, a corner region of $O(\mathrm{Ha}^{-1/2})\times O(\mathrm{Ha}^{-1})$ size should appear near the end-walls (Hunt & Stewartson 1965). The radial scale of the corner region is much larger than the axial one. So, it is easy to check that both h and g take the following asymptotic form in the corner region: $g(\eta,z)=g_c(\eta)(1-e^{-\zeta})$ and $h(\eta,z)=h_c(\eta)-g_c(\eta)e^{-\zeta}$, where $g_c(\eta)$ and $h_c(\eta)$ represent the values of functions on the border between the side layer and the corner. Substituting of this corner solution into (29) yields $g_c(\eta)=\mathrm{Ha}^{-1}$. Thus, the drop of angular velocity in the corner is equal to the core velocity. Notice, that the estimate $\partial h/\partial z=O(\mathrm{Ha}^{-1})$ follows from (27) on the border between the corner and the side layer. Suppose, the order of solution g and h is higher than $O(\mathrm{Ha}^{-1})$. Then the asymptotic side layer solution of (27–30) can be found in the following form:

$$h(\eta,z)=\sum_{n=0}^{\infty}h_n(\eta)\sin(\lambda_n z), \quad \text{and} \quad g(\eta,z)=\sum_{n=0}^{\infty}g_n(\eta)\cos(\lambda_n z), \tag{31}$$

where $\lambda_n=(2n+1)\pi$, $n=0,1,2...$ (cf., Hunt 1965). Substituting of (31) into (27) and (28) yields the same equation for both g_n and h_n:

$$g_n^{(4)}+\lambda_n^2 g_n=0,\ h_n^{(4)}+\lambda_n^2 h_n=0\ ,\ \text{and additionally } h_n=-g_n''/\lambda_n.$$

A corresponding characteristic equation has 4 complex roots: $\pm(\lambda_n/2)^{1/2}\pm i(\lambda_n/2)^{1/2}$. Since g_n and h_n vanish in the infinity (i.e., the core), then those with positive real parts should be dropped. According to the no-slip condition on the side wall ($g_n(0)=0$) it follows:

$$g_n(\eta)=b_n\sin(\kappa_n\eta)\exp(-\kappa_n\eta) \text{ and } h_n(\eta)=b_n\cos(\kappa_n\eta)\exp(-\kappa_n\eta),\ \kappa_n=(\lambda_n/2)^{1/2}. \tag{32}$$

The boundary condition (30) for $h(\eta)$ determines b_n:

$$b_n=a_n\frac{1+\dfrac{2\alpha_\tau}{R}}{1+\alpha_\tau \mathrm{Ha}^{1/2}\kappa_n}, \tag{33}$$

where $a_n=4(-1)^n/\lambda_n^2$ are coefficients in the expansion of $z=\sum a_n\sin(\lambda_n z)$, $z\in[-0.5,0.5]$. So, the solution (31–33) for perfectly conducting ends and an arbitrary conducting side wall, being the first term of asymptotic expansion, has been expressed as a rapidly converging series of elementary functions. In case of insulating side walls ($\alpha_\tau=0$), this solution exactly coincides with one found by Hunt (1965) for the rectangular duct flow. The analogy seems to be obvious, since the curvature effect in a narrow boundary layer is of a higher order of magnitude. Nevertheless, this analogy is not complete. The curvature effect in the boundary condition (26) is characterized by the term $2\alpha_\tau\Phi/R$. When the conductance α_τ increases, the characteristic Φ drop in the tangential boundary layer (and, consequently, the derivative,) decreases if compared to Φ itself. So, the increasing of conductivity increases the role of the curvature. It follows from (33) that the curvature effect governs at $\alpha_\tau>>R$.

The maximum angular velocity calculated from the first term of expansion is

$$\Omega_\tau = \frac{T}{Ha}\frac{4}{\lambda_0^2}\frac{1+2\alpha_\tau/R}{1+\alpha_\tau(0.5Ha\lambda_0)^{1/2}}\sin(\pi/4)\exp(-\pi/4) \approx \frac{T}{Ha}0.13\frac{1+2\alpha_\tau/R}{1+1.25\alpha_\tau Ha^{1/2}} \qquad (34)$$

Suppose, $\alpha_\tau >> R$. Then $\Omega_\tau \approx 0.2/(RHa^{3/2})$ that agrees with the results of a previous numerical solution (Figure 6). The tangential boundary layer velocity scale $\Omega_\tau \sim THa^{-3/2}$ takes place for poorly conducting side wall and negligible curvature as well ($Ha^{-1/2} << \alpha_\tau << \min(0.1Ha^{1/2}, R)$). In this case $\Omega_\tau \approx 0.1T/(\alpha_\tau Ha^{3/2})$. It means that there is a range of tangential wall conductivity, when $\Omega_\tau = O(T/Ha^{3/2})$ for the duct flow ($R\to\infty$), too. As well as for the flow in the cylinder, it is necessary that $\alpha_\tau Ha^{1/2} >> 1$. Of course, the "–3/2" scaling law takes place only when the characteristic value of the solution (34) dominates over the dropped $O(Ha^{-1})$ term in the "sewing" condition. It is ensured by $\alpha_\tau << 0.1Ha^{1/2}$. Notice that this poorly conducting wall limit depends on the Hartmann number. If $Ha >> 100$, then even the side wall with $\alpha_\tau >> 1$ may turn out "poorly conducting". If the side wall is perfectly conducting, the solution (31–33) for the duct flow looses its sense, because the dropped $O(Ha^{-1})$ term in the "sewing" condition becomes a leading one. Evidently, Hunt's (1965) solution for all perfectly conducting walls sets in then.

The analytical boundary layer type solution (31–33) for large Ha and perfectly conducting end-walls was compared with the numerical one (Figure 6 and 8). Figure 8 (*a* and *b*) depicts the velocity profiles in the mid-height of vessel for perfectly conducting and insulating side walls. In the first case, even a rather strong SMF does not ensure good agreement because the core velocity remains comparable to the maximum boundary layer velocity. However, an algebraic sum of analytical maximum boundary layer (34) and core (20) angular velocity fits well to the numerical results (Figure 6). Besides, the characteristic profile behavior and extreme location turned out well predicted, even when the core and boundary layer velocities were of the same order (Figure 8 *a*).

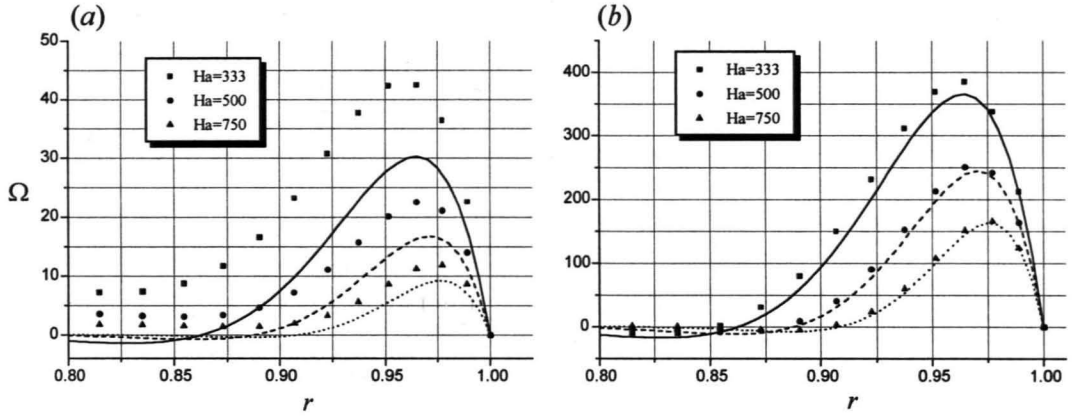

Figure 8. Radial profiles of angular velocity in the tangential boundary layer. $T=10^6$, $R=1.0$, $\alpha_n >> 1$. (a) — perfectly conducting, (b) — insulating side wall. Dots — numerical, curves — analytical boundary layer type solution.

The case of poorly conducting end-walls and insulating side wall has a special practical importance, since the mentioned combination of wall conductance is characteristic for semiconductor crystal growth processes. A problem similar to (27–30) follows. The characteristic value of $g(\eta\to\infty)$ in the core is $O(Ha^{-1}\alpha_n^{-1}) << 1$, so a solution similar to (31–33) can be found. The problem essentially differs with the force distribution, which is nearly the same as for the insulating ends. It should be

integrated to receive the base solution Φ_0 analogous to $\Phi_0=-\mathrm{THa}^{-2}z$ for perfectly conducting ends. After that, the solution (31–33) can be applied with the corresponding coefficients of expansion a_n of the base solution Φ_0. The values of first two coefficients depending on the aspect ratio are presented in table 3.

R	a_0	a_1
0.1	0.41	–0.056
0.25	0.37	–0.037
0.5	0.27	–0.022
1.0	0.15	–0.012
2.0	0.072	–0.0056
4.0	0.035	–0.0027

Table 3. Driving force expansion coefficients depending on the aspect ratio.

We see from (26) or (30) that the curvature of sidewall is significant only when it is conducting. Therefore, if a vessel has all insulating walls, the tangential boundary layer solution should coincide with the corresponding one in the duct flow. It has a thickness varying along the side wall and a characteristic velocity of the same order as in the core (Shercliff 1953, Williams 1963). The numerical simulation has confirmed that.

The last characteristic case deals with the insulating end walls and a perfectly conducting side wall. Similarly to the duct flow, the numerical simulation revealed no essential influence of the side wall conductance. There was an analytical solution found for a corresponding duct flow (see, Hunt & Stewartson 1965, Grinberg 1961 and 1962). No essential novelty is expected, since then it has to reveal itself in the numerical solution. Thus, we restricted our consideration of this case to the numerical simulation.

7. Meridional flow under a strong steady magnetic field

It is shown in §6 that the variation of angular velocity takes place in the axial direction of side layer regardless of the wall conductivity. Thus, an additional meridional flow is generated. The angular velocity drop in the longitudinal direction of the side layer is of the same order as the angular velocity itself. So, the axial pressure gradient there can be estimated as follows:

$$\partial p/\partial z \sim \delta_\tau/L\,\partial p/\partial r \sim \delta_\tau/L\,\rho\Omega_\tau^2 L.$$

It should be balanced by a shear: $\partial p/\partial z \sim \rho\nu v_\tau/\delta_\tau^2$. Combining two previous expressions, an estimated meridional velocity in the boundary layer follows:

$$v_\tau \sim \nu^{-1}\Omega_\tau^2\delta_\tau^3, \tag{35}$$

which always vanishes slower than the characteristic meridional flow velocity v_n in the normal boundary layer. From (23) and flow continuity it follows that $v_n \sim \nu^{-1}\Omega_0^2\delta_n^2 L$. The comparison of the scales of characteristic flow velocities at different wall conductance is presented in table 4.

	$\alpha_n=0$	$\alpha_n >>1$	
	$\alpha_\tau=0$	$\alpha_\tau =0$	$\alpha_\tau >>0.1Ha^{1/2}$
$O(\Omega_0)$	THa^{-1}	THa^{-2}	THa^{-2}
$O(\Omega_\tau)$	THa^{-1}	THa^{-1}	$THa^{-3/2}$
$O(v_n)$	T^2Ha^{-4}	T^2Ha^{-6}	T^2Ha^{-6}
$O(v_\tau)$	$T^2Ha^{-7/2}$	$T^2Ha^{-7/2}$	$T^2Ha^{-9/2}$

Table 4 Characteristic velocities of azimuthal swirl and meridional flow.

These scales fit well to the results of numerical simulation. Figure 9 depicts the dependence of stream function maximum ψ_{max} on Hartmann number for three characteristic cases of wall conductivity. Note that $v_\tau \sim \psi_{max}/\delta_\tau$.

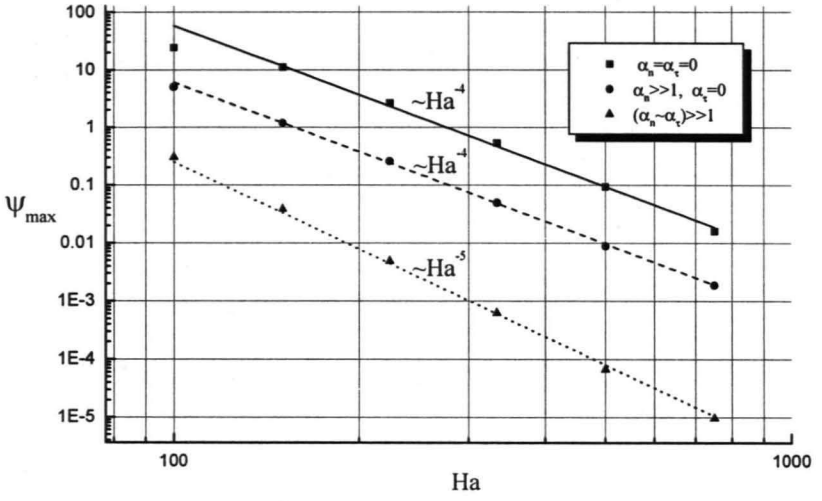

Figure 9. Stream function maximum versus Ha. $T=10^6$, $R=1$.

Figure 10 illustrates the consequent feature of a strong SMF field to "push" the meridional flow towards the side wall.

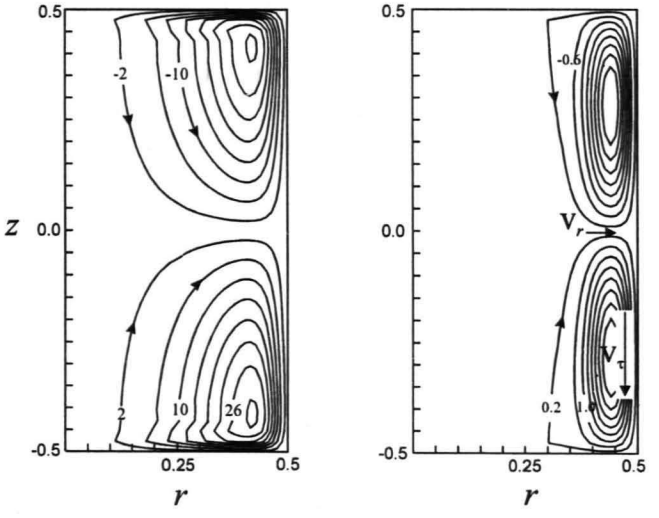

Figure 10. Meridional flow under weak and strong SMF. All walls are insulating.

Since the meridional flow in the boundary layer vanishes slower, the inertia is expected to dominate longer there. Let us estimate a limiting value of strong SMF induction. The field will be strong, if the Coriolis force $O(\rho v_r \Omega_\tau)$ becomes negligible in comparison to the e.m. driving force $O(\rho\nu^2/L^3 T)$. A characteristic radial velocity of secondary flow in the boundary layer at side wall v_r can be estimated from expression (35) for v_τ. Due to continuity, $v_r \sim v_\tau \delta_\tau / L$. Thus, the estimates of large Ha numbers follow:

$$(Ha^{-1/2})(T^2 Ha^{-7/2})(THa^{-1}) \sim T \text{ or } Ha \sim T^{2/5}, \text{ if } \Omega_\tau \sim T/Ha \text{ and} \tag{36}$$

$$(Ha^{-1/2})(T^2 Ha^{-9/2})(THa^{-3/2}) \sim T \text{ or } Ha \sim T^{4/13}, \text{ if } \Omega_\tau \sim T/Ha^{3/2}. \tag{37}$$

One can see that these limiting values are larger than the ones for the core. The effect manifests itself in the unsteady numerical solution. Strong forcing by RMF gives rise to continuous flow oscillations. Richardson (1974) examined the stability of purely azimuthal flow in an infinite cylinder. The Taylor–Götler type instability appears near the side wall. The numerical simulation in the cylinder of finite length revealed essential stabilization by recirculation (Gelfgat *et al.* 1991, Priede 1993, Barz *et al.* 1997, Grants 1998, ch. 2). We investigated the flow stability depending on the imposed SMF. Our numerical simulation has revealed that the oscillations disappear together with the determining role of inertial forces at SMF of $Ha \sim T^{2/5}$ (Figure 11). The numerical results were confirmed experimentally only for a strong SMF.

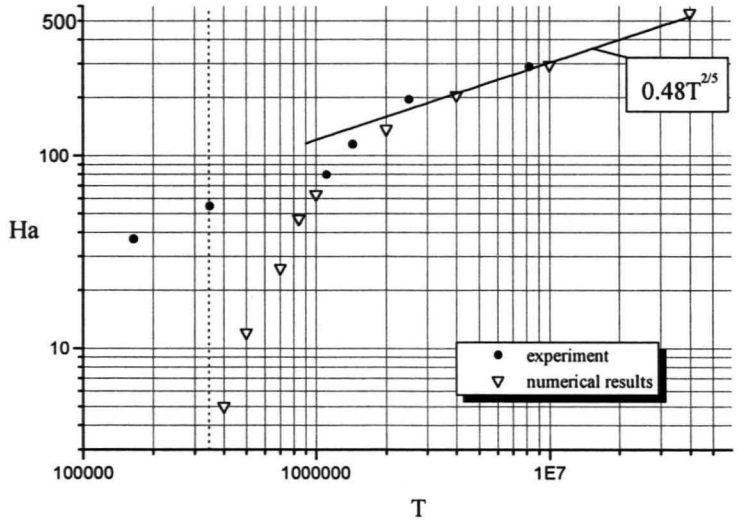

Figure 11. Neutral stability curve at a strong SMF. Comparison of numerical and experimental results. R=1. Dashed line depicts the limit of Ha→0.

8. Oscillating body force

Note that the model is based on the assumption of negligible oscillating body force (§2). Let us estimate the amplitude of angular velocity oscillations. According to the Maxwell's equation, a uniform magnetic field rotating in a (θ,r) plane induces a purely axial alternating e.m.f. of magnitude $\omega_0 r B_0$. If the end walls are perfectly conducting, the induced currents are purely axial ($j_z' \sim \sigma\omega_0 B_0 R_0$).

If the end walls have finite conductance, then radial current of magnitude j_r' appears. Similarly to (8), the relationship: $j_z' + j_r' \sim \sigma\omega_0 B_0 L$ for oscillating current density

follows from the Ohm's law. Contrary to the SMF induced currents, there are no boundary layers for the oscillating ones. The current continuity requires $j_z' R_0 \sim j_r' L + j_{wr}' \Delta_n$, where j_{wr}' is radial current density in the endwall. Expressing j_{wr}' from the continuity condition for tangential electric field on the end wall ($j_r'/\sigma \sim j_{wr}'/\sigma_n$) and considering $R_0 \sim L$, it follows that $j_z' \sim j_r'(1+\alpha_n)$. Hence, j_r' can be estimated as:

$$j_r' \sim \frac{\sigma \omega_0 L B_0}{1+\alpha_n} .$$

The SMF induced steady current is $j \sim (\sigma \Omega_0 L B)$ (9–11). Suppose, α_n is finite. Since $\omega_0 >> \Omega_0$, an oscillating body force jB_0 due to the interaction between SMF induced current and RMF will be negligible. A dominating oscillating body force $j_r'B$, in its turn, will be balanced by the inertia: $j_r'B \sim \rho \Omega' L \omega_0$, where Ω' is amplitude of angular velocity oscillations. Now we can estimate the amplitude of oscillations as:

$$\Omega' \sim \frac{\sigma B B_0}{\rho} .$$

It should grow together with B while the mean flow angular velocity decreases. So, in case of insulating wall, the velocity oscillation amplitude becomes comparable to the mean flow velocity at $Ha \sim (T/Ha_e)^{1/2}$. Here Ha_e denotes the Hartmann number of RMF. In this case the SMF induction threshold hardly lies in the range of practical interest.

If the end walls' conductance is $\alpha_n = O(1)$, then the amplitude of velocity oscillations in the core reaches the magnitude of the core velocity already at $Ha \sim (T/Ha_e)^{1/3}$. Contrary to the insulating wall case, the threshold induction seems quite realistic. However, the characteristic mean and oscillating core angular velocities stay very small in comparison to the mean angular velocity of boundary layer. Further increase of the end wall conductance reduces the radial part of oscillating current and, consequently, the phenomenon takes place later.

9. Experiment.

The experiment was carried out on In-Ga-Sn eutectic (table 5) poured in a vessel of the radius equal to the height of 50 millimeters (figure 12 *a*). The vessel walls were insulating. A maximum induction of rotating magnetic field was about 6 mT ($T=10^7$) that provided a maximum azimuthal velocity about 15 cm/s, or the Reynolds number about 10^4. The rotating magnetic field was generated by a one pole pair inductor of dimensions: diameter D=29 cm, height H=19 cm. The inductor was fed by 50 Hz three phase alternating current. A maximum steady magnetic field induction was 180 mT, or the Hartmann number about 300. SMF was generated by a water-cooled coil with the internal diameter approximately equal to the height of 17 cm. The field non-uniformity in the experimental volume was less than 10%.

The presence of the imposed steady axial magnetic field and thin hydrodynamic boundary layers at the end walls allows to use simply a couple of electrodes to measure the azimuthal velocity. Suppose, the normal to field end walls are insulating or poorly conducting. The induced current density in the core can be estimated then as: $j_0 \sim \sigma \Omega_0 \delta_n B$ (9) or $j_0 \sim \sigma \Omega_0 L B \alpha_n$ (10), correspondingly. So, if both δ_n/L and α_n are much smaller than unity, then the contribution of current density is negligible in the Ohm's law if compared to the one of characteristic e.m.f. $O(\sigma \Omega_0 L B)$, and, hence,

$$v_\theta B_z = \partial \phi / \partial r .$$

Figure 12 (*b*) schematically depicts the probe. Distance between electrodes Δl in our experiments varied from 4 to 12 mm and measured potential difference $\Delta\phi$ was of the order of 1–100 μV.

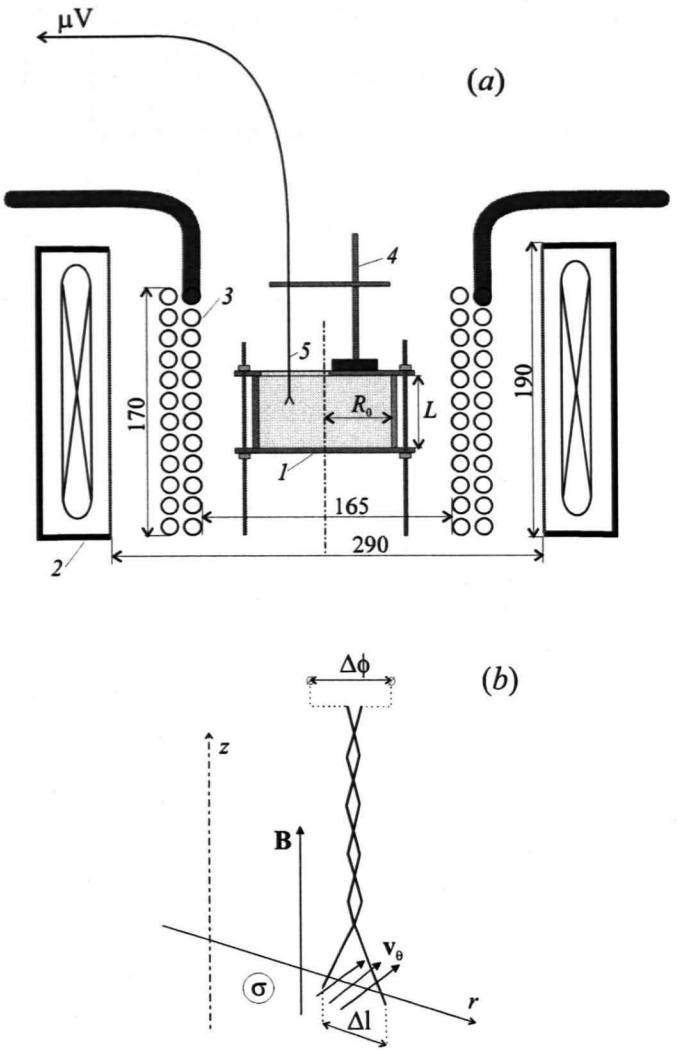

Figure 12. Sketch of experimental device. (a) general view. 1 – experimental volume; 2 – RMF inductor; 3 – SMF inductor; 4 – probe positioner; 5 – probe. (b) probe.

Content	67% Ga, 20.5% In, 12.5% Sn
Density	ρ=6.4 g/cm^3
Conductivity	$\sigma=3.46\times10^6$ S/m
Viscosity (20°C)	$\nu=62.3\times10^{-8}$ m^2/s

Table 5. Properties of experimental liquid.

We measured the total applied e.m. torque acting on the liquid instead of the RMF induction. For this purpose we hung our volume on a calibrated string and measured steady rotation angle.

The experiment showed a good agreement with the theoretical results (Figure 13). Note that both experimental and laminar numerical results fitted well to the theoretical results for a turbulent flow obtained by Davidson (1992): $\max(v_\theta)\approx1.98T^{5/9}R^{11/18}$. At a

lower forcing, the coincidence to the selfsimilar solution at weak ($\Omega_0 \sim 0.52T^{2/3}$) and strong ($\Omega_0 = 0.5THa^{-1}$) steady magnetic field limit has been found in experiments.

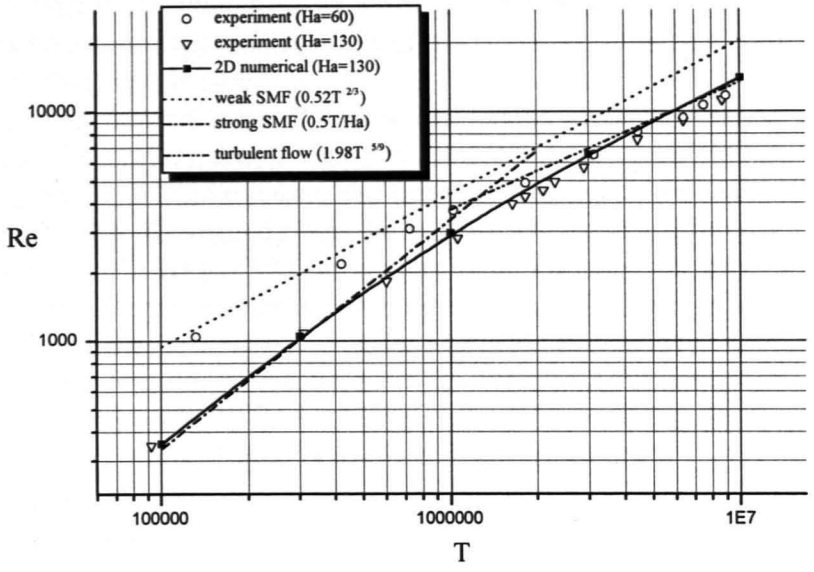

Figure 13. Reynolds number of induced flow versus Taylor number of forcing. Here Re is based on the azimuthal velocity at r=0.86, z=0.

An important theoretical fact is the appearance of a new source of meridional flow in the tangential layer. The experiment has confirmed the presence of an essential angular velocity drop in the axial direction at a strong steady magnetic field (figure 14).

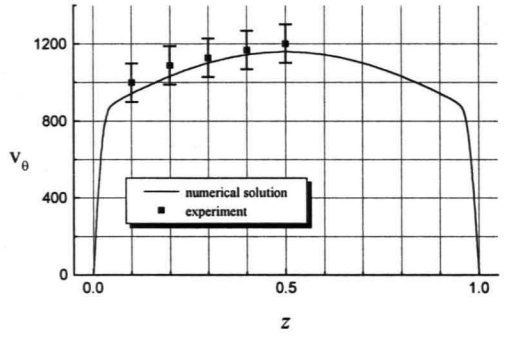

Figure 14. Azimuthal velocity profile along the tangential boundary layer. $T=2.2\times10^5$, Ha=90.

In order to verify numerical results concerning the SMF influence on the flow stability, we performed experimental measurements of time dependent azimuthal velocity. For a strong SMF ($Ha > T^{1/3}$), the experimental and numerical results coincide well (figure 11). Unfortunately, we could not increase T above 10^7 in the experiment. Nevertheless, at least the possibility to generate a stable rotating-recirculating flow with $Re \approx 10^4$ has been shown.

The relationship between the Reynolds number and Hartmann number necessary to stabilize the flow can be introduced. The oscillations were found to disappear at a strong SMF threshold ($Ha \sim T^{2/5}$), when the velocity scale $Re \sim THa^{-1}$ sets in. Consequently, a maximum stable flow velocity is $Re \sim T^{1-2/5} \sim T^{3/5}$. Thus, the imposed SMF of induction Ha allows to generate a stable flow of velocity $Re \sim Ha^{3/2}$. The "$T^{2/5}$"

law can be broken at a certain higher Reynolds number. This question lies beyond the scope of the current investigation, so we can refer to the general similarity to the duct flow only. The stability threshold Re/Ha=$O(10^2)$ was introduced by Branover & Tsinober (1970) for the duct flow at a strong transverse field. Unfortunately, their conclusion is based on experimental data at the Reynolds number below some 2×10^4. So, it worth nothing in our case.

Our experiment showed that a 2D numerical axially symmetric model considerably overestimated the experimental stability threshold in case of a weak SMF. Unfortunately, we could not measure the flow oscillations below Ha=35 because of a very low signal. The discrepancy may be caused by the 3D instability of Bödewadt layer (Lingwood 1997, Savas 1987) as well as by perturbation of probe.

Figures 15 and 16 present some examples of the experimental results illustrating the unsteady flow behavior. Figure 15 depicts time dependencies of azimuthal velocity and corresponding amplitude spectrum in the vicinity of a neutral stability curve. Rather monochrome oscillations are characteristic for a strong imposed SMF. The relative amplitude grows and spectra widen at a lower induction.

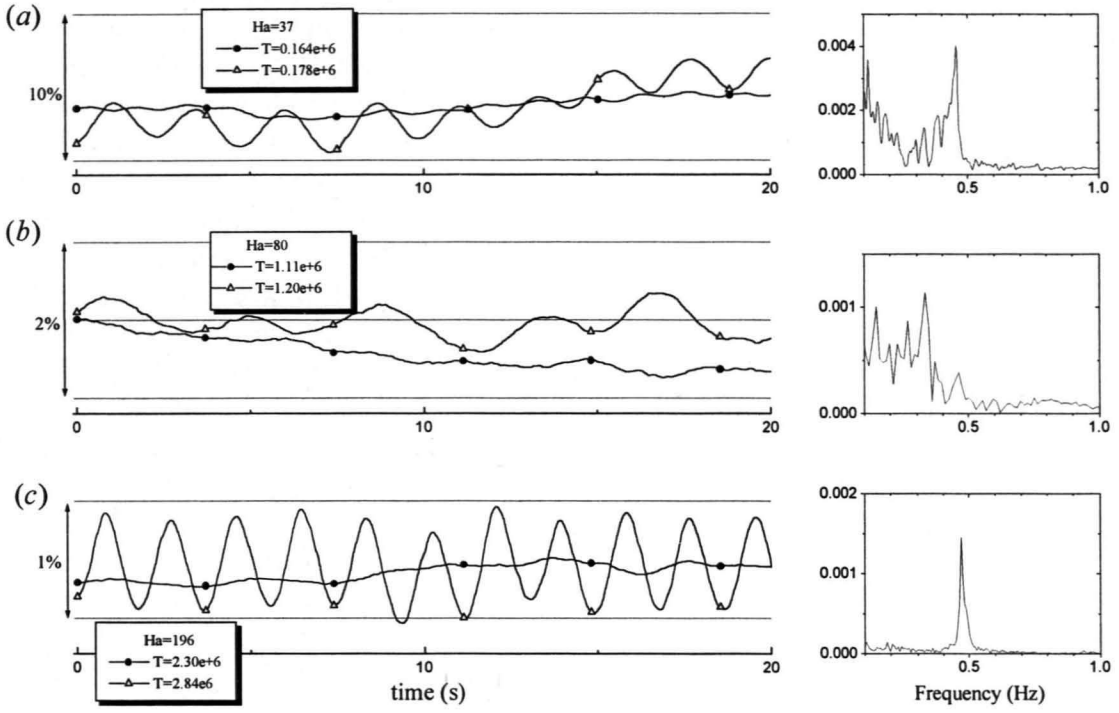

Figure 14. Azimuthal velocity oscillations and amplitude spectrum (fast Fourier transformation) in the vicinity of neutral stability (See, figure 11).

In practical applications RMF is known not only as a tool for stirring but as a mean to "stabilize" the flow as well. An undesirable strong oscillating convection due to buoyancy takes place during crystal growth processes. It turned out that the period and amplitude of oscillations of RMF driven flow was much smaller (Dold & Benz 1995, Fischer *et al* 1997). Unfortunately, the increase of necessary forcing that accompanies linear scale enlargement, can increase the flow oscillations, too. The imposed SMF reduce them or eliminate at all. Figure 16 illustrates the above said.

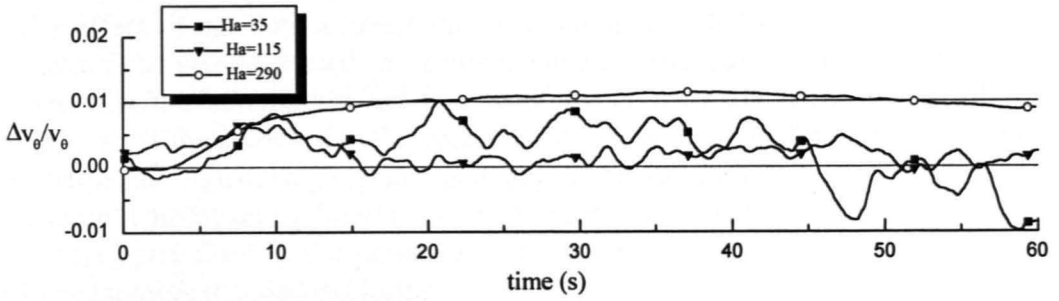

Figure 15. SMF effect on flow oscillations at strong forcing $T\approx 0.8\cdot 10^7$, $Re\approx 10^4$

10. Concluding remarks

This chapter presents a theoretical investigation of main features of the mean flow of conducting liquid generated by rotating and steady axial magnetic fields in a cylindrical vessel. The influence of a variety of main dimensionless parameters is examined. Some results are verified experimentally.

On the one hand, the flow is related to the RMF alone driven flow when the induction of imposed SMF is small. On the other hand, it becomes similar to the well-studied rectangular duct flow at a strong SMF. If the conductance the of end walls is comparable or much larger than the conductance of an adjacent boundary layer, the core is subject to the influence of SMF before the normal boundary layer is. Hence, an intermediate range of SMF action appears. The rotating boundary layer thickness $(\nu/\Omega_0)^{1/2}$ remains, while SMF brakes the core as $\Omega_0=O(\mathrm{THa}^{-2})$. Thus, the normal boundary layer grows wider until the inertia is suppressed in the whole layer.

The order of magnitude estimates was confirmed by a selfsimilar numerical solution, which, in its turn, agreed with the results of 2D numerical simulation. The Taylor number of forcing based on the average torque can be used to predict maximum angular velocity in case, when the end walls are insulating. A strong SMF increases the role of radial non-uniformity of the force distribution. So, the core angular velocity in the vicinity of the axis is about $(1+1.5R^{-3})$ times smaller than the maximum one near the side wall.

A tangential boundary layer appears at the side wall under the influence of a strong SMF. This boundary layer is generally analogous to the one in the 2D duct flow. However, in case of considerably conducting end and side walls ($\alpha_n>>1$ & $\alpha_\tau>>R$), an unexpected "–3/2" scaling appears for the boundary layer velocity. The analytical solution has revealed the role of curvature causing this discrepancy. It also demonstrated that the same $O(\mathrm{Ha}^{-3/2})$ velocity scale should take place in case of conducting end walls and a poorly conducting side wall ($\mathrm{Ha}^{-1/2}<<\alpha_\tau<<0.1\mathrm{Ha}^{1/2}$) regardless of the curvature (i.e., for the duct flow as well). Notice, if the Hartmann number is $O(10^4)$ or more, then the side wall with a relative conductance exceeding the unity ($\alpha_\tau>>1$) may turn out "poorly" conducting.

An essential angular velocity drop in the axial direction of tangential boundary layer causes the meridional flow, which is less influenced by SMF than the "usual" one. The inertia persists in the tangential layer until the Hartmann number reaches a value $\mathrm{Ha}\sim T^{2/5}$. Both, the numerical and experimental investigations showed that the flow oscillations disappeared at this threshold. The maximum velocity of stabilized flow scales as $\mathrm{Re}\sim\mathrm{Ha}^{3/2}$.

The effect of oscillating forces due to alternating radial currents and steady axial magnetic field was neglected in our investigation. The order of magnitude estimates showed that the assumption justified itself under common industrial or laboratory conditions. At the same time, the core flow considerably oscillating with the rotating field frequency ω_0 can be generated under special conditions.

One can employ an analogy to the rectangular duct flow if plans any experiment on fully developed flow in the presence of a strong SMF. However, this analogy then may need a more detailed exploring.

The imposed SMF often allows simple azimuthal velocity measurements. If the flow has thin boundary layers near the insulating or poorly conducting end walls, a couple of electrodes is helpful enough for measuring the azimuthal velocity.

The present investigation reveals and illustrates the ability of SMF to control both the mean and unsteady characteristics of the RMF driven flow. A strong SMF brakes the meridional flow drastically. Therefore, the superimposed rotating and steady magnetic fields can be efficiently used to control the heat transfer and solidification interface, at the same time ensuring axial symmetry due to a residual strong azimuthal flow (Grants & Gelfgat 1997). On the other hand, SMF reduces or even eliminates the flow oscillations, which are undesirable in crystal growth.

REFERENCES

Barz, R. U., Gerbeth, G., Wunderwald, U., Buhrig, E., Gelfgat, Y. M. 1997 *J. Crystal Growth* 180, 3/4, 410

Branover, H. & Tsinober A. B. 1970 *Magnetohydrodynamics of incompressible media*, Nauka, Moscow (in Russian)

Chang, C. C. and Lundgren, T. S. 1961 *Z. angew. Math. Mech.* 12, 100

Davidson, P. A. 1989 *JFM* 209, 35-56

Davidson, P. A. 1992 *JFM* 245, 669

Davidson, P. A. and Hunt, J. C. R. 1987 *JFM* 185, 67-106

Dold, P. & Benz, K. W. 1995 *Cryst. Res. Technol.* 30, 1135

Fischer, B., Friedrich, J., Kupfer, C., Müller, G. and Vizman, D. 1997 In: *Proc. on 3rd Int. Conf. on Energy Transfer in MHD Flows.* Vol. 2, pp. 337-342. Aussois, France.

Gelfgat, Yu. M. and Priede, J. 1995, *Magnetohydrodynamics* 32, 1/2

Gelfgat, Yu. M. and Priede, J. 1996, *Magnetohydrodynamics* 33, 3

Gelfgat, Yu. M., Priede, J., Sorkin, M. Z. 1991 *Proceed. on Int. Conf. on Energy Transf. in MHD Flows*, France, pp. 181-186.

Grants, I. 1998 *Magnetically driven swirling flow guided by steady magnetic field and imposed rotation.* Thesis, Salaspils, Latvia

Grants, I. and Gelfgat, Yu. M. 1997 In: *Proceed. of 3rd Int. Conf. on Transf. Phen. in MHD flows*, Aussois, France. Vol. 2, pp. 351-356.

Grants, I., Priede, J. and Gelfgat, Yu. M. 1996, *Magnetohydrodynamics*, 32, 3, 210

Greenspan, H. P. 1968 *The Theory of Rotating Fluids.* Cambridge University Press.

Grinberg, G. A. 1961. *Appl. Math. & Mech (PMM)* 25, 1536

Grinberg, G. A. 1962. *Appl. Math. & Mech (PMM)* 26, 106

Hjelming, L. N. and Walker, J. S. 1986. *JFM* 164, 237

Hunt, J. C. R. 1965. *JFM* 21, 4, 577

Hunt, J. C. R. and Shercliff, J. A. 1971. *Ann. Rew. Fluid Mech.* 3, 37

Hunt, J. C. R. and Stewartson, K. 1965. *JFM* 23, 3, 563

Lingwood, R. J. 1997 *JFM* 331, 405-428

Priede, J. 1993 *Theoretical study of a flow in an axisymmetric cavity of finite length, driven by a rotating magnetic field.* Thesis, Salaspils
Richardson, A. T. 1974. *JFM* 63, 593
Robinson, T. 1973 *JFM* 60, 641-664
Savas, Ö. 1987 *JFM* 183, 77-94
Shercliff, J. A. 1953. *Proc. Camb. Phil. Soc.* 49, 136
Shlichting, H. G. 1979 *Boundary Layer Theory*, 7th edn. McGraw-Hill.
Sterl, A. 1990 *JFM* 216, 161
Trombetta, P., Marty, P., Martin Witkowski, L. and Tomasino, T. 1997 In: *Proc. on 3rd Int. Conf. on Energy Transfer in MHD Flows.* Vol. 2, p. 463. Aussois, France.
Ungarish, M. 1997 *JFM* 347, 105
Williams, W. E. 1963 *JFM* 16, 2, 262

Chapter IV

Rotating magnetic field driven flow in a rotating cylinder

Azimuthal body force driven swirling flow in a rotating vessel is examined theoretically. The core region appears surrounded by von Kármán swirling layers. Steady flow is controlled by a boundary layer type similarity solution of the so-called one disk problem. This solution predicts the existence of several steady states as well as the absence of any solution in a certain range of imposed rotation. A corresponding numerical simulation of full original problem confirms the feasibility of those branches which tends to the Ekman type flow at increasing of the vessel's speed. Instability of the force balance in the core is shown for a branch which tends to the Cohran's solution. An essentially 2D flow with separating layers or an additional couple of meridional recirculation loops appear in the range of absent similarity solution. An asymptotic solution is given for the Stewartson's type side layer at almost rigid rotation. The results on the stability of rotating boundary layers are reviewed. The investigation shows a possibility to generate controllable and stable flows needed in the crystal growth technologies.

1. Introduction.

Guided melt flow can serve as an effective tool to optimize heat and mass transfer as well as solidification interface in the crystal growth processes (Gelfgat & Priede 1995, Grants & Gelfgat 1997). Since the semiconductor melt has a considerable conductivity, magnetohydrodynamic (MHD) methods can be used (Langlois 1987). The rotating magnetic field recently has received attention as a tool to generate swirling flow and, thus, to control convection of the melt. A practical point is that the induced artificial flow is more uniform and less oscillating than the natural buoyant one (Gelfgat & Priede 1995, Dold & Benz 1995, Fischer *et al* 1997). Besides, the necessary induction of rotating field is of the order of few militeslas that is much smaller than in case of the steady magnetic field application.

The rotating magnetic field (RMF) is considered to be a uniform magnetic field rotating in the plane perpendicular to the axis of symmetry. An induced Lorentz force drives a swirling-recirculating flow with strong coupling between swirl and poloidal recirculation. An exhaustive work of Davidson (1992) explains the key features of mean flow, and the theory was shown in a good agreement with previous experimental investigations. A review of RMF driven flow is given by Gelfgat and Priede (1995). The pattern of the induced flow is rather fixed. A uniformly rotating core region occurs surrounded by thin boundary layers. The main flow characteristics are determined by a single applied magnetic torque. Centrifugal force in the core is balanced by a radial pressure gradient. Therefore, in the boundary layer, where the azimuthal velocity falls to zero, a radial inflow of the order of azimuthal velocity is generated. Due to continuity, the flow is always directed from rigid walls (the solidification interface) towards the bulk of melt. The fixed flow structure is shortcoming from the point of view of optimization. A superimposed steady axial

magnetic field may improve characteristics of RMF driven flow (Grants, Priede & Gelfgat 1996, Grants 1998, ch. 3). The steady magnetic field can control the pattern and magnitude of velocities of meridional flow but its direction.

Priede (1993, 1994) proposed the imposed rotation of vessel (IRV) to control RMF driven flow. He used steady self-similar (laterally unbounded) boundary layer type approach transforming the original problem to the well-known single parameter problem of the flow due to the disk rotation (see, review by Zandbergen and Dijkstra 1987). Besides, Priede proposed a new effective analytical method to solve it. The main results of the analytical solution were:

(i) Possibility of meridional flow direction change;

(ii) Possibility to control flow velocities and boundary layer thickness;

(iii) Existence of two steady state solutions for counter-rotation;

(iv) Absence of a solution for a certain range of counter-rotation.

However, some questions can not be answered by similarity solution. The first one is on capability of selfsimilar approach to describe the flow in the cylinder of finite dimensions. Next one is on existence and additional conditions to obtain a laterally bounded flow corresponding to each of the steady solutions possible at the same imposed rotation. Last but one question is on the actual flow in the range of counter-rotation where a steady self-similar solution is absent. In order to answer these questions, we resorted to a direct numerical simulation of the problem in both self-similar and axially symmetric (2D) approximations.

Notice that the current problem gives a certain example of single parameter von Kármán flow which had received much attention of researchers in the past. On the other hand, the current paper continues the recent investigation of certain MHD application. The single parameter, that governs the solution, can be introduced in several ways. Usually the ratio of fluid (core) and disk (vessel) angular velocity is used. However, referring to the original problem it is more convenient to use the terms of differential rotation as Priede did. The original problem, in its turn, deals with a fixed angular velocity of the vessel and unknown angular velocity of the core flow to be found. So, different formulations arises, which are sequentially examined in the current chapter. The problem of von Kármán swirling flow has been attacked by a variety of methods (numerical solutions, different expansions as well as rigorous provements of existence and uniqueness) during several decades as described in the review by Zandbergen and Dijkstra (1987). Thus, we aimed our efforts mainly to study applicability of the associated single parameter solution to the original problem.

Our investigation confirmed the feasibility of two solution branches tending to an almost rigid (Ekman type) flow. The steady solution at counter-rotation, which tends to the Cohran solution with the core in rest (von Kármán type flow), was unreachable numerically from a variety of initial conditions. We have found a corresponding solution of the original problem to be unstable.

Section 2 deals with model and governing equations in both 2D and self-similar approximations. In §3 we introduce connection between the original and the one disk problems. Simple order of magnitude estimates are given in §4 for the case of almost rigid rotation. An analytical boundary layer type solution of both full and linearized equations is compared with a corresponding numerical similarity solution of the original problem in §5. An original 2D flow in the range of absent selfsimilar solution is examined in §6. A Stewartson's type boundary layer appears at the side wall in case of a rapid vessel's rotation. We examined it in §7. Section 8 deals with the stability of flow.

2. Equations

Consider magnetic field vector $\mathbf{B}_0$=const rotating with a constant angular velocity ω_0 in a plane perpendicular to the axis of cylinder filled with a conducting liquid. The rotating field induces an oscillating current, that interacts with RMF itself, so giving rise to an oscillating body force with a frequency $2\omega_0$ and averaged value in the direction of field rotation. This volumetric force drives a swirling flow. Besides, the cylinder itself rotates with an angular velocity Ω_d^*. The meridional flow appears due to the so-called Ekman pumping at differently rotating endwalls. A theoretical model is based on the following assumptions:

(i) Frequency of RMF rotation is too low to cause an essential skin-effect;

(ii) Induction of RMF is too low to drive a flow with an angular velocity comparable to that of RMF rotation.

Under these assumptions the driving body force is purely azimuthal and flow independent (Davidson 1992). In an infinitely long cylinder (liquid enclosed by thick and well conducting endwalls) the induced magnetic force is $F_\theta^\infty(r)=0.5\rho\Omega_f^2 r$, where Ω_f is angular velocity of forcing $\Omega_f=(\sigma\omega_0/\rho)^{1/2}B_0$ (Davidson 1992); σ and ρ is conductivity and density of liquid, respectively. The induced currents have to bend along the insulating endwalls making body force zero here. An analytical expression of the force distribution in a truncated cylinder with insulating ends is given by Trombetta *et al.* (1997):

$$F_\theta = B_0^2\sigma\omega_0\left(\frac{r}{2}-\sum_{k=1}^{\infty}\frac{R_0 I_1(\lambda_k r/R_0)}{(\lambda_k^2-1)I_1(\lambda_k)}\left\{\frac{\sinh\left(\lambda_k\frac{z+0.5L}{R_0}\right)-\sinh\left(\lambda_k\frac{z-0.5L}{R_0}\right)}{\sinh(\lambda_k L/R_0)}\right\}\right),$$

where the axial coordinate z is measured from the midheight of cylinder of lenght L and radius R_0; $I_\nu(x)$ is the Bessel function of first kind and λ_k are the roots of $I_\nu'(x)=0$.

The flow is considered to be axially symmetric, laminar but already inertia dominated. These assumptions turn out to be applicable under the common crystal growth conditions. On the other hand, they permit to separate electromagnetic and hydrodynamic problems and provide the reception of 2D or even 1D (self-similar) sets of equations. (Davidson 1992, Priede 1993, 1994, Gelfagt and Priede 1996).

Let us write a non-dimensionalized† axially symmetric Navier-Stokes set of equations in a form of:

$$\frac{\partial\Omega}{\partial t}+H\frac{\partial\Omega}{\partial z}+\frac{r}{2}\left(\frac{\partial H}{\partial r}\frac{\partial\Omega}{\partial z}-\frac{\partial H}{\partial z}\frac{\partial\Omega}{\partial r}\right)-\frac{\partial H}{\partial z}\Omega=\frac{\partial^2\Omega}{\partial r^2}+\frac{3}{r}\frac{\partial\Omega}{\partial r}+\frac{\partial^2\Omega}{\partial z^2}+\mathrm{Te}f(r,z)\,, \quad (1)$$

$$\frac{\partial W}{\partial t}+H\frac{\partial W}{\partial z}+\frac{r}{2}\left(\frac{\partial H}{\partial r}\frac{\partial W}{\partial z}-\frac{\partial H}{\partial z}\frac{\partial W}{\partial r}\right)-\frac{\partial\Omega^2}{\partial z}=\frac{\partial^2 W}{\partial r^2}+\frac{3}{r}\frac{\partial W}{\partial r}+\frac{\partial^2 W}{\partial z^2}, \quad (2)$$

$$\frac{\partial^2 H}{\partial r^2}+\frac{3}{r}\frac{\partial H}{\partial r}+\frac{\partial^2 H}{\partial z^2}+2W=0\,. \quad (3)$$

† Vessel's height L and diffusion time $\tau=L^2/\nu$ are used as characteristic values. No special notation is introduced for the dimensional variables used further in scaling analysis.

Functions Ω, W, H are defined as follows: $\Omega=v_\theta/r$; $W=w/r=(\nabla\times\mathbf{v},\mathbf{e}_\theta)/r$; $H=2/r^2\psi$, where ψ is stream function and w is worticity of the meridional flow. Hence, physical velocities are expressed as follows

$$v_\theta=r\Omega, \qquad v_z=H+0.5r\partial H/\partial r, \qquad v_r=-0.5\partial H/\partial z. \tag{4}$$

The magnetic Taylor number $Te=0.5\sigma\omega_0 B_0^2 L^4/(\rho\nu^2)$ characterizes the magnetic forcing; ν denote kinematic viscosity of liquid. Force distribution $f(r,z)$ is defined here as $f(r,z)=F_\theta(r,z)/F_\theta^\infty(r)$. Imposed rotation of a vessel is encountered through boundary conditions for angular velocity:

$$\Omega|_\Sigma=\Omega_d,$$

where $\Omega_d=\Omega_d^* L^2/\nu$ is non-dimensional angular velocity of a vessel and Σ is vessel's surface.

The numerical simulation in a resting vessel shows (e.g., Gelfgat, Priede & Sorkin 1991, Priede 1993) that under considered conditions RMF driven flow has an almost uniformly rotating core. If so, it is insensitive to the force distribution and is determined by a sole total applied torque. Let us substitute the actual force distribution in a truncated cylinder by an idealized one linearly increasing with the radial distance from the axis (Ungarish 1997). It implies a substitution of actual source $Te\,f(r,z)$ by a constant T, called here the Taylor number of forcing

$$T=\frac{M}{M_0}Te=\frac{2ML^4}{mR_0{}^2\nu^2}=\frac{M}{0.5m\left(R_0/\tau\right)^2}, \tag{4}$$

where M/M_0 is ratio of an actual driving torque to the one acting on a corresponding piece of infinite cylinder; m is mass of liquid. Then a 1D set of similarity equations can be obtained assuming Ω, H and W constant in the radial direction (e.g., Shlicting 1979):

$$\frac{\partial\Omega}{\partial t}+H\Omega'-H'\Omega=\Omega''+T \tag{5}$$

$$\frac{\partial H''}{\partial t}+HH'''+2(\Omega^2)'=H^{(4)} \tag{6}$$

The boundary conditions for (5–6) are: $\Omega(\pm0.5)=\Omega_d$; $H(\pm0.5)=H'(\pm0.5)=0$. We used an idealized source characterized by T in self-similar analysis and an actual driving force distribution $Te\,f(r,z)$ in a 2D simulation.

3. Connection to one disk problem

Consider a selfsimilar problem. As shown by Davidson (1992), magnetic forcing T is balanced by the Coriolis force $H'\Omega$ in the core. Hence, the angular and radial velocity is constant along the height: $\Omega=\Omega_0$ and $H=-2H_0z$, $\Omega_0H_0=2T$. The core solution does not satisfy the boundary conditions, so hydrodynamic boundary layers appear. Due to continuity, the radial velocity and, consequently, the Coriolis force are much larger there than those in the core. Therefore, the magnetic force is negligible in the boundary layer. Let us introduce reference values for dimensionless angular

velocity $\Omega^{ref}=T^{2/3}$, axial velocity $H^{ref}=T^{1/3}$ and an axial scale $\delta^{ref}=T^{-1/3}$. Then the steady boundary layer problem follows (Priede 1994):

$$h_0 g_0' - h_0' g_0 = g_0'', \tag{7}$$

$$h_0 h_0''' + 4 g_0' g_0 = h_0^{(4)} \tag{8}$$

$$g_0(0)=\Omega_d/\Omega^{ref},\ g_0'(\infty)=0, \tag{9}$$

$$h_0(0)= h_0'(0)= h_0'(\infty)=0, \tag{10}$$

$$h_0(\infty)g_0(\infty)=2, \tag{11}$$

where $g_0(\xi)=\Omega/\Omega^{ref}$, $h_0(\xi)=H/H^{ref}$, $\xi=(0.5\pm z)/\delta^{ref}$. Condition (11) follows from the force balance in the core. Terms of $O(T^{-1/3})$ has been dropped in (7–11), so solutions h_0, g_0 represent the first terms of asymptotic expansion. This problem can be further transformed into the problem on disk and liquid differential rotation. Let us use a substitution (Priede 1994):

$$g_0(\xi)= (g_0(\infty)-g_0(0))g(y),\quad h_0(\xi)= (g_0(\infty)-g_0(0))^{1/2}h(y),\quad y=(g_0(\infty)-g_0(0))^{1/2}\xi, \tag{12}$$

that affects only boundary conditions, as follow:

$$hg' - h'g = g'', \tag{13}$$

$$hh''' + 4g'g = h^{(4)}, \tag{14}$$

$$g(0)=\mathcal{R}-1/2,\ g(\infty)=\mathcal{R}+1/2 \tag{15}$$

$$h(0)= h'(0)= h'(\infty)=0, \tag{16}$$

where $\mathcal{R}$ is inverse Rosby number representing an inverse value of a relative differential angular velocity $\mathcal{R} = 0.5\dfrac{g_0(\infty)+g_0(0)}{g_0(\infty)-g_0(0)} = 0.5\dfrac{\Omega_0+\Omega_d}{\Omega_0-\Omega_d}$. Values of $\mathcal{R}=0.5$ (when $\Omega_d=0$, Bödewadt's solution) and $\mathcal{R}=-0.5$ (when $\Omega_0=0$, Cohran's solution) mark the boundaries of three different flow regimes. If $|\mathcal{R}|>0.5$, then the sign of the core and vessel velocity coincides with the sign of $\mathcal{R}$. If $-0.5<\mathcal{R}<0.5$, then the core and the vessel rotate in different directions. Large inverse Rosby number $|\mathcal{R}|\to\infty$ correspond to the Ekman type almost rigid flow.

The link to the original problem (7–11) is introduced via the solution of associated problem (13–16) for axial velocity $h_\infty(\mathcal{R})$ in the liquid bulk far from the disk, where the force balance in the core (11) should be satisfied. It yields $g_0(0)=\Omega_d/\Omega^{ref}=(\mathcal{R}-0.5)(2h_\infty(\mathcal{R}+0.5))^{-2/3}$.

Priede (1994) has solved the associated problem using an expansion in form of a double sum of complex exponentials. Substituting into (13–14) he showed all the coeficients depending on three real parameters: h_∞ and a complex constant. These parameters were found to satisfy three boundary conditions (16) on the disk. A full asymptotic expansion containing only exponentials is briefly described also by Zandbergen & Dijkstra (1987) with a reference to Dijkstra (1978). Unfortunately, the latter one was not available to the author and made the comparison impossible. Figure

1 depicts solution h_∞ as a function of the inverse Rosby number. Different flow regimes (further called branches) are denoted by numbers 1–5.

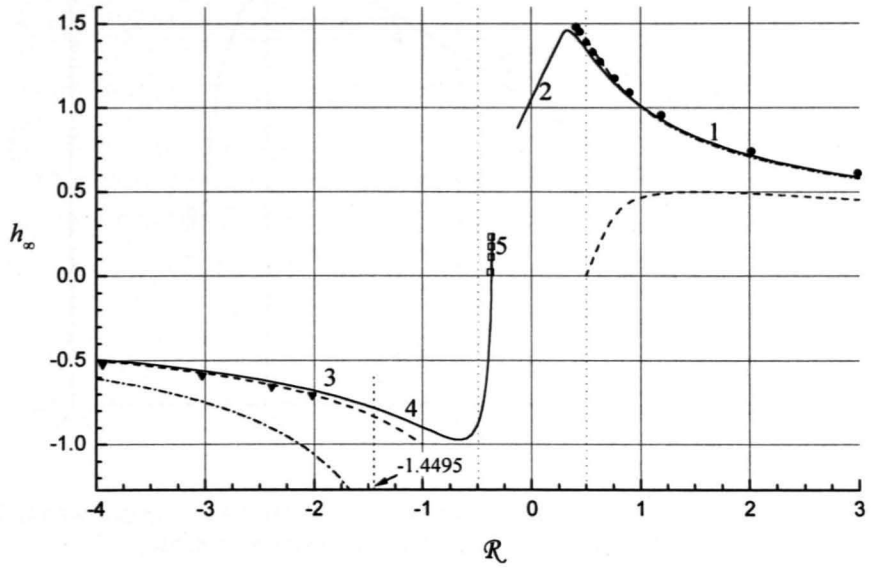

Figure1. Axial velocity at infinity as a function of the inverse Rosby number. — exact solution of associated problem (13–16); – – linearized solution of original problem (5–6); – · – linearized solution of associated problem; numerical solution of (5–6) is depicted by dots. Value of $\mathcal{R}$=-1.4495 separates branches 3 and 4 (See, also figures 3 and 11).

The associated one disk problem is traditionally investigated in the terms of velocity ratios $s=\Omega_0/\Omega_d$ and functions $f(x)$ and $g(x)$, defined

$$v_r = rf'(x), \qquad v_\theta = rg(x), \qquad v_z = -2f(x),$$

where v_r, v_θ and v_z are dimensionless radial, azimuthal and axial velocities, respectively. Under this formulation further referred as a classic one, the problem takes the following form (e.g., Zanbergen & Dijkstra 1987)

$$f''' + 2ff'' = f'^2 + s^2 - g^2, \tag{17}$$

$$g'' + 2fg' = 2f'g, \tag{18}$$

with the boundary conditions

$$f=f'=0,\ g=1,\ x=0 \text{ and } f'\to 0,\ g\to s,\ x\to\infty \tag{19}$$

The link to the terms of problem (13–16), that is the inverse Rosby number $\mathcal{R}$ and the value of function $h(\infty)=h_\infty$, follows:

$$s=1+1/(\mathcal{R}-0.5), \qquad f_\infty=-0.5|s-1|^{1/2}h_\infty.$$

A solution in terms of s and f_∞, is shown in figure 2.

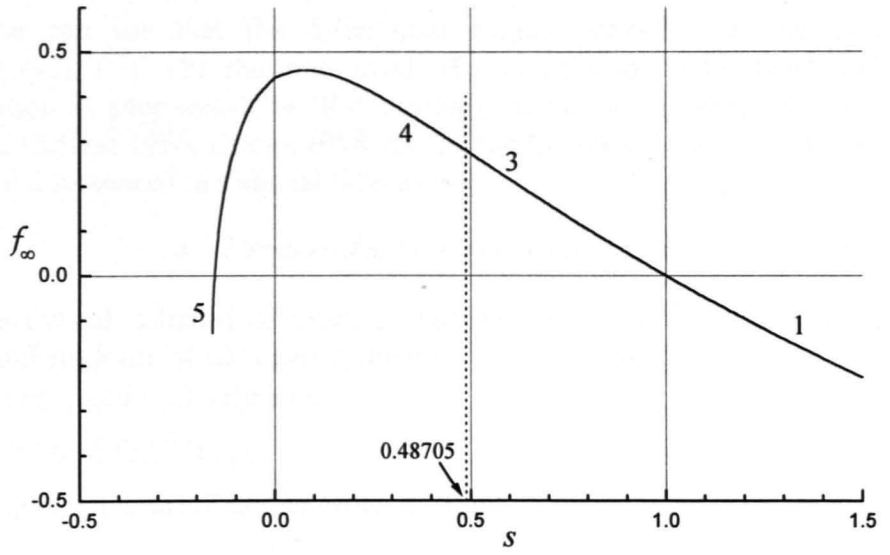

Figure 2. Solution of one-disk problem in the terms of ratio parameter. Value s=0.48705 separates solution branches 3 and 4 (See, also figures 3 and 11).

4. Orders of magnitude and linearized solution

4.1 Orders of magnitude at almost rigid rotation

Suppose, the imposed rotation is much larger than the differential rotation of liquid evoked by body force. Then the core rotates with an angular velocity close to that of the vessel. Since the flow is inertia dominated, it has the core and boundary layers. The core radial velocity v_0 is determined by the balance of driving magnetic body force due to RMF and braking Coriolis force:

$$\rho v_0 \Omega_d^* \sim F_\theta, \tag{20}$$

from which the estimate $v_0 \sim F_\theta/(\rho\Omega_d^*)$ follows. Thus, the sign of radial velocity depends on the direction of imposed rotation. An obtained obvious suggestion on the meridional flow direction change is consistent with the sign of centrifugal force drop driving the meridional recirculation. Differential rotation of the core causes a imbalance between the centrifugal force and radial pressure gradient in the boundary layer. The sign of centrifugal force drop depends on the direction of imposed rotation (Davidson & Hunt 1987). If the vessel and RMF co-rotates, then, obviously, the centrifugal force in the core is larger than in the boundary layer and, therefore, a radial inflow is generated. On the contrary, if RMF acts in the direction opposite to a strong vessel's rotation, then it can only slightly brake the core. Consequently, the centrifugal force in the core is less than in the boundary layer and the radial outflow occurs there.

Since the boundary layers are *ex hypotesis* thin, the radial velocity in these layers is much larger than in the core. Consequently, the Coriolis force is much larger than the driving body force and, thus, is balanced only by a shear: $\rho\Omega_d^* v_n \sim \rho\nu L\Delta\Omega/\delta^2$. A characteristic velocity of meridional flow is determined by the balance of the aforementioned drop of centrifugal force $O(\rho L(\Omega_0^2 - \Omega_d^{*2})) = O(\rho L\Omega_d^*\Delta\Omega)$ and frictional force $O(\rho\nu v_n/\delta^2)$. A characteristic Ekman boundary layer thickness $\delta \sim |\nu/\Omega_d^*|^{1/2}$ follows from two previous relations (Greenspan 1968). Now applying

(20), one can see that the differential angular velocity can be expressed as $\Delta\Omega \sim F_\theta/(\rho|\nu\Omega_d^*|^{1/2})$. On the one hand, the velocity of both swirl and poloidal recirculation is suppressed by IRV similarly to the steady magnetic field (Grants, Priede & Gelfgat 1996, Grants 1998, ch. 3). On the other hand, IRV has a possibility to control direction of meridional flow as well.

4.2 Linearized solution of original problem

An analytical solution of original problem (5–6) can be easily found using a dimensionless form of obtained estimates. Let us rewrite (5–6) for boundary layer variables $u(\zeta)$ and $v(\zeta)$ defined as

$$\Omega=\Omega_d+T|\Omega_d|^{-1/2}v(\zeta), \qquad H=T\Omega_d^{-1}u(\zeta), \qquad \zeta=|\Omega_d|^{1/2}(0.5+z),$$

neglecting small terms of higher order. A simple linear problem follows

$$v''=-u', \quad 4v'=u^{(4)} \tag{21}$$

$$u(\infty)=0.5, \; v(0)=u(0)=u'(0)=0. \tag{22}$$

Condition $u(\infty)=u_\infty=0.5$ follows from the force balance in the core. The solution of the linearized problem is well-known (e.g, Rogers and Lance 1960, Greenspan 1968):

$$v(\zeta)= u_\infty(1-\cos(\zeta)e^{-\zeta}) \tag{23}$$

$$u(\zeta)= u_\infty(1-(\sin(\zeta)+\cos(\zeta))\, e^{-\zeta}) \tag{24}$$

It can be expressed in terms of associated problem as follows: $h_\infty(\mathcal{R})=|\mathcal{R}-0.5|^{1/2}/(\mathcal{R}+0.5)$, that differs from the solution of linearized associated problem $h_\infty(\mathcal{R})=|\mathcal{R}|^{1/2}/\mathcal{R}$ (Priede 1993). Both are compared to the exact solution in figure 1.

5. Numerical similarity solution

Figure 3 depicts the results of numerical solution of the original selfsimilar problem (5–6) as well as the comparison to the linearized and exact boundary layer type solutions. The feasibility of a branch denoted by 1 at co-rotation and slight counter-rotation has been confirmed. A steady numerical solution disappears at $\Omega_d/\Omega^{ref}=-0.075$ ($\mathcal{R}=0.36$ or $\sigma=1/s=-0.16$) together with an unlimited growth of velocities. That agrees with the results of an unsteady numerical solution of the associated problem performed by Bodonyi (1978). He recovered a limit-cycle character of time-dependent similarity solution at $\sigma=-0.1$ ($\mathcal{R}=0.41$, $\Omega_d/\Omega^{ref}=-0.05$). Beyond $\sigma=-0.15$ ($\mathcal{R}=0.37$, $\Omega_d/\Omega^{ref}=-0.07$) his numerical solution diverged.

According to the investigations by Priede (1994), another branch denoted by 2 takes place in the range from $\mathcal{R}=0.325$ ($\Omega_d/\Omega^{ref}= -0.097$) where function $h_\infty(\mathcal{R})$ reaches its maximum (figure 1), down to $\mathcal{R}=-0.125$ ($\Omega_d/\Omega^{ref}=-0.83$). An indicative case of this branch with $\mathcal{R}=0$ or $s=-1$ corresponds to equally counter-rotating disk and liquid, which does not possess any solution (McLeod 1970). Priede concluded the solution of this branch to be unstable due to an abnormal dependence between the disk rotation and the rate of meridional recirculation.

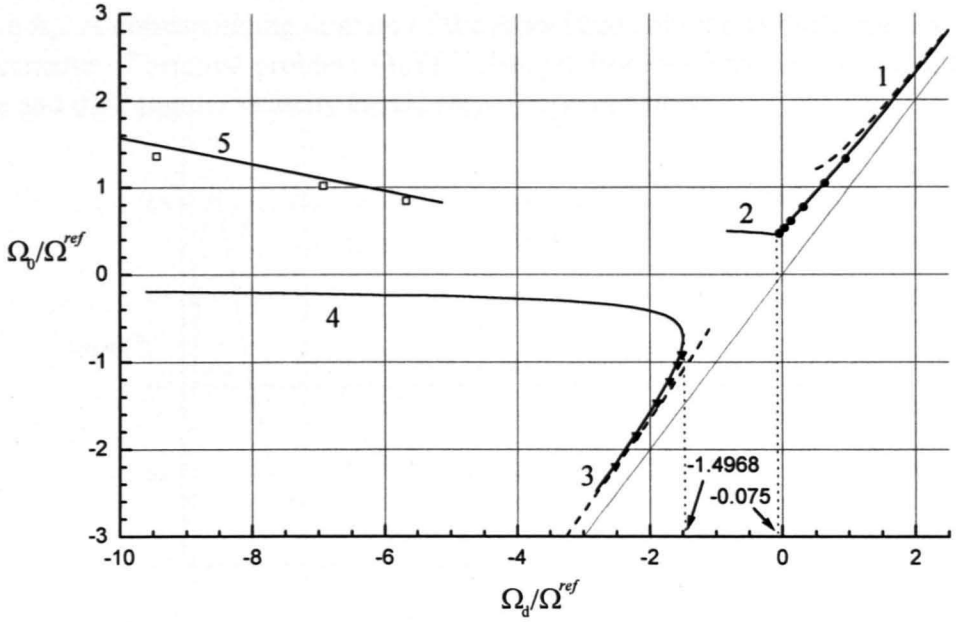

Figure 3. Core angular velocity versus disk rotation rate. — exact solution of associated problem (13–16); – – linearized solution of original problem (5–6); numerical solution of (5–6) is depicted by dots. Branches 3 and 4 appear simultaneously at $\Omega_d/\Omega^{ref}=-1.4968$ (See, also figure 11).

Lack of corresponding steady numerical solution agrees with this. However, the offered suggestion seems not convincing since it is based on the analysis of a steady solution behavior instead of the dynamic terms. Besides, our more careful investigation revealed that the analytical similarity solution disappeared already at $\mathcal{R}=0.29$ ($\sigma=-0.266$ or $\Omega_d/\Omega^{ref}=-0.12$). Thus, Branch 2 turns out quite narrow $\mathcal{R}\in[0.29; 0.325]$. Note that Bodonyi & Ng (1984) stated the disk similarity solution to be unstable below $\sigma=-0.03$.

Neither analytical nor numerical steady solution exists at further increasing of counter-rotation until the interaction parameter reaches the value $\Omega_d/\Omega^{ref}=-1.497$, when two branches of the analytical solution appear simultaneously (figure 3; see, also figure 11). Only one of them, namely, Branch 3 already examined in the limits of a strong counter-rotation (§4.2) was detected numerically. A variety of initial conditions have been tried. The von Kármán type analytical solution of Branch 4 has been taken as an initial condition at last. Nevertheless, the Ekman type solution of Branch 3 set in. The instability of force balance in the core of Branch 4 type solution is discussed below in §8.1.

We detected another steady numerical solution denoted by 5 at a rapid counter-rotation $\Omega_d/\Omega^{ref}<-5.5$. It developed in an initially resting or co-rotating layer. In spite of rapid vessel's counter-rotation, the core co-rotated with RMF (See, figure 3). Moreover, the core angular velocity increased together with a rate of vessel's counter-rotation ($\partial\Omega_0/\partial\Omega_d<0$). A corresponding associated solution (denoted by 5) possesses to the well-known solution at vessel's counter-rotation (figure 1 and 2). Priede (1994) has missed the analytical solution already at $\mathcal{R}=-0.38$ ($s=-0.134$), before the core axial velocity h_∞ changed sign. Notice, that the force balance in the core (11) requires a positive $h_\infty(\mathcal{R})$ at $\mathcal{R}>-0.5$ ($\Omega_0>0$). Thus, the solution ranged between $\mathcal{R}=-0.5$ up to $\mathcal{R}=-0.3664$ ($s=-0.1542$), when h_∞ reaches zero, has no consequences to the original problem. However, the solution continues up to $\mathcal{R}=-0.3617$ ($s=-0.16054$) with a

positive h_∞. A corresponding domain of the associated solution is quite narrow, while the parameter of original problem Ω_d/Ω^{ref} changes from -5.5 to $-\infty$. Hence, the ratio of core and disk angular velocity Ω_0/Ω_d stays nearly constant.

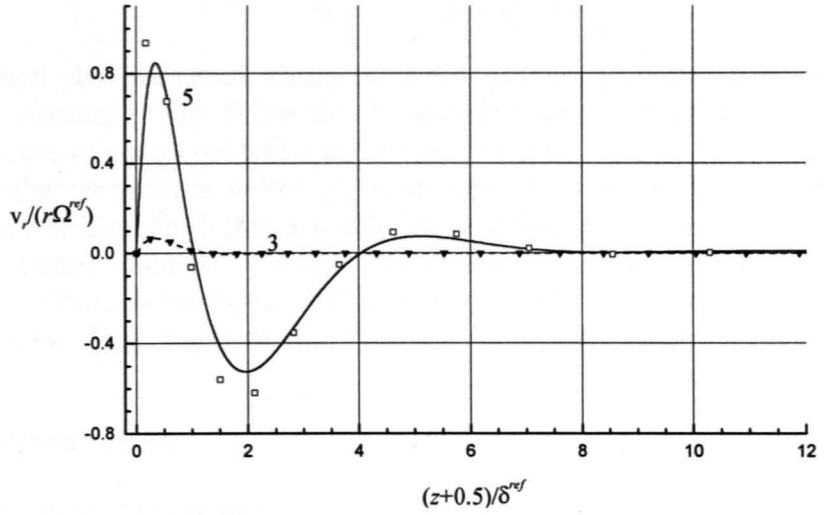

Figure 4. Axial profile of Branches 3 and 5 type solution at $\Omega_d/\Omega^{ref}=-5.67$. The results of numerical and analytical solution are depicted by dots and lines, respectively.

Branch 5 type steady solution has a much higher rate of the differential rotation and, hence, the meridonal recirculation if compared to Branch 3 (see, figure 4). The meridional flow is redistributed between two eddies (figure 5) depending on the rate of imposed rotation. In the limits of a very strong vessel's counter-rotation, the core circulation tends to zero and the entire meridional flow is localized in the boundary layer. A zero core circulation gives rise of the infinite growth of core angular velocity. It implies a limit of infinite imposed rotation accompanied by infinite opposite rotation of the core surrounded by infinitesimally thin boundary layers in the original solution.

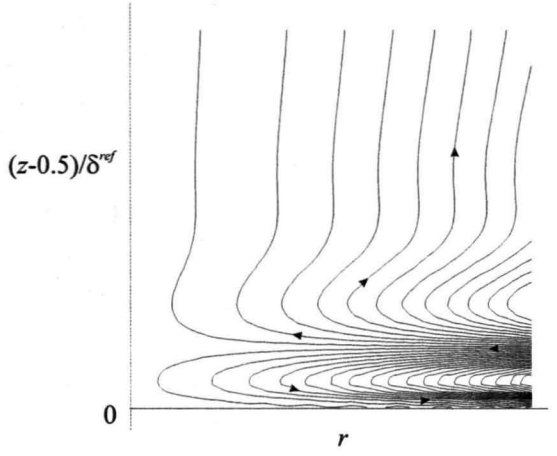

Figure5. Streamlines of meridional flow for Branch 5 steady solution. $\Omega_d/\Omega^{ref}=-5.67$

It is worth mentioning that the self-similar model does not control the balance of angular momentum. So, e.g., only 57% of the angular momentum production due to body force is driven out by shear on the resting end walls (Davidson 1992). The residue is carried away by radial outflow in the core. The ratio of frictional outflux to

magnetic production of angular momentum can be used as a measure of this imbalance:

$$S = \frac{2\Omega'(z=-0.5)}{\mathrm{T}} = \frac{g'(\xi=0)}{2h_\infty(\mathcal{R}+0.5)} \tag{25}$$

Notice that the linearized steady solution (23–24) provides a conservation of angular momentum (S=1). Since the linearized solution underestimates differential rotation in case of counter-rotation and overestimates it in case of co-rotation (figure 3), the angular momentum deficit (S>1) or residue (S<1) appears, correspondingly. The solution of Branch 5 has a much larger differential rotation and, hence, the angular momentum deficit is much larger than the production (S>10). Hence, a corresponding laterally bounded 2D flow should be supported by an additional forcing outside the core. An example of such flow is given below in §6.

6. 2D numerical solution

Neither analytical nor numerical self-similar steady solution was found in the range of counter-rotation $\Omega_d/\Omega^{ref} \in [-1.5,-.12]$. So, what actually happens to the flow in this range? Besides, a question on the ability of self-similar solution to describe the real flow in the cylinder of finite dimensions arises. In order to answer these questions, we performed a direct numerical 2D simulation. An exponential finite difference scheme obtained by the integral identity technique as well as Peaceman–Rachford implicit alternating direction time-stepping scheme were employed (Priede 1993). We considered an actual source of swirl $\mathrm{Te}\,f(r,z)$ instead of the idealized constant one T used so far in the selfsimilar formulation.

A numerical 2D simulation confirmed the results of similarity solution for Branches 1 and 3. The boundary layer thickness and characteristic velocities scaled in agreement with the estimates (§4). A considerably oscillating pattern of Bödewadt's type boundary layer about $\mathcal{R}$=0.5 was replaced by an Ekman type behavior at almost rigid rotation $|\mathcal{R}|>>1$. Solutions at rapid co- and counter-rotation of the vessel differed in the direction of meridional velocity only, similarly as solution (23–24) describes both cases. The increase of imposed rotation increased the role of force distribution in the core. We shall see in §7 that at almost rigid rotation the radial profile of the core differential angular velocity adjusts to the body force averaged over the height.

A significantly thicker boundary layer appeared near the side wall at almost rigid rotation. According to Stewartson (1957), it has $O(|\Omega_d|^{-1/4})$ thickness and, so, is somehow analogous to the magnetohydrodynamic side layer at the wall parallel to the field (Hunt & Shercliff 1971). Contrary to the MHD side layer, an angular velocity drop in the axial direction vanishes, decoupling the meridional flow. Thus, the almost rigid flow in the system under consideration turns out physically simple. The side layer is briefly examined below in §7.

The numerical simulation showed that the flow becomes essentially two-dimensional in the range of absent similarity solution. That implies the appearance of a radial non-uniformity of angular velocity distribution even in the very vicinity of the axis (figure 6, *a* and *b*) as well as separating boundary layers (figure 6, *a* and *c*). An intermediate stage includes the development of an additional couple of meridional flow loops near the side wall (figure 6, *d*). As a result, the boundary layer at side wall grows much wider (figure 6, *b*). A more detailed examination of the flow ranged to

the absent similarity solution lies beyond the scope of our investigation. These flow structures are expected to be less stable and, hence, suitable for intense stirring.

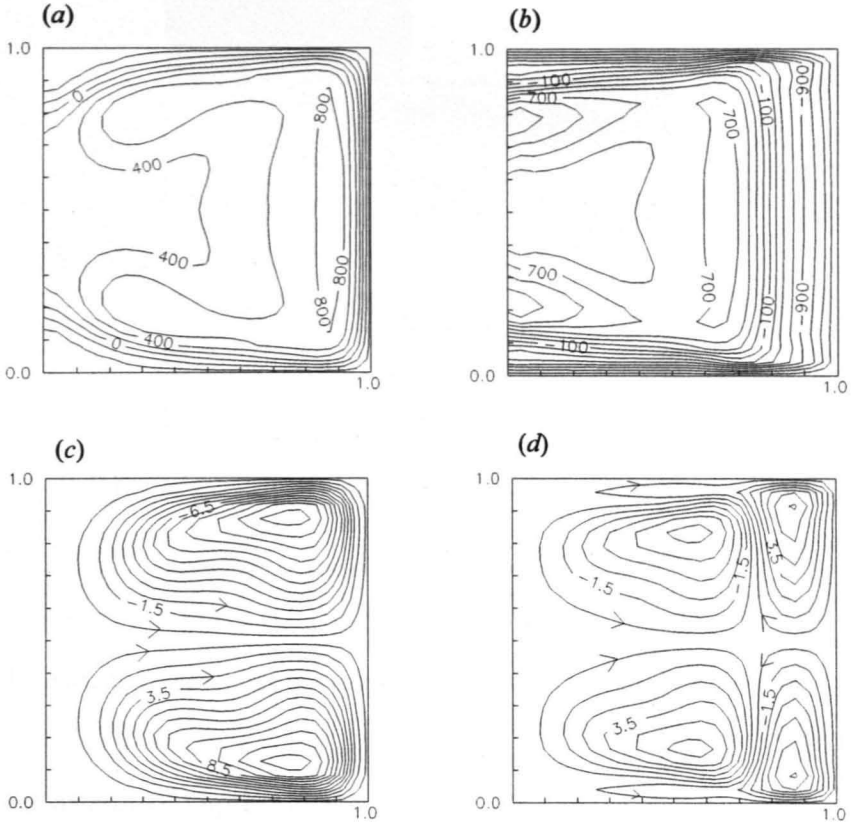

Figure 6. Isolines of angular velocity (a, c) and streamlines of meridional flow (b, d) at: Ω_d/Ω^{ref}=-0.25 (a, b) and Ω_d/Ω^{ref}=-0.75; (c, d).

A probably aphysical Branch 5 with a huge deficit of angular momentum has been detected in the selfsimilar solution. Evidently, such flow should be supported by an "injection" of angular momentum outside the core. One can realize such a support by RMF forcing beyond "open" side wall or by co-rotating with the RMF "closed" side wall. The "open" side wall implies the disks surrounded by an unbounded liquid, but "closed" side wall corresponds to the discs enclosed by a cylinder (Brady & Durlofsky 1987). A certain "open" side wall occurs, for example, below the edge of crystal in the Czochralski process (Figure 7). Besides, the side wall of the crucible serves as a "closed" wall in this case. Thus, the flow could pick up a necessary amount of angular momentum to provide a "wasteful" boundary layer of Branch 5 type in two regions: (i) at the free surface and (ii) near the side wall of co-rotating cruicible. We performed numerical 2D simulation in following case: $\Omega_{crystal}$=−7000; $\Omega_{cruicible}$=700; $\Omega^{ref}=T^{2/3}$=1170 ; $R_{crystal}$=0.5R, where $R=R_0/L$=1 is dimensionless radius of crucible, or the aspect ratio. The steady solution revealed a boundary layer of Branch 5 under the crystal depicted in figure 7. Thus, the numerical 2D solution confirmed the feasibility of second branch at rapid counter-rotation.

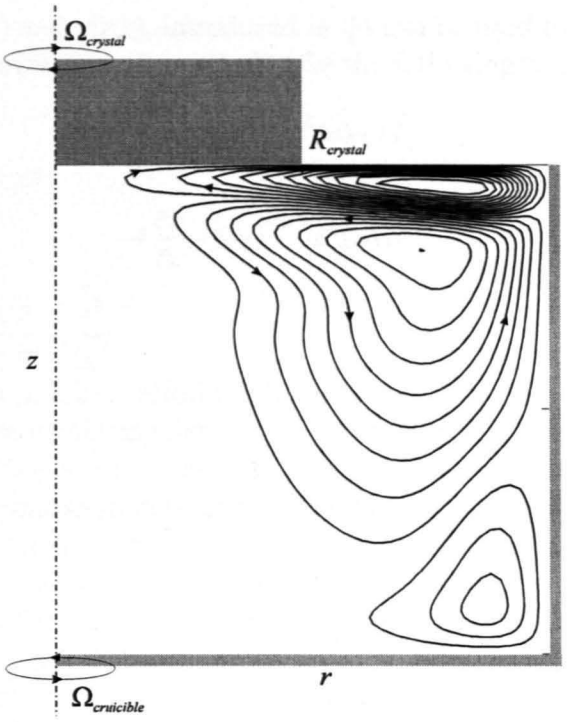

Figure 7. Example of Branch 5 type boundary layer in the Czohralski crystal growth configuration.

7. Side layer at almost rigid rotation

The 2D numerical simulation of the RMF induced flow under conditions of almost rigid rotation revealed a constant along the height angular velocity distribution with a rather thick boundary layer near the side wall. A radial variation of the angular velocity appeared in the core due to a non-uniform force distribution. In order to simplify further investigation of principal features of this side layer, let us restrict ourselves to a constant force distribution $f(r,z)=1$ temporary. A corresponding characteristic angular velocity distribution is depicted in figure 8.

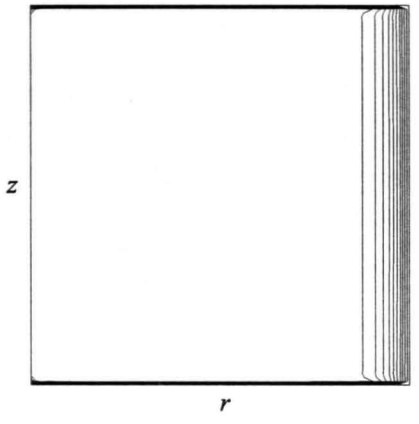

Figure 8. Isolines of a characteristic angular velocity distribution for a rapid imposed rotation ($f(r,z)\equiv 1$).

Functions $u(r,z)$ and $v(r,z)$, introduced in §4 can be used to describe the side layer, too. Then the linearized equations (1–3) take the following form:

$$\frac{\partial u}{\partial z} = |\Omega_d|^{-1/2} \mathcal{L}^2(v) + 1, \tag{26}$$

$$-4\frac{\partial v}{\partial z} = |\Omega_d|^{-3/2} \mathcal{L}^4(u), \tag{27}$$

where $\mathcal{L}^2 = \frac{\partial^2}{\partial r^2} + \frac{3}{r}\frac{\partial}{\partial r} + \frac{\partial^2}{\partial z^2}$.

Evidence of an axially uniform differential angular velocity distribution now is seen from (27). The whole angular velocity drop occurs in thin corner regions of usual thickness $O(|\Omega_d|^{-1/2})$ separating the side layer from the rigid end-walls. Consequently, the meridional recirculation decouples from the angular velocity in the side layer. At the same time, the angular velocity distribution remains coupled with recirculation via the Coriolis force. Since the angular velocity is constant along the height, the meridional flow is generated in the corner. Hence, the corner is expected to play the key role. Its radial scale is much larger than the axial one. Consequently, the corner flow is described by set (21–22). The most important feature of its solution (23–24) is the equivalence of functions u and v in infinity, i.e., on the boundary between the side layer and the corner. Let us split the solution for angular velocity in the side layer as $v(r,z)=v_0(r)+v_1(r,z)$, where v_0 is the main part being constant along the height. Notice that it should match the corner solution, i.e., $v_0(r)=v_\infty(r)=u_\infty(r)$. Now we can rewrite equation (26) for the side layer as follows:

$$\frac{\partial u_0}{\partial z} = \frac{1}{|\Omega_d|^{1/2}}\left(u_\infty''(r) + \frac{3}{r}u_\infty'(r)\right) + 1, \tag{28}$$

where u_0 is the main part of axial velocity. The right-hand side does not depend on the axial coordinate. Thus, the main radial velocity $\partial u_0/\partial z$ should be constant along the height and, consequently, $u_0(r,z)=-2u_\infty(r)z$, to match the corner solution. An asymptotic solution of (28) for large $|\Omega_d|$ has a $O(|\Omega_d|^{-1/4})$ thickness, discussed by Stewartson (1957, 1966):

$$u_\infty(r)=0.5(1-\exp(-|4\Omega_d|^{1/4}(R-r)), \tag{29}$$

where R is dimensionless radius or the aspect ratio of vessel.

Figure 9 depicts the comparison of 2D numerical solution and asymptotic solution (29) at $T=10^5$, $\Omega_d=40000$, $R=1$. In real applications, however, the aspect ratio may be much less than unity and, therefore, boundary layer may turn out of the order of radius. A limit for solution (29) applicability can be estimated from (28) as $3/(R|4\Omega_d|^{1/4})<O(\varepsilon)$, where ε is maximum tolerance.

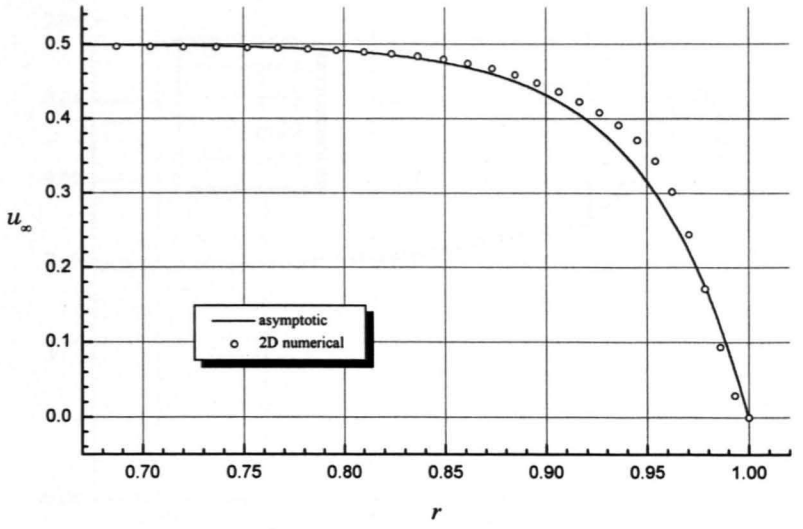

Figure 9. Radial profile of side layer at almost rigid rotation. $T=10^5$, $\Omega_d=40000$, $R=1$.

Evidently the main part $u_0(r,z)=-2u_\infty(r)z$ does not satisfy the boundary condition $\partial u/\partial r=0$ ($r=R$) for axial velocity neither equation (27). Thus, some correction $u_1(r,z)$ and, consequently, $v_1(r,z)$ should be added. Substituting a corrected solution into (26–27), the problem for u_1

$$\frac{|\Omega_d|^{-2}}{4}\mathcal{L}^6(u_1)+\frac{\partial^2 u_1}{\partial z^2}+\frac{|\Omega_d|^{-2}}{4}\mathcal{L}^6(u)=0, \tag{30}$$

$$\left.\frac{\partial u_1}{\partial r}\right|_{r=R}=\left.\frac{\partial u_0}{\partial r}\right|_{r=R}\approx\frac{\sqrt{2}}{2}|\Omega_d|^{1/4} \tag{31}$$

follows. The equation is singularly perturbed and, thus, an inner boundary layer of $O(|\Omega_d|^{-1/3})$ thickness must appear (Stewartson 1957, 1966). A characteristic value of the correction now can be estimated from boundary condition (31) $O(u_1)=|\Omega_d|^{1/4}\delta_\tau=|\Omega_d|^{-1/12}$, where δ_τ is thickness of the inner layer. A correction to angular velocity can be estimated now from (27) $O(v_1)=|\Omega_d|^{-3/2}\delta_\tau^{-4}O(u_1)=|\Omega_d|^{-1/4}$ that is $O(u_1)$ times smaller than for the case considered by Stewartson (1957). In order to obtain more information on this correction, we performed a direct numerical simulation ($|\Omega_d|=4\times10^4$). Figure 10 depicts the results of calculation for correction to radial velocity $\frac{u_1}{-2z}=\frac{u-u_0}{-2z}$, where u is numerical solution. One can see that a contribution of u_1 does not exceed ten percents of maximum u_0. Taking into account its poor dependence on imposed rotation, we concluded that the primary solution (29) provides accuracy sufficient for intended practical needs.

So far we ignored the body force distribution. However, it plays an important role in the core if its rotation is almost rigid. The angular velocity profile there adjusts the force distribution $\bar{f}(r)$ averaged over the height. Let us consider an actual force distribution $f(r, z)$ instead of idealized unity source in (26) and integrate the equation along a line passing between the both Ekman layers at a fixed radius. Then the relation $u_\infty(r)=0.5\bar{f}(r)$ follows for the core, where diffusive terms are negligible.

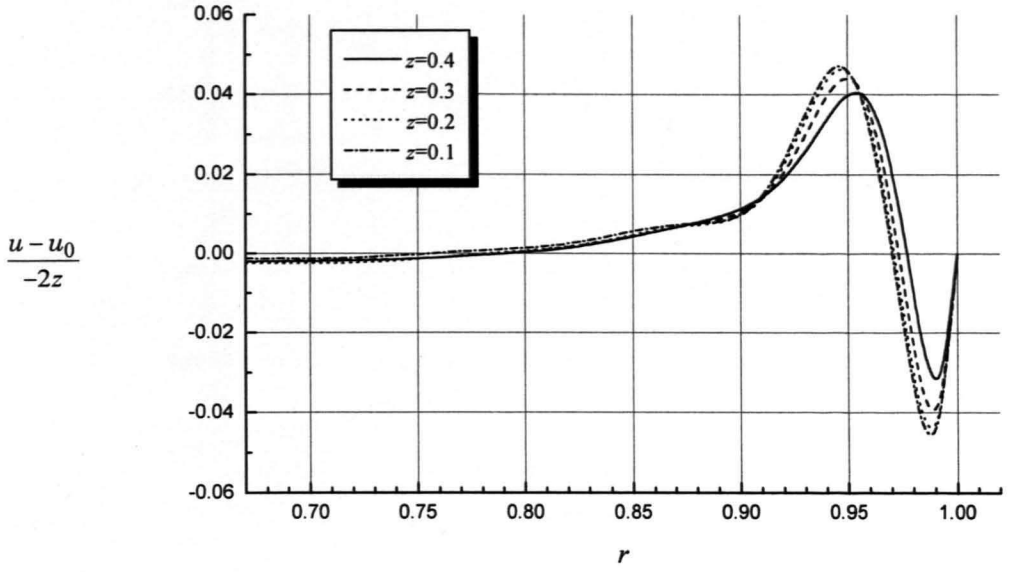

Figure 10. Correction to main radial velocity.

8. Stability

8.1 Instability of force balance in the core of von Kármán type solution

The instability of force balance in the core of von Kármán type solution (Branch 4) can be easily shown. It takes place due to a positive derivative of the Coriolis force with respect to differential angular velocity $\partial F_C/\partial\Delta\Omega$. It implies that the perturbation of a steady core angular velocity reflects in the force balance giving rise of its further growth. Coriolis force is $F_C=-2v_0\Omega_0=-2(v_0(\Omega_d+\Delta\Omega))$. Its derivative can be expressed in terms of (7–11) as follows:

$$\frac{\partial F_C}{\partial\Delta\Omega}=-2\left(v_0+\Omega_0\frac{\partial v_0}{\partial\Delta\Omega}\right)=-H^{ref}\left(h_0(\infty)+g_0(\infty)\frac{\partial}{\partial\mathcal{R}}(h_0(\infty))\left(\frac{\partial}{\partial\mathcal{R}}(g_0(\infty)-g_0(0))\right)^{-1}\right) \quad (32)$$

If the core radial velocity is directed towards the axis ($v_0<0$), the flow is potentially unstable. The second term, however, can eliminate instability due to an influence of perturbation on the meridional flow. One can conclude from (32) that a flow at counter-rotation with a lower core angular velocity and a higher radial velocity (i.e., Kármán type Branch 4) is less stable. Expressions

$$h_0(\infty)=h_\infty^{2/3}(2(\mathcal{R}+0.5))^{-1/3},\qquad (g_0(\infty)-g_0(0))=(2h_\infty(\mathcal{R}+0.5))^{-2/3},$$
$$g_0(\infty)=(g_0(\infty)-g_0(0))(\mathcal{R}+0.5)$$

follows from (12). Substituting in (32), the stability criterion yields

$$h_\infty\left(1+(\mathcal{R}+0.5)\frac{0.5h_\infty-(\mathcal{R}+0.5)\partial h_\infty/\partial\mathcal{R}}{h_\infty+(\mathcal{R}+0.5)\partial h_\infty/\partial\mathcal{R}}\right)>0 \quad (33)$$

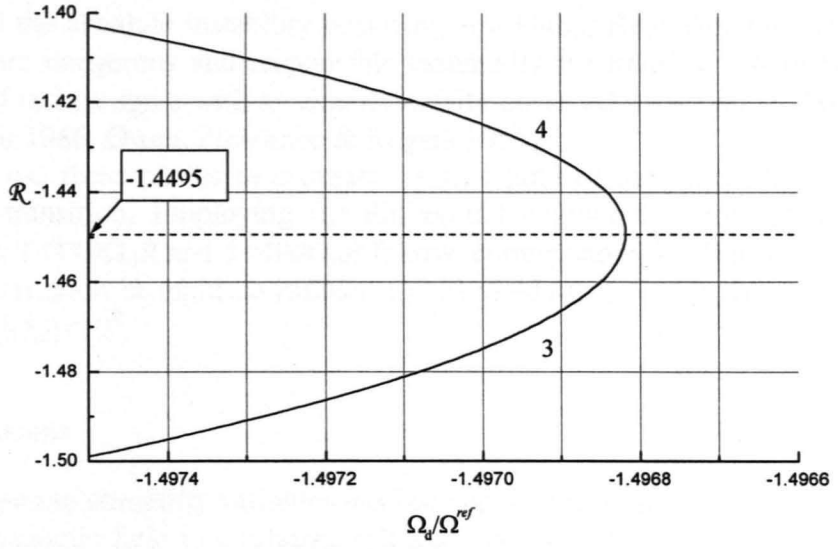

Figure 11. Bifurcation of similarity solution at counter-rotation. Stability limit (33) depicted by a doted line.

The expression is positive for the entire domain of $\mathcal{R}$ except Branch 4. Notice, that threshold value $\mathcal{R}$=–1.4495 coincides with the bifurcation point within four decimal digits, at least (figure 11). Thus, a von Kármán type solution 4 of original problem is unstable. This conclusion agrees with the numerical solution, where the Branch 3 steady solution set in even from Branch 4 initial state.

8.2 Rayleigh criterion at almost rigid rotation.

Similarity of the side layer to the Taylor–Couette flow between cylinders has been employed from very first works in field of RMF driven flow (Moffat 1965). The Taylor–Couette flow is stable if the Rayleigh criterion is satisfied. It requires a positive derivative of squared angular momentum $\partial(\Gamma^2)/\partial r=\partial/\partial r(v_\theta^2 r^2)>0$ (see, e.g., Greenspan 1968). If the core counter-rotates to RMF, the Rayleigh criterion is satisfied. Indeed, the absolute value of angular velocity increases in the radial direction, since RMF brakes the core.

At almost rigid co-rotation the criterion is $\partial(\Gamma^2)/\partial r\approx 2\Omega_d r^4(\partial\Delta\Omega/\partial r+2\Omega_d/r)>0$. Let us use asymptotic solution (28) to estimate $\partial\Delta\Omega/\partial r$. Then the satisfaction of the Rayleigh criterion is guaranteed by $T|\Omega_d|^{-1/4}<\Omega_d/R$, or $T<\Omega_d^{5/4}/R$.

8.3 Stability of Ekman layer.

Stability of boundary layers occurring on a horizontal wall in rotating flow has been studied both theoretically and experimentally for several decades. A review of these studies as well a recent investigations recovering the absolute instability are given by Lingwood (1997). An inviscid crossflow instability of Ekman type flow occurs at Re=125 observed experimentally by Faller (1963). It agrees closely with Lilly's (1966) and Lingwood's (1997) calculations Re=115 and 116, correspondingly. The flow has a second unstable mode which is stable in inviscid limit and has a lower critical Reynolds number Re=56 (Lilly 1966, Melander 1983). The Reynolds number is defined here as $Re=\Delta v_\theta l/\nu$; Δv_θ is differential azimuthal velocity of the disk, l is characteristic boundary layer thickness $l=(\nu/\Omega_d)^{1/2}$. However, Lingwood (1997)

concluded the absolute instability occurring at a higher Reynolds number Re=198 to be far more dangerous and responsible essentially for transition to turbulence. Her theoretical results agree with an experimentally observed transition at Re≈200 (Faller and Keylor 1966, Owen, Pincombe & Rogers 1985).

Let us use these results to estimate the threshold of first instability and laminar-turbulent transition. Employing the differential angular velocity obtained in §4.2, conditions $T<110\Omega_d R$ and $T<400\Omega_d R$ follow, correspondingly. The comparison to the Raylaigh criterion at rapid co-rotation (§7.2) yields that side layer become unstable first, if $O(|\Omega_d|)<10^8$.

9. Conclusions

Von Kármán similarity variables has been applied to study a swirling flow due to a rotating magnetic field in a rotating cylinder. As showed by Priede (1993, 1994), the problem reduces to the so-called one-disk problem. Different solutions of this classic problem are reviewed by Zandbergen and Dijkstra (1987). However, only some parts of this solution has consequences to the original problem. Besides, a steady solution, corresponding to the von Kármán type flow, turns out unreachable due to an unstable force balance in the core of the original flow. A direct numerical solution in both self-similar and axially symmetric (2D) formulations confirmed the feasibility of both Ekman type branches. So, one of practically most important features, namely, the possibility to control the meridional flow intensity and direction has been confirmed. A solution with a small negative ratio parameter s about –0.16 and axial velocity towards the disk was achieved numerically as well. The latter has a closed loop of meridional flow inside the boundary layer. A corresponding solution of the original problem appears at a rapid counter-rotation. The solution has a huge angular momentum deficit, so it cannot be observed in a laterally bounded flow without additional forcing. However, such boundary layer is feasible in certain technological processes with differently rotating rigid boundaries.

Self-similar analysis can not answer the question on the flow in an intermediate range of vessel's counter-rotation, when simlarity solution is absent. A corresponding numerical 2D simulation revealed a peculiar flow patterns with separating boundary layers and additional couples of secondary recirculation.

The numerical simulation showed an increasing of the side layer with vessel's rotation rate, until the condition of almost rigid rotation is satisfied. Further increasing of the imposed rotation gives rise to the constant along the height angular velocity in the side layer. Thus, the recirculation remains coupled with the angular velocity in the corner regions only. As a result, an asymptotic similarity of radial and angular velocity profiles is established. A simple singularly perturbed equation yields the thickness of side layer $O(|\Omega_d|^{-1/4})$. This primary boundary layer solution does not satisfy the no-slip condition for axial flow. Therefore, an inner boundary layer of $O(|\Omega_d|^{-1/3})$ thickness appears. Contrary to Stewartson's (1957) solution, only axial velocity has a discontinuity of primary boundary layer solution on the sidewall. It yields the correction $O(|\Omega_d|^{-1/12})$ and $O(|\Omega_d|^{-1/4})$ for radial and angular velocities, respectively.

The Rayleigh criterion is satisfied, if the core counter-rotates to the magnetic field, as well as for a rapid co-rotation. Thus, the imposed rotation stabilizes the side layer. Besides, the imposed rotation reduces the differential core rotation and boundary layer thickness, so stabilizing the Ekman type layers as well. The comparison of instability

estimates yields that the side layer at co-rotation is less stable, if $O(|\Omega_d|)<10^8$ that completely includes the crystal growth conditions. The Rayleigh criterion is satisfied if core counter-rotates to the magnetic body force. Hence, the imposed rotation directed opposite to the driving body force is expected to produce a more stabilizing action.

REFERENCES

Bodonyi, R. J. & Ng, B. S. 1984 *JFM* 144, 311-28

Bodonyi, R. J. 1978 *Q. J. Mech. Appl. Math.* 31, 461-72

Brady, J. F. & Durlofsky, L. 1987 *JFM* 175, 363-394

Davidson, P. A. 1992 *JFM 245, 669-699*

Davidson, P. A. and Hunt, J. C. R. 1987 *JFM* 185, 67-106

Dijkstra, D. 1978 *TW-Memo. 205*, Dep. Math., T.H.T. Enschede, Neth.

Dold, P. & Benz, K. W. 1995 *Cryst. Res. Technol.* 30, 1135-1145

Faller, A. J. 1963 *JFM* 15, 560-576

Faller, A. J. and Keylor, R. E. 1966 *J. Atmos. Sci.* 23, 466-480

Fischer, B., Friedrich, J., Kupfer, C., Müller, G. and Vizman, D. 1997 In: *Proc. on 3rd Int. Conf. on Energy Transfer in MHD Flows.* Vol. 2, pp. 337-342. Aussois, France.

Gelfgat, Yu. M. and Priede, J. 1995, *Magnetohydrodynamics* 32, 1/2

Gelfgat, Yu. M. and Priede, J. 1996, *Magnetohydrodynamics* 33, 3

Gelfgat, Yu. M., Priede, J., Sorkin, M. Z. 1991 *Proceed. on Int. Conf. on Energy Transf. in MHD Flows*, France, pp. 181-186.

Grants, I. and Gelfgat, Yu. M. 1997 In: *Proceed. of 3rd Int. Conf. on Transf. Phen. in MHD flows*, Aussois, France. Vol. 2, pp. 351-356.

Grants, I. 1998 *Magnetically driven swirling flow guided by steady magnetic field and imposed rotation.* Thesis, Salaspils, Latvia

Grants, I., Priede J., Gelfgat Y. M. *1996 Magnetohydrodynamics* 33, 3

Greenspan, H. P. 1968 *The Theory of Rotating Fluids*. Cambridge University Press.

Hunt, J. C. R. and Shercliff, J. A. 1971 *Ann. Rew. Fluid Mech., 3, 37*

Langlois, W. E. 1985 *Ann. Rev. Fluid Mech.* 17, 191-215.

Lilly, D. K. 1966 *J. Atmos. Sci.* 23, 481-494

Lingwood, R. J. 1997 *JFM* 331, 405-428

McLeod, J. B. 1970 *Mathematika* 17, 243-49

Melander, M. V. 1983 *JFM* 132-293

Moffat, H. K. 1965 *JFM* 22, 521-528 (Corrigendum 1973 *JFM* 58, 823)

Owen, J. M., Pincombe, J. R., Rogers, R. H. 1985 *JFM* 155, 233-265.

Priede, J. 1993 *Theoretical study of a flow in an axisymmetric cavity of finite length, driven by a rotating magnetic field.* Thesis, Salaspils

Priede, J. 1994 In: *Proc. on 2nd Int. Conf. on Energy Transfer in MHD Flows.* Vol. 1, pp. 87-97, Ausois, France

Rogers, M. H. & Lance, G. N. 1960 *JFM* 7, 617-31

Shlicting, H. 1979 *Boundary Layer Theory*, 7th edn. McGraw-Hill.

Stewartson, K. 1957 *JFM* 3, 17

Stewartson, K. 1966 *JFM* 26, 131-144

Trombetta, P., Marty, P., Martin Witkowski, L. and Tomasino, T. 1997 In: *Proc. on 3rd Int. Conf. on Energy Transfer in MHD Flows.* Vol. 2, p. 463. Aussois, France.

Zandbergen, P. J. and Dijkstra, D. 1987 *Ann. Rev. Fluid Mech. 19, 465-91*

Chapter V

Simplified theoretical model of hydrodynamically guided solidification

A simplified theoretical model for the solidification interface shape prediction is introduced and tested. We linearised a coupled hydrodynamic-solidification problem about the state with a flat interface. In such a way we split the problem into a hydrodynamic part with a flat solid-liquid front and a solidification part with a calculated heat flux from the liquid phase. The method allows obvious conclusions on optimum heat conditions near the solidification interface providing its flatness and maximum pulling velocity at the same time. Comparison to the results by *FLUENT* package showed that the method provides a reasonable accuracy even for a noticeably deformed interface shape. Another part of the contribution deals with an influence of artificial swirling-recirculating flow due to a rotating magnetic field with an optional superimposed steady axial field or rotation of crucible. Estimates of necessary forcing to suppress buoyancy are given and illustrated by numerical simulation. The limits of possibilities to control heat regime (consequently, the interface shape and pulling velocity) are discussed and illustrated.

1. Introduction

The current chapter concerns an artificial flow as a means to optimise the solidification interface shape during crystal growth. Traditionally solidification problems are solved numerically on adapting meshes or in enthalpy-porosity formulation on a fixed mesh (Voller & Cross 1980, Bennon & Incropera 1987, Voller & Prakash 1987). Both methods are widely used including commercial codes. However, the numerical simulation of full problem takes much time and gives less understanding of the physical process. The shape of solidification front has a significant influence on the quality of produced crystals. There are optimum growth conditions with a flat solidification interface and a strong and stable motion of melt. These conditions are expected to ensure a minimum concentration of dislocations. I split a coupled problem, in order to obtain an obvious model of guided solidification. Such model is expected to provide more understanding of the process and, hence, possibilities of its control. Besides, it can be used in estimates as well as for testing of numerical codes. The method is originally intended for the vertical gradient freeze growth, but it can be easily generalised.

The shape of solid-liquid interface is closely linked to a heat flux between both phases. If crystals are small, then the heat transfer is diffusive and completely determined by thermal boundary conditions. In recent technologies, however, the size of grown crystals is more and more enlarged. If a properly defined Peclet number is more than unity, then the melt motion can significantly influence the heat transfer near the solid-liquid front and, hence, its shape, too. Thus, there are two tools to control the interface shape: thermal boundary conditions and the artificial flow of melt controlling a convective heat flux. As mentioned, there is an optimum solidification interface that

simply has a flat shape. Suppose, both controlling tools allow to obtain an almost flat quasi-steady interface. In order to find corresponding conditions, we can linearise a full problem about this optimum state. It implies neglecting of the influence of actual shape of almost flat interface on the melt motion and heat transfer within it. Having solved a hydrodynamic-thermal problem with an isotermic flat interface, we receive heat flux from the liquid phase. Together with a latent heat flux due to pulling and heat transfer in the solid phase it determines the shape of actual quasi-steady almost flat front. Besides, I considered a non-isotermic flow of melt. Natural motion occurs due to buoyancy. An artificial swirling-recirculating flow of conducting liquid with a number of favourable properties (Priede 1993) can be induced by a rotating magnetic field (Moffat 1965, Davidson 1992). Superimposed actions such as a steady axial magnetic field (Grants, Priede & Gelfgat 1996, Grants 1998, ch. 3) or imposed rotation of crucible (Priede 1993, 1994, Grants 1998, ch. 4) significantly widen possibilities to control the induced base flow and its stability. A first question arises on necessary strength of imposed forcing to suppress buoyancy, i.e., to make the flow completely artificial. Another question is the influence of considered artificial flow on a heat flux through the solidification interface and its shape.

The obtained method reveals a close relationship among heat flux from the melt, pulling velocity and shape of quasi-steady solidification interface. It follows from this relationship that optimum growth conditions are provided by a minimum heat flux with a uniform distribution, especially in the middle part of new solidified crystal. Our numerical simulation showed that the buoyancy increased this flux in comparison to a purely diffusive regime. A swirling-recirculating flow due to a rotating magnetic field (RMF) of sufficient strength suppresses the buoyancy and changes the direction of meridional flow. As a result, the heat flux can be significantly reduced. An imposed steady magnetic field (SMF) or rotation of crucible promotes a transition to a swirl dominated flow and provides additional options to improve the thermal conditions.

Section 2 introduces the model and governing equations. A link is established for the shape of quasi-steady solidification interface, heat flux conditions on it and pulling velocity in §3. Estimates of necessary forcing are made in §4. Section 5 discusses the influence of artificial flow on the heat transfer. Section 6 proceeds with the main results of numerical simulation. The summary is given in §7.

2. Model and equations

Consider a solidification problem in a cylindrical vessel schematically depicted in figure 1. Basic assumptions of our model are:

(i) Melt motion considerably influences the solidification interface $\zeta^*(r)$. In terms of dimensionless criteria it requires the Peclet number more than unity.

(ii) A guided artificial flow allows to transform the interface into almost flat.

Besides, the solidification interface was considered to be isotermic and quasi-steady. A non-isotermic interface may take place when a binary system solidifies. We neglected a possible morphological instability and consequent dendrite growth with respect to a strong azimuthal flow due to a rotating magnetic field considered for the generation of artificial flow (Priede 1993, 1994, Grants *et al.* 1996, Grants 1998, ch. 1–4). A condition of quasi-steady interface shape requires that its change in time is much slower than pulling velocity $\partial\zeta^*/\partial r << u_p$. This condition is consistent with our task to keep the front as flat as possible. Under these assumptions a full solidification

problem can be easily split. First, let us find a heat flux through a flat isotermic interface $\zeta^*(r)=0$ solving a corresponding hydrodynamic-thermal problem in the melt.

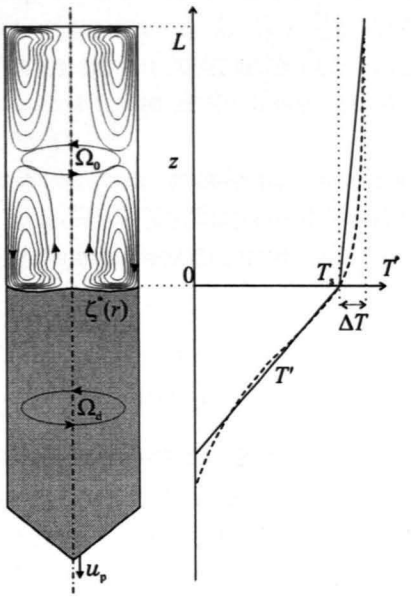

Figure 1. Sketch of the model.

We assumed fixed temperature profile on crucible surface as schematically shown in figure 1. Besides, we substituted an actual temperature distribution by a stepwise linear function that is characterised by a temperature drop ΔT in the liquid phase and a temperature gradient T' on the crystal surface. Of course, such assumption seems inappropriate for a modelling of real process. However, our task was mostly the developing and testing of the method itself rather than the investigation of specified technological process. Thus, to avoid less important details, we restricted ourselves to a minimum set of parameters.

The assumptions for heat transfer in the liquid phase included axial symmetry, laminar motion, lack of volumetric heat sources as well as Bussinesq approximation for buoyancy. Axial symmetry is ensured by a strong swirling flow. The motion is stabilised and, hence, laminar due to a superimposed steady axial magnetic field or rotation of crucible (Grants 1998, ch. 3–4). A rotating magnetic field is usually generated by AC of industrial frequency that can not rise a considerable heating. Under these assumptions, the Navier–Stokes equations were supplemented by a buoyant body force $\mathbf{f}_b$ that is proportional to a temperature $\mathbf{f}_b=\rho\beta g T^* \mathbf{e}_z$, where $\mathbf{e}_z$ is unity vector in the axial direction, T^* is the temperature, ρ is the density and β is the coefficient of thermal expansion of the melt, but g is the gravity acceleration. According to the assumptions, the temperature field is described by an equation in dimensionless form

$$\frac{\partial T}{\partial t} + (\mathbf{v}\nabla)T = \frac{1}{\mathrm{Pr}}\nabla^2 T, \tag{1}$$

with the boundary conditions

$$T|_{z=1}=1,\quad T|_{r=R}=z,\qquad T|_{z=0}=0, \tag{2}$$

where $T=(T^*-T_s)/\Delta T$ is the dimensionless temperature, T_s is the solidification temperature, **v** is the velocity of melt motion, Pr is the Prandtl number defined as $\mathrm{Pr}=\nu/a$, ν is the kinematic viscosity, a is the thermal diffusivity, $R=R_0/L$ is a dimensionless crucible radius or aspect ratio of liquid zone. The characteristic height of liquid zone L is used as a linear lenghtscale since usually it is a determining scale in a rotating flow (Greenspan 1968).

Having solved hydrodynamic-heat problem, we found an axial heat flux on isotermic flat bottom $q^*(r)=\lambda(\Delta T/L)\partial T/\partial z$ that substituted the actual one on an almost flat front in our model (λ is a thermal conductivity of liquid). Write a heat balance on the solidification interface

$$\left.\frac{\partial \mathcal{T}}{\partial z}\right|_{z=\zeta(r)} = \mathrm{St} + q(r), \tag{3}$$

where $\mathcal{T}$ is the dimensionless crystal temperature defined as $\mathcal{T}=(T^*-T_s)/(T'R_0)$, St is the Stenton number $\mathrm{St}=u_p\rho_s\Lambda/(\lambda_s T')$, ρ_s and λ_s are density and thermal conductivity of crystal, but Λ is the latent heat of solidification. We used another lenghtscale that was the radius of crystal R_0 for a thermal problem in the solid phase since here it was more convenient than the previous one L used in the hydrodynamic part. Both parts are linked by the heat flux written in dimensionless form $q(r)=q^*(r)/(\lambda_s T')$. We considered a slow pulling with a Peclet number $\mathrm{Pe}_p=u_pR_0/a_s \ll 1$ and constant thermal conductivity. Actual conditions in technological processes may turn out different. However, they play a secondary role and may be easily incorporated into the present model. Under these assumptions the temperature distribution T in crystal is described simply by the Laplace equation

$$\nabla^2\mathcal{T}=0, \tag{4}$$

with Dirichlet boundary conditions on the crucible wall

$$\mathcal{T}|_S=z. \tag{5}$$

3. Stefan problem with a known heat flux from the liquid phase

There are two boundary conditions on the quasi-steady solidification interface of unknown shape. Obviously, an isothermal solidification front will move, to finally adjust the second boundary condition for the heat flux, too. Suppose, we have found a heat flux q^* from the liquid phase to a flat isotermic bottom that substitutes an almost flat front. Remember that our practical interest was exactly to find the conditions for a flat solidification interface. Of course, even under optimal conditions, the heat flux continuity on the assumed flat front may be unsatisfied. The disbalance in the heat flux continuity will be a measure of shift of actual solidification front from the assumed flat one. This section concerns in a link between these variables.

The shape of quasi-steady solidification interface is described by a solution of (3–5). Let us introduce a temperature correction due to an actual deformed interface as follow

$$\mathcal{Y}(r,z)=\mathcal{T}(r,z)-\mathcal{T}_0(r,z),\qquad (z<\zeta(r)) \tag{6}$$

where $\mathcal{T}_0(r,z)$ is the temperature field in crystal with a flat front. From (4–5) it follows that $\mathcal{T}_0(r,z)=z$ in our model. Hence, the heat flux continuity (3) on an almost flat interface takes the form of

$$\left.\frac{\partial \Upsilon}{\partial z}\right|_{z=\zeta(r)} = \mathrm{St} - 1 + q(r), \tag{7}$$

The correction $\Upsilon(r,z)$ satisfies the Laplace equation and takes zero value on crystal surface with Dirichlet boundary conditions used in our model. Definition (6) establishes a relationship between the correction $\Upsilon(r,z)$ and corresponding profile of front $\zeta(r)$

$$\Upsilon(r,z)|_{z=\zeta(r)} = \mathcal{T}(r,z)|_{z=\zeta(r)} - \mathcal{T}_0(r,z)|_{z=\zeta(r)}. \tag{8}$$

The solidification interface $z=\zeta(r)$ is isotermic, so the temperature $\mathcal{T}(r,z)|_{z=\zeta(r)}=0$ takes zero value on it, but $\mathcal{T}_0(r,z)|_{z=\zeta(r)} = \zeta(r)$ in case of the assumed linear temperature profile and slow pulling. Thus, the profile $\zeta(r)$ to be found coincides with a value of temperature correction $\Upsilon(r,z)$ on surface defined by this profile itself

$$\zeta(r) = -\Upsilon(r,z)|_{z=\zeta(r)}. \tag{9}$$

The problem is still defined by the boundary condition on unknown surface $\zeta(r)$. However, it can be easily found iteratively, e.g.,

$$\left.\frac{\partial \Upsilon^{n+1}}{\partial z}\right|_{z=\zeta^n(r)} = \mathrm{St} - 1 + q(r), \quad \zeta^{n+1}(r) = -\Upsilon^{n+1}\Big|_{z=\zeta^n(r)}, \quad \zeta^0(r) = 0. \tag{10}$$

The first approximation $\zeta^1(r)$ is expected to provide a reasonable accuracy for an almost flat solidification interface. It is defined simply by a solution of Laplace equation with homogenous Dirihlet conditions on the crucible wall and Neuman condition (7) on a flat front $z=0$.

Now we can derive some rather evident conclusions, that define certain optimal conditions for the heat flux. A flat quasi-steady front corresponds to zero right hand expression of (7). Hence, from the point of view of optimum solidification interface and maximum pulling velocity, a minimal heat flux $q(r)$ is required. The heat flux through the interface may be reduced either by thermal boundary conditions (such as a temperature drop ΔT in melt or gradient T' on the crystal surface) or by a guided motion of the melt. Second, the solidification interface is more sensitive to the heat flux in the central part of new solidified crystal. If this flux has a uniform distribution $q(r)=q_0$ and a magnitude below unity $q_0<1$ there, then an almost flat front can be achieved by an appropriate pulling velocity that follows from (7) $\mathrm{St}=1-q_0$.

4. Estimates of buoyancy suppression

Consider an artificial swirling flow of the melt driven by azimuthal body force due to a rotating magnetic field in a rotating vessel. Different rotation of the core region that appears in such flow (Priede 1993, 1994) leads to a secondary recirculation. At a certain threshold of magnetic forcing and imposed rotation of vessel this flow is expected to suppress the natural buoyant one. In order to estimate this limit, let us consider a circulation of centrifugal and buoyant forces over a closed loop *ABCDA* in

figure 2. Horizontal parts AB and DC give no contribution to the circulation of a buoyant force $\mathbf{f}_b=\rho\beta g T^* \mathbf{e}_z$, since it is purely axial

$$\Phi_b = \oint_{ABCDA} \mathbf{f}_b d\mathbf{l} = \rho\beta g \left(\int_B^C T(r,z)dz - \int_A^D T(r,z)dz \right) = \rho\beta g O(\Delta TL). \qquad (11)$$

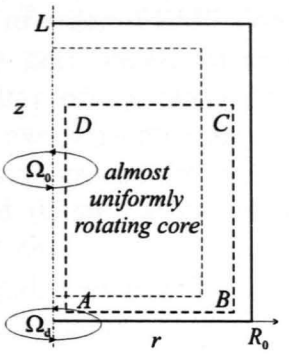

Figure 2. Sketch of swirl dominated flow.

A centrifugal force $\mathbf{f}_c=\rho\Omega^2\mathbf{e}_r$ is purely radial (Ω is the angular velocity). Consider a completely artificial (swirl dominated) flow. Then the circulation of $\mathbf{f}_c$ can be estimated as follow

$$\Phi_c = \oint_{ABCDA} \mathbf{f}_c d\mathbf{l} = \rho \left(\int_A^B \Omega^2(r,z) r dr - \int_D^C \Omega^2(r,z) r dr \right) \approx \frac{\rho R_0^2}{2} \left(\Omega_d^2 - \Omega_0^2 \right), \qquad (12)$$

where Ω_d and Ω_0 are the angular velocities of the crucible and the core, respectively. Suppose, the buoyancy is suppressed, if $\Phi_c >> \Phi_b$. Then, the threshold forcing can be estimated comparing (11) and (12).

First, consider a sole rotating magnetic field driven flow $\Omega_d=0$. Grants (1997) numerically found that the core angular velocity (for moderate Reynolds numbers $\mathrm{Re} \le O(10^4)$) is approximately $\Omega_0 \approx \nu / L^2 \mathrm{T}^{2/3} R^{1/2}$, where $R=R_0/L$ is the aspect ratio of liquid zone and T is the Taylor number of forcing $\mathrm{T} = \dfrac{ML^4}{0.5 m R_0^2 \nu^2}$ proportional to a driving magnetic torque M (Grants & Gelfgat 1997, Grants 1998, ch. 1 and 3); m is the mass of enclosed liquid. Substituting in (12) and comparing to (11) yields the following estimate of strong forcing:

$$\mathrm{T} \sim (\mathrm{Gr} R^{-3})^{3/4}. \qquad (13)$$

The Grashoff number Gr is defined here as $\mathrm{Gr} = \dfrac{\beta g \Delta T L^3}{\nu^2}$. Estimate (13) differs from the one given by Fischer *et al.* (1997). They simply compared $O(\mathrm{T})$ and $O(\mathrm{Gr})$. One should notice that both these parameters characterise the body forces that act in perpendicular directions, so such straightforward comparison hardly justifies itself. On the other hand, results of such comparison agreed with the experimental and

numerical results on the stabilising action of rotating field. In our case, however, we are interested mostly in the effect on heat flux and, thus, characteristics of base flow. To verify (13), we performed a numerical simulation with a forcing rate ranging about the estimated threshold value. The results for different aspect ratios are depicted in figure 5.

We restricted our study of action of superimposed SMF to a "small" induction. From practical point of view the imposed steady magnetic field is expected to be "hardly strong" that is with about a minimum strength providing a stable flow. The angular velocity of such flow is of order of RMF alone driven flow. Hence, the above estimate (13) is sufficient for such cases. In case of a strong steady field, a considerable angular velocity drop occurs along the height of $O(\mathrm{Ha}^{-1/2})$ side layer. Besides, this layer may have its own velocity scale of a higher order of magnitude. As a result, an axial pressure gradient appears driving the meridional flow that vanishes slower in a strong steady field (Grants *et al.* 1996, Grants 1998, ch. 3). Hence, estimate (12) is not suitable any more.

Now, consider an almost rigidly rotating flow ($\Omega_0 \approx \Omega_d$). Then the circulation of centrifugal forces (12) can be estimated as

$$\Phi_c \approx \frac{\rho R_0^2}{2}\left(\Omega_d^2 - \Omega_0^2\right) \approx \rho R_0^2 \Omega_d \Delta\Omega . \tag{14}$$

The differential rotation $\Delta\Omega$ of such flow is (Priede 1993, Grants 1998, ch. 4)

$$\Delta\Omega \sim \nu / L^2 \mathrm{T}|\mathrm{E}|^{1/2}, \tag{15}$$

where $\mathrm{E}=\nu/(\Omega_d L^2)$ is the Ekman number of crucible rotation. Then the comparison of (11) and (14) yields:

$$\mathrm{T}|\mathrm{E}|^{-1/2} \sim \mathrm{Gr} R^{-2}. \tag{16}$$

The condition of almost rigidly rotating flow requires $|\mathrm{E}|^{-1} >> \mathrm{T}^{2/3}$ (Priede 1993).

Notice that expression (11) overestimates the contribution of buoyancy and it is valid only for large Peclet numbers, when the recirculation significantly deforms a diffusive temperature field. The circulation of buoyant forces (11) vanishes as the Peclet number tends to zero in our model, since no radial temperature gradient occurs according to boundary conditions (2).

5. Heat transfer

In the previous section we estimated a limit of necessary forcing to suppress a buoyancy driven flow. Now let us consider heat transfer in swirl dominated flow as a limiting case of non-isotermic motion. An azimuthal body force due to a rotating magnetic field induces a swirling flow that provides axial symmetry of time-averaged characteristics. However, the main role belongs to an induced secondary recirculation that influences the heat transport in the normal direction to the solidification interface.

Flows of all three types considered in this chapter have a single vortex structure as schematically depicted in figure 3. From the point of view of heat transfer through the solid-liquid interface this vortex can be characterised by two parameters: the core axial velocity v_z and the location of vortex eye r^*. We see in §3 that the solidification interface is more sensitive to the heat flux in its central part. The direction of core axial velocity determines whether the heat flux is reduced or increased here in

comparison to a purely diffusive regime. The magnitude of core axial velocity H_0 determines the role of convection. Peclet number $Pe=H_0L/a$ should be larger than unity according to our basic assumption on a hydrodynamically guided solidification. The radial location of vortex eye determines the place where the influence of convection on heat transfer is inverted. Thus, it marks out the place, where a significant non-uniformity of convection dominated heat flux is expected. From the practical point of view the vortex eye should be pushed towards the side wall as far as possible, since exactly such configuration could increase the size of flat part of the heat flux profile and, hence, the solidification interface.

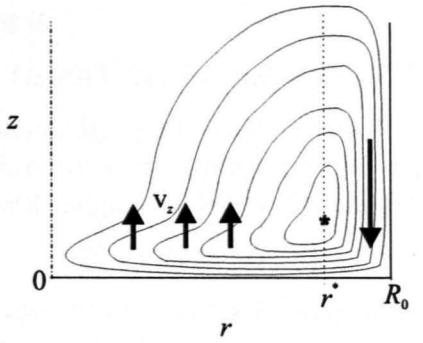

Figure 3. Characteristic pattern of swirl dominated motion near the solidification interface.

Let us consider a sole rotating field driven flow. According to Grants' (1997) numerical simulation of moderate Reynolds number flow in an elongated cylinder (the aspect ratio $1/8<R<1$), the core angular velocity is $\Omega_0 \approx 0.52\nu/L^2T^{2/3}R^{1/2}$. This expression for $R=1$ coincides with the corresponding similarity solution (Davidson 1992, Ungarish 1997). Employing a Bödewadt's solution (e.g., Greenspan 1968), we obtained the core axial velocity and Peclet number in form

$$H_0 \approx 1.35(\nu\Omega_0)^{1/2}=\nu/L\,0.97T^{1/3}R^{1/4}, \quad Pe \approx 0.97T^{1/3}R^{1/4}Pr\,. \tag{17}$$

Evidently, the location of vortex eye is closely connected to the thickness of side layer. Grants (1998, ch. 2) found that the relative thickness of this layer is $(\delta_\tau/R_0)\sim 0.075R^{-2/3}$ for moderate Reynolds numbers near the onset of Taylor–Götler instability and the aspect ratios ranging $1/8<R<1$. Here the side layer was defined via the location of maximum in the azimuthal velocity profile. Correspondingly, the "thickness of side layer" in an infinite cylinder is $(\delta_\tau/R_0)=1-3^{-1/2}\approx 0.422$ (Richardson 1974). The current investigation revealed that such widening of side layer persisted in elongated cylinders for the Reynolds numbers far beyond the onset value as well. One can see that in case of elongated liquid zone that is characteristic for the initial stage of the vertical gradient freeze method, the vortex eye moves away from the side wall. It reflects in the heat flux distribution so that the central uniform part is less expressed (cf. figure 5 *a* and *b* for forcing rate $T=3T_0$). The thickness of critical side layer is depicted here by a vertical dashed line.

Under the magnetic field with a large Hartmann number the core angular velocity of flow greatly depends on a relative conductance of new solidified crystal $\alpha_n=\sigma_s L_s/(\sigma L)$, where σ_s is the conductivity of crystal and L_s is its height. In case of semiconductor growth it is of order of few percents (Hjelming & Walker 1986). Such seemingly negligible conductance, however, is much larger than that of adjacent

Hartmann layer if the imposed field is strong $\alpha_n >> Ha^{-1}$; $Ha=(\sigma/(\nu\rho))^{1/2}LB$ is the Hartmann number; B is the induction of steady magnetic field. As a result, the swirling flow is braked more efficiently than in case of insulating walls (Grants *et al.* 1996, Grants 1998, ch. 3). Besides an indirect braking via the reduction of swirl, the meridional flow is suppressed directly as well. The core axial velocity scales as

$$H_0 \sim \frac{L^3}{\nu}\Omega_0^2 Ha^{-3}, \qquad \text{where} \quad \Omega_0 = \frac{\nu}{L^2}\frac{T}{Ha^2}\left(\frac{0.5+\alpha_n}{\alpha_n + Ha^{-1}}\right). \tag{18}$$

One can see that a strong SMF brakes recirculation drastically and, thus, it is appropriate to control the heat transfer and solidification in a narrow range beyond the threshold of strong field that is

$$Ha=O(T^{1/4}\alpha_n^{-1/4}) \quad \text{and} \quad Ha=O(T^{1/3}) \tag{19}$$

for poorly conducting and insulating walls, respectively.

A rapid imposed rotation rises an almost rigidly rotating flow with the axial velocity sign as that of crucible angular velocity (Priede 1993)

$$H_0 \sim \nu/LTE. \tag{20}$$

Priede predicted that there was a second branch of steady similarity solution at counter-rotation with a larger axial velocity and lower core angular velocity. However, Grants (1998, ch. 4) showed that this solution was not feasible due to an unstable force balance in the core. Thus, both imposed actions reduce the core axial velocity. Consequently, they can not reduce the heat flux more than a sole rotating field does. A rapid counter-rotation of crucible changes the direction of normal to bottom flow towards it. As a result, the heat flux increases and, consequently, an optimum pulling velocity decreases. There is the so-called Stewartson layer near the curved side wall in an almost rigidly rotating flow. It has an exponentially rising profile, a thickness of $O(L|E|^{1/4})$ and an inner more complicated layer of $O(L|E|^{1/3})$ order that smoothes out a discontinuity in the primary axial velocity profile (Stewartson 1957). Besides, the radial profile of core axial velocity is no more uniform but fits the driving magnetic body force distribution averaged over the height (Grants 1998, ch. 4). Minding that (20) expresses a softer damping law than (18), the above features of almost rigid flow make it more suitable for the controlling of heat flux distribution.

6. Numerical results

First, let us consider a buoyancy dominated flow (figure 4). The melt moves upward at a warmer side wall and is directed towards the solidification interface in its middle part. As a result, the buoyancy considerably increases the heat flux from the liquid phase in comparison to a diffusive regime (figure 5).

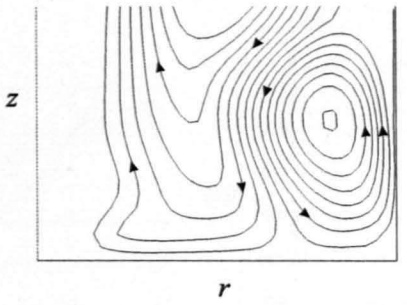

Figure 4. Characteristic pattern of buoyancy dominated motion near the solidification interface.

A magnetic forcing of sufficient strength changes the pattern of recirculation similar to the one depicted in figure 3. In such a way the heat flux is reduced. Figure 5 illustrates the above said. The heat flux from the liquid phase is depicted here in several regimes of forcing about estimated threshold value (13) for aspect ratio R=1/2 and R=1/8. The Grashoff number is $Gr=4\times10^6\times R^{-3}$ with corresponding threshold value $T_0=3.2\times10^7$ and $T_0=10^9$ for aspect ratios 1/2 and 1/8, respectively. One can see that a transition between buoyancy and swirl dominated regimes really occurs as predicted by scaling. The numerical simulation showed that the heat flux could be more reduced in a shorter cylinder (figure 5 *a*). Transition regime with an almost uniform heat flux was detected for an elongated cylinder (figure 5 *b*). The effect of sidelayer widening together with a relative height of liquid zone (§5) restricts possibilities to reduce the heat flux from an elongated liquid zone.

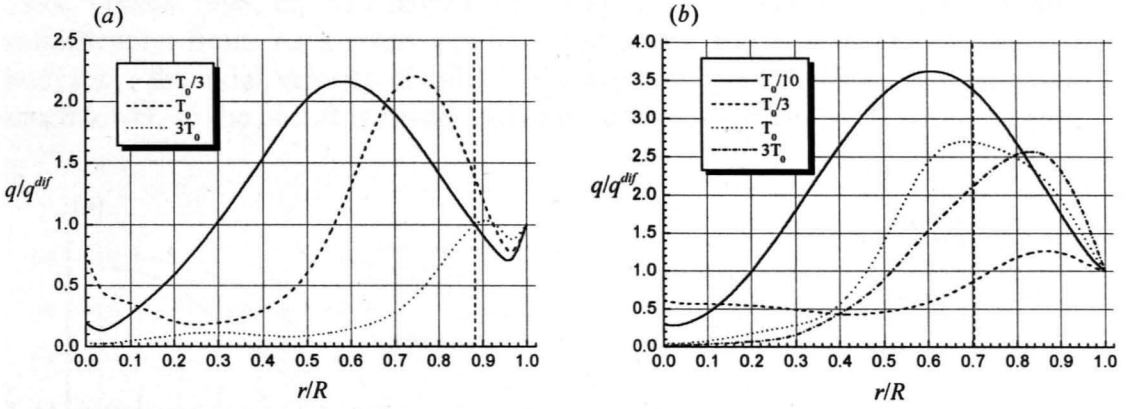

Figure 5. The heat flux distributions in the range at transition from buoyancy to swirl driven motion. (a) the aspect ratio R=1/2, the Grashoff number $Gr=4\times10^6R^{-3}=32\times10^6$ and estimated rate of threshold forcing $T_0=2\times10^6$. (b) R=1/8, $Gr=4\times10^6R^{-3}=2\times10^9$, $T_0=10^9$. A constant q^{dif} characterises purely diffusive heat flux.

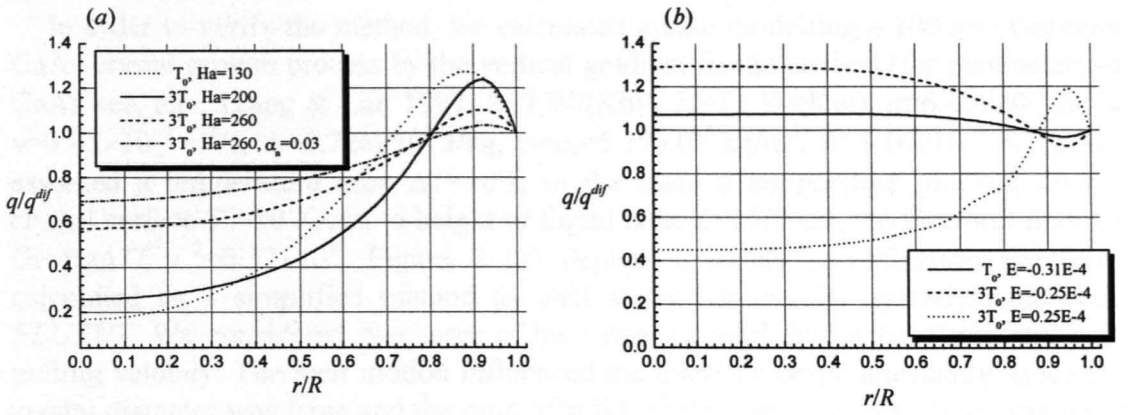

Figure 6. The heat flux profiles under imposed: (a) steady magnetic field or (b) rotation of crucible. The aspect ratio of liquid zone R=1/2, Gr=32×10⁶, estimate of forcing threshold rate T_0=2×10⁶. A constant q^{dif} characterises a purely diffusive heat flux.

Figure 6 depicts the characteristic heat flux distributions under a superimposed steady magnetic field or rotation of crucible. The aspect ratio is R=1/2, the Grashoff number is Gr=32×10⁶ and a corresponding threshold forcing is T_0=2×10⁶. An imposed steady magnetic field promotes a transition to the heat regime characteristic for a magnetically driven flow. Figure 6 (*a*) illustrates the role of seemingly negligible conductance of grown crystal α_n=3% as well.

The imposed rotation of vessel (figure 6 *b*) provided a more uniform heat flux distribution. A counter-rotation of magnitude about $\Omega_d \approx -1.5\nu/L^2T^{2/3}$ (Priede 1993, 1994, Grants 1998, ch. 4) changed the direction of core axial velocity towards the solidification front. As a result, the heat flux grows. Contrary to the motion due to buoyancy, the axial velocity distribution is more uniform. Besides, its magnitude is much lower, so the heat flux hardly increases in comparison to the diffusive regime.

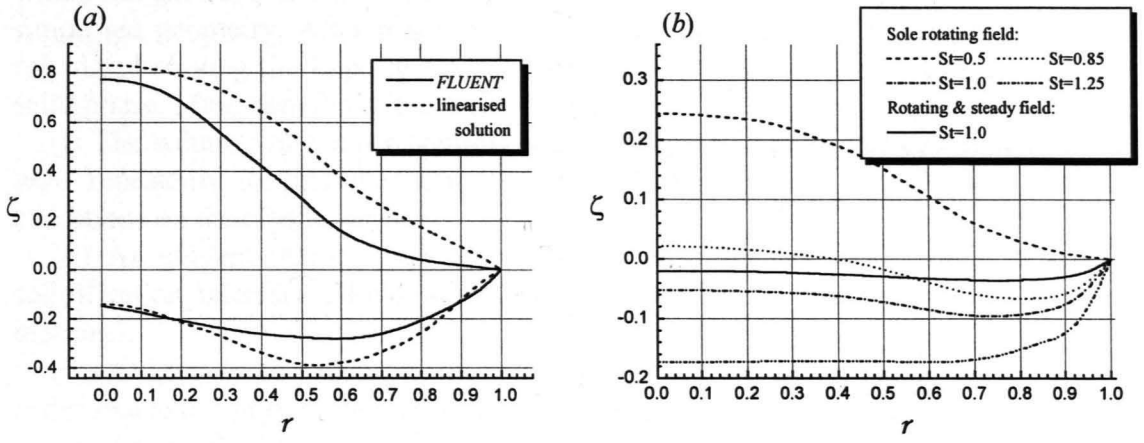

Figure 7. (a) comparison of front shape calculated by simplified model and FLUENT*; zero pulling velocity; Gr=0.31×10⁹; R=1/3. Lower and upper curves correspond to buoyancy and swirl (T=0.2×10⁹) dominated flow, respectively. (b) an example of solid-liquid interface optimisation. Dashed curves depict sole rotating field guided profiles at different pulling velocities. Solid curve corresponds to rotating (T=0.2×10⁸) and steady (Ha=510) magnetic field driven regime.*

In order to verify the method, we calculated a case modelling a 100 mm diameter GaAs crystal growth process by the vertical gradient freeze method (for parameters of GaAs see, e.g., Liang & Lan 1997: λ=7 W/(Km), λ_s=14 W/(Km), a=6.45×10^{-6} m^2/s, ν=3.45×10^{-7} m^2/s, Λ=0.726×10^6 J/kg, ρ=ρ_s=5.17×10^3 kg/m^3, β=1.16×10^{-4} K^{-1}). We assumed a temperature drop ΔT=10 K in the melt, a temperature gradient on the crystal surface T'=10 K/cm, a height of liquid zone L=150 mm, the Grashoff number $Gr=\beta g \Delta T L^3 \nu^{-2}=0.32\times10^9$. Figure 7 (*a*) depicts a steady solidification interfaces calculated by a simplified method as well as by commercial hydrodynamic code *FLUENT*. We considered two cases of buoyancy or swirl dominated flows and zero pulling velocity. The melt motion influenced the interface shape drastically, since the crystal diameter was large and the ratio of solid-liquid thermal conductivity was poor. One can see that our simplified method provided a reasonable accuracy even for a large front deformation of crystal radius order. In case of a buoyancy driven motion, the front is noticeably concave to the melt even for zero pulling velocity and favourable thermal boundary conditions used. According to (7) and its consequences, interface convex to the melt, that occurs for a swirl driven motion, can be always smoothed out by an appropriate pulling velocity (see, figure 7 *b*). However, a non-uniformity of heat flux distribution always manifested itself in a corresponding profile of the front (compare figure 7 *b* with the results by Friedrich *et al.* 1997). An imposed steady magnetic field reduced this non-uniformity and, thus, improved the growth interface.

7. Summary

This chapter concerns the solid-liquid interface between a grown crystal and the melt in the vertical gradient freeze method. We considered a lenghtscale large enough to significantly influence the heat transport by forced motion of melt. We linearised the coupled hydrodynamic-solidification problem about the optimum state simply with a flat growth interface. Thus, the hydrodynamic problem is to be solved in a fixed simplified geometry. After that a corresponding quasi-steady interface shape can be calculated solving the Laplace equation with the previously found flux source in the solid phase. Main benefits of the method are:

(i) The solution of a more complicated hydrodynamic part once calculated can be used repeatedly to find the corresponding optimum pulling velocity and thermal conditions on the crystal surface;

(ii) An evident relation between the heat flux from the melt and the shape of solidification interface allows obvious conclusions on an optimum pattern of melt motion;

(iii) Originally intended for the vertical gradient freeze technique with a lot of additional assumptions, the model can be easily generalised and supplemented;

(iv) The method provides a reasonable accuracy even for a significantly deformed interface.

We considered an artificial swirling-recirculating flow of conducting melt forced by a rotating magnetic field under an action of either steady magnetic field or rotation of crucible. The estimates of necessary forcing to suppress a natural buoyant flow are given and illustrated by the results of numerical simulation for different aspect ratios of the liquid zone. A sole rotating field driven flow could significantly reduce the heat flux from the liquid phase in comparison to a purely diffusive one. Hence, the

optimum pulling velocity can be increased. An imposed steady field or co-rotation of crucible control the heat flux in the range between sole rotating field driven and purely diffusive regimes. At the same time, the above actions allow to manipulate its distribution. Therefore the front shape can be noticeably improved with an additional benefit to the pulling velocity. The goal of imposed steady field or crucible rotation is to provide a certain compromise between the magnitude of heat flux and its uniformity (or, in other words, the optimum velocity of pulling and flatness of the front). The imposed counter-rotation increases the heat flux from the liquid phase in comparison to diffusive regime. Thus, from the point of view of solidification interface shape and pulling velocity, it is not an optimal case. However, the heat flux is reduced in comparison to the buoyancy driven flow. Besides, exactly such a configuration with a uniform flow towards a new solidified crystal may have benefits in quality characteristics that depend on mass transfer.

REFERENCES

Bennon, W. D. and Incropera, F. P. 1987 *Int. J. Heat Mass Transfer* 30, 2171

Davidson, P. A. 1992 *JFM* 245, 669-699

Fischer, B., Friedrich, J., Kupfer, C., Müller, G. and Vizman, D. 1997 In: Proc. on 3rd Int. Conf. on Energy Transfer in MHD Flows. Vol. 2, p. 337. Aussois, France.

Friedrich, J., Kupfer, C., Fischer, B., Müller, G. 1997 In: Proc. on 3rd Int. Conf. on Energy Transfer in MHD Flows. Vol. 2, p. 439. Aussois, France.

Grants, I. 1998 *Magnetically driven swirling flow guided by steady magnetic field and imposed rotation.* Thesis, Salaspils, Latvia

Grants, I. 1997 In: Proc. on 3rd Int. Conf. on Energy Transfer in MHD Flows. Vol. 2, p. 409. Aussois, France.

Grants, I., Priede J., Gelfgat Y. M. 1996 *Magnetohydrodynamics* 33, #3, 281

Greenspan, H. P. 1968 *The Theory of Rotating Fluids.* Cambridge University Press.

Hjelming, L. N. and Walker, J. S. 1986 *JFM* 164, 237

Liang, M.C. and Lan, C. W. 1997 *J. Cryst. Growth* 180, 587

Moffat, H. K. 1965 *JFM* 22, 521

Priede, J. 1993 *Theoretical study of a flow in an axisymmetric cavity of finite length, driven by a rotating magnetic field.* Thesis, Salaspils

Priede, J. 1994 In: Proc. on 2nd Int. Conf. on Energy Transfer in MHD Flows. Vol. 1, p. 87, Ausois, France

Richardson, A. T. 1974 *JFM* 63, 593

Stewartson, K. 1957 *JFM* 3, 17

Ungarish, M. 1997 *JFM* 347, 105

Voller, V. R. and Cross M. 1980 *Int. J. Heat Mass Transfer* 24, 545

Voller, V. R. and Prakash, C., 1987 *Int. J. Heat Mass Transfer* 30, 1709

Summary

The present thesis concerns a cylindrical, swirling-recirculating, azimuthal body force driven flow of conducting, incompressible liquid guided by a steady axial magnetic field or imposed rotation. Such flow is considered as a tool to control the convective transport in crystal growth from the melt. The optimum conditions of the intended application require an axially symmetric, uniform, controllable and steady flow. The natural buoyancy driven one usually does not satisfy any of these conditions. An azimuthal body force due to a rotating magnetic field drives an artificial flow with a number of advantages. However, it usually is neither stable nor controllable enough. The current thesis paper reveals and illustrates an ability of both imposed actions under consideration to control the base flow characteristics and its stability. I used mostly theoretical methods including scaling analysis, analytical solutions of simplified indicative cases as well as numerical simulation in selfsimilar or axially symmetric formulation.

The thesis paper consists of five independent contributions (chapters). A review of flows related to the investigated ones is given in the first chapter. The cited literature clearly shows that the problem under consideration is closely related to famous and well known problems on: (i) fully developed (2D) magnetohydrodynamic boundary layers under a strong transverse magnetic field; (ii) von Kármán swirling flow in half-space above a rotating disk. However, only few of existing results can be directly applied in our case.

The second chapter concerns the stability of sole rotating magnetic field driven flow in a truncated cylinder of aspect ratio (radius vs. height) below a unity. The numerical investigation showed that the Taylor–Götler type instability onset delays in a shorter cylinder due to a stronger recirculation that reduces the relative thickness of side layer. A numerically found criterion expressed in terms of maximum azimuthal velocity and the relative thickness of sidelayer approximates the corresponding one in the Taylor–Couette flow with an inner cylinder rotating. The investigation of base flow yielded the expressions for the characteristic velocity and boundary layer thickness thus introducing a link to the critical forcing rate. The comparison to a 3D instability onset in the Bödewadt layer yields that this type of instability is expected to take place first in the vessel with the aspect ratio (radius vs. height) above one third.

Chapter III deals with a body force driven flow under the action of steady axial magnetic field. The force balance analysis revealed a significant role of conductivity of normal to field end-walls. Magnetic braking starts to dominate first in the core if conductivity of end-walls is larger than that of adjacent boundary layer. Consequently, an intermediate range of braking occurs when the core is already braked but inertia perists to dominate in the boundary layer. The phenomenon is accompanied by a boundary layer widening with induction of the imposed field. Under a strong steady field the core rotation is braked exactly as the classic Hartmann flow. The source of core recirculation is proportional to a squared angular velocity drop in the boundary layer. Besides, a steady field brakes the recirculation directly as well that results in a drastic damping law of core recirculation. A strong field provides an axial uniformity of core rotation if the end-walls are insulating or thin. However, a strong field increases the role of radial distribution of driving body force.

A tangential boundary layer near a curved wall demonstrated an unexpected behavior in case of a reasonable conductivity of side wall. So, in case of all perfectly conducting walls, a sidelayer's velocity scale turned out much larger than that of the core. It differs essentially from the related classic case where both these scales are equal. A simple approximate analytical solution revealed that the difference occured due to curvature. An angular velocity drop along the height of side layer rises the meridional flow being less suppressed than the normal one in a horizontal layer. Therefore, in the side layer inertia persists for a higher induction of steady field. The numerical simulation showed that the Taylor-Götler type instability in the side layer is suppressed together with inertia. An imposed steady magnetic field allowed simple azimuthal velocity measurements by a couple of electrodes. Such technique is validated by the closure of steady field induced current through thin boundary layers or poorly conducting end-walls. The experiment has confirmed some theoretical results including the neutral stability curve at a strong steady field, the presence of essential azimuthal velocity drop in vertical direction of side layer as well as the numerically found (by a laminar model) base flow velocity in the range of Reynolds numbers up to 10^4.

Chapter IV concerns a flow driven by a rotating magnetic field and vessel's rotation. A steady solution of such flow is greatly controlled by the core force balance and a solution of associated so-called one disk problem. This classic problem describes a flow in a layer between a rotating bulk (i.e., the core in our case) over a differently rotating infinite disk (i.e. horizontal end-wall). According to its solution, the flow velocities can be controlled by imposed rotation similarly as it is done by a steady magnetic field. Contrary to the steady field, an imposed counter-rotation allows to change the direction of recirculation. A range of absent similarity solution appears as well as multiple solutions for counter-rotation. The numerical solution has confirmed the feasibility of those branches tending to an Ekman type almost rigid flow at a rapid vessel's rotation. Hence, the controllability of flow has been confirmed. Contrary to the steady field, the imposed rotation does not brake the recirculation directly. Thus, the decay law is softer. Axial variation of angular velocity occurs neither in the core nor in the side layer of almost rigid flow. The radial profiles of both the axial and angular velocities match each other and fit to an averaged over the height driving force distribution in the core. An approximate analytical solution was received for Stewartson's type vertical side layer.

The numerical simulation exhibited essentially 2D flow structures with separating layers and additional couples of recirculation loops in the range of absent similarity solution. The second solution at counter-rotation turned out unreachable due to an unstable force balance in the core. However, another branch of similarity solution was confirmed tending to the state with zero core circulation at a rapid counter-rotation. This solution was observed in a laterally bounded volume with differently rotating boundaries (e.g. Czohralski growth).

The existing results of rotating flow stability, as well as simple estimates using the Rayleigh criterion showed the stabilizing action of imposed rotation, especially of rapid counter-rotation.

In Chapter V a simplified model of hydrodynamically guided solidification is given. The method was obtained by linearizing a coupled hydrodynamic-solidification problem with an almost flat growth interface. The proposed technique allows to clarify optimum thermal and hydrodynamic conditions ensuring a maximum pulling velocity and flat solidification front. Besides, the method significantly simplified

calculations providing a reasonable accuracy at the same time. A minimum heat flux with a uniform distribution in the middle part is required. A natural buoyant flow is directed towards the solidification interface in its middle part. Hence, the heat flux is large and non-uniform there. A rotating field of sufficient strength drives a swirling-recirculating flow with axial velocity towards the bulk of melt. Consequently, the heat flux can be considerably reduced. The imposed steady magnetic field or rotation of vessel promoted a transition from buoyancy to a swirl dominated flow. Besides, both these actions allowed to control the heat flux distribution. Thus, they provided a certain compromise between the magnitude of heat flux and its non-uniformity. In terms of solidification front, it corresponds to its maximum flatness and an additional benefit to the pulling velocity rate.

The thesis offers a rich material to one wishing to optimize the melt motion during crystal growth. I believe, it somehow supplements the knowledge on famous theoretical problems in magnetohydrodynamic and rotating boundary layers, as well, or at least, gives several illustrative examples. Most of theoretical results wait for further experimental checking.

Acknowledgment

The work has been done under the grant by Latvian Council of Sciences from 1995 till 1998. I wish to acknowledge everyone who supported this investigation, especially Prof. Y. M. Gelfgat and Dr. J. Priede.